U.PORTO

DOUTORAMENTO

BIOLOGIA BÁSICA E APLICADA

The relationship between naïve pluripotency and X-chromosome inactivation

Elsa Sousa

D

2018

U.PORTO

Elsa Sousa The relationship between naïve pluripotency and X-chromosome inactivation

The relationship between naïve pluripotency and X-chromosome inactivation

Elsa Sousa

D.ICBAS **2018**

SEDE ADMINISTRATIVA

INSTITUTO DE CIÊNCIAS BIOMÉDICAS ABEL SALAZAR

FACULDADE DE CIÊNCIAS

FACULDADE DE MEDICINA

ELSA JOANA FERREIRA DE SOUSA

THE RELATIONSHIP BETWEEN NAÏVE PLURIPOTENCY AND X-CHROMOSOME INACTIVATION

Tese de Candidatura ao grau de Doutor em Biologia Básica e Aplicada submetida ao Instituto de Ciências Biomédicas Abel Salazar da Universidade do Porto.

Orientador

Doutor José Silva
Senior Investigator
Wellcome-MRC Cambridge Stem Cell Institute, University of Cambridge

Co-orientador

Professora Doutora Carmen de Lurdes Fonseca Jerónimo
Professora Associada convidada com Agregação
Departamento de Patologia e Imunologia Molecular
Instituto de Ciências Biomédicas Abel Salazar - Universidade do Porto
&
Investigadora Auxiliar e Coordenadora do Grupo de Epigenética e Biologia do Cancro
Centro de Investigação
Instituto Português de Oncologia do Porto Francisco Gentil, E.P.E.

Publication

Sousa, E.J., Stuart, H.T., Bates, L.E., Ghorbani, M., Nichols, J., Dietmann, S., and Silva, J.C.R. (2018). Exit from Naive Pluripotency Induces a Transient X Chromosome Inactivation-like State in Males. Cell Stem Cell *22*, 919-928 e916.

Acknowledgements

First, I would like to convey my gratitude to my supervisor, José Silva, for the opportunity to carry out my PhD studies in his lab. I am thankful for his support, guidance and endless optimism throughout this journey.

I am very grateful to Prof. Carmen Jerónimo, who encouraged me to apply to the GABBA programme and then accepted to be my co-supervisor. I thank her for all the help and for always being available when needed.

I would like to thank the GABBA programme for giving me the freedom to pursue my PhD studies in a lab of my choice.

I thank Hannah Stuart, Lawrence Bates, Mohammadmersad Ghorbani, Jennifer Nichols and Sabine Dietmann for their contribution to this work. I am also grateful to the core facilities of the Wellcome-MRC Cambridge Stem Cell Institute for their invaluable help.

I would like to thank all the members of the Silva lab, past and present, for creating such a friendly work environment and for always contributing with good ideas and insightful feedback. Special thanks to Lawrence for taking such good care of the lab and for making sure we would not run out of all the reagents, even though this was not his job. I am deeply grateful to Hannah and Charlotte, the best housemates ever, for their friendship, kindness and encouragement. I also thank Hannah for the invaluable comments on this thesis.

I am very grateful to all the good friends I made in Cambridge for making this city feel like home.

I would like to express my gratitude to my parents for the unconditional love and for always being my biggest supporters.

I am immensely grateful to my sister, Inês, for inspiring me every day and for always encouraging me to pursue my dreams.

Finally, I would like to thank Diogo, who shared with me all the ups and downs of this PhD, for always putting a smile on my face and reminding me what really matters in life.

Abstract

In mammals, females have two X-chromosomes, while males have one X- and one Y-chromosome. In order to equalise X-linked gene expression between the sexes, one of the two X-chromosomes is transcriptionally inactivated in female mammals, a process called X-chromosome inactivation (XCI). This process starts very early in female mouse embryonic development, with imprinted inactivation of the paternally inherited X-chromosome in all cells of the embryo. The silent X-chromosome is then transiently reactivated exclusively in the naïve epiblast, which contains the cells that will generate the entire embryo proper. Shortly after implantation, one of the two X-chromosomes is randomly inactivated in epiblast cells. The transient stage between imprinted and random inactivation is characterised by the presence of two active X-chromosomes. In fact, the presence of two active X-chromosomes in female cells is one of the epigenetic signatures of naïve pluripotency, a feature of the late pre-implantation epiblast and of its *in vitro* counterpart, embryonic stem cells. As female naïve pluripotent stem cells (nPSCs) differentiate, the master regulator of XCI, *Xist,* is upregulated monoallelically and coats the inactivating X-chromosome. Even though there is a strong correlation between differentiation and XCI, it is not known whether prevention of XCI is mediated by gene networks that also preserve the naïve pluripotent state. Thus, the main aim of this work was to explore the link between naïve pluripotency and XCI.

Here, I show that expression of *Xist* is repressed by a robust naïve transcription factor network, which can be achieved through the use of optimal nPSC culture conditions. When perturbation of the naïve network was induced through ablation of key components of the network, *Xist* expression was highly upregulated not only in female but also in male cells. This prompted me to revisit the kinetics of *Xist* expression during nPSC differentiation.

Surprisingly, I found that *Xist* is transiently and rapidly upregulated in early differentiating male cells. The data presented here show that *Xist* upregulation is gender-independent and linked to the downregulation of naïve pluripotency factors. Moreover, I demonstrate that nPSCs accumulate *Xist* on the single male X-chromosome and on both female X-chromosomes as they become NANOG-negative at the onset of differentiation. This is accompanied by appearance of a repressive chromatin signature and partial X-linked transcriptional silencing.

Xist expression was also assessed in male and female mouse embryos at different stages. I observed that *Xist* is not expressed in pre-implantation naïve epiblast cells in either sex, and that it is transiently expressed in males from the single X-chromosome and in females from both X-chromosomes at the onset of naïve epiblast differentiation.

In conclusion, these findings demonstrate that XCI initiation is gender-independent, and that it is triggered by destabilization of naïve identity. Importantly, this suggests that gender-specific mechanisms follow, rather than precede, XCI initiation. This change in the paradigm of XCI opens up new avenues to investigate how this process is regulated.

Resumo

As fêmeas de mamíferos possuem dois cromossomas X, enquanto que os machos possuem um cromossoma X e um Y. De forma a equalizar a expressão dos genes localizados no cromossoma X entre os dois sexos, um dos dois cromossomas X é inactivado transcricionalmente em mamíferos fêmea através de um processo chamado inactivação do cromossoma X (XCI). Este processo começa durante as etapas iniciais do desenvolvimento embrionário da fêmea de murganho com a inactivação "imprinting" do cromossoma X de origem paterna em todas as células do embrião. O cromossoma X inactivo é depois reactivado de forma transiente exclusivamente no epiblasto "naïve" que contém as células que darão origem ao embrião propriamente dito. Logo após a implantação, um dos dois cromossomas X é inactivado aleatoriamente nas células do epiblasto. O estado transiente entre a inactivação "imprinting" e a aleatória é caracterizado pela presença de dois cromossomas X activos. De facto, a presença de dois cromossomas X activos em células fêmea é uma das "assinaturas" epigenéticas da pluripotência "naïve" que, por sua vez, pode ser encontrada no epiblasto pré-implantação tardio e no seu homólogo *in vitro*, as células estaminais embrionárias. Durante a diferenciação das células estaminais pluripotentes naïve (nPSCs) fêmea, o principal regulador da XCI, *Xist*, aumenta a expressão de um dos seus alelos e reveste o futuro cromossoma X inactivo. Embora exista uma forte correlação entre a diferenciação e a XCI, não se sabe se a XCI é regulada pelos mesmos genes que regulam a pluripotência naïve. Assim, o principal objectivo deste trabalho foi explorar a relação entre a pluripotência naïve e a XCI.

Aqui, demonstro que a expressão do *Xist* é reprimida por uma rede robusta de factores de transcrição associados ao estado "naïve", que pode ser obtida através do uso de condições de cultura ideais para as nPSCs. Quando esta rede de factores de transcrição foi perturbada através da remoção dos seus componentes, a expressão do *Xist* aumentou não só em células fêmea, mas também em células macho. Estes resultados levaram-me a revisitar a cinética da expressão do *Xist* durante a diferenciação de nPSC.

Surpreendentemente, descobri que a expressão do *Xist* aumenta de forma transiente e rápida no início da diferenciação das células macho. Os dados aqui apresentados demonstram que este aumento na expressão do *Xist* é independente do género e que está ligado à diminuição da expressão dos factores de transcrição "naïve". Também demonstrei que as nPSCs acumulam *Xist* no único cromossoma X dos machos e em ambos os cromossomas X das fêmeas, assim que as células se tornam negativas para a proteína NANOG no início da diferenciação. Isto é acompanhado pelo aparecimento de uma

“assinatura” repressiva da cromatina e pelo silenciamento parcial dos genes localizados no cromossoma X.

A expressão do *Xist* foi também avaliada em embriões de murganho macho e fêmea em diferentes estadios do desenvolvimento. Constatei que o *Xist* não é expresso nas células do epiblasto “naïve” pré-implantação em nenhum dos sexos, e que é posteriormente expresso de forma transiente em machos no seu único cromossoma X e em fêmeas em ambos os cromossomas X no início da diferenciação do epiblasto “naïve”.

Em conclusão, estes resultados demonstram que a iniciação da XCI é independente do género e que é desencadeada pela desestabilização da identidade “naïve”. Isto sugere que, ao contrário do que se pensava, mecanismos específicos do género ocorrem após a iniciação da XCI. Esta mudança no paradigma da XCI abre novos caminhos na investigação da regulação deste processo.

Table of contents

List of figures

List of tables

List of abbreviations

2iL:	2i/LIF medium
4-OHT:	4-hydroxytamoxifen
BSA:	bovine serum albumin
DAPI	4’,6-diamidino-2-phenylindole
DMSO:	dimethylsulfoxide
dNTP:	deoxyribonucleotide
Ds:	double-strand
E:	embryonic day
EB:	embryoid body
ECC:	embryonal carcinoma cell
EDTA:	ethylenediaminetetraacetic acid
EGF:	epidermal growth factor
EGTA:	ethylene glycol tetraacetic acid
EpiSC:	epiblast stem cell
ERK:	extracellular-signal-regulated kinase
ESC:	embryonic stem cell
FA:	FGF2/Activin A medium
FACS:	fluorescence-activated cell sorting
FAX:	FGF2/Activin A/XAV 939 medium
FBS:	fetal bovine serum
Fgf2:	fibroblast growth factor 2
FISH:	fluorescence in situ hybridization
G418:	geneticin
Gapdh:	glyceraldehyde 3-phosphate dehydrogenase
GFP:	green fluorescent protein
GSK3β:	glycogen synthase kinase-3 beta
GY118F:	JAK/STAT3 activating receptor
H:	histone
HEPES:	4-(2-hydroxyethyl)-1-piperazineethanesulfonic acid
ICM:	inner cell mass
iPSC:	induced pluripotent stem cell
IRES:	internal ribosomal entry site
JAK/STAT3:	janus kinase/signal transducer and activator of transcription 3
JAKi:	janus kinase inhibitor

K:	lysine
Klf4:	Kruppel-like factor 4
LIF	leukemia inhibitory factor
me:	methylation
MEK:	mitogen-activated protein kinase
Myc:	v-myc avian myelocytomatosis viral oncogene homolog
N2B27:	basal media complemented with N2 and B27
Nanog-GFP:	reporter where GFP is expressed under the control of Nanog
NEAA:	non-essential aminoacids
nPSC:	naïve pluripotent stem cell
NSC:	neural stem cell
Oct4:	octamer binding protein 4
Oct4-GFP:	reporter where GFP is expressed under the control of Oct4
PBS:	phosphate buffered saline
PCA:	principal component analysis
PCR:	polymerase chain reaction
PLAT-E:	platinum E 239T cells
pMX:	retrovirus
qRT-PCR:	reverse transcription quantitative Real-Time PCR
Rex1:	reduced expression protein 1
Rex1-dGFP:	reporter where GFP is expressed under the control of Rex1
RNA-seq:	RNA sequencing
SL:	serum/LIF
Sox2:	SRY (sex determining region Y)-box 2
Ss:	single-strand
SSC:	saline sodium citrate
Taq:	*Thermophilus aquaticus* DNA polymerase
Tris:	Tris(hydroxymethyl)aminomethane
WT:	wild type
Xa:	Active X-chromosome
XAV 939:	tankyrase (TNKS) inhibitor
XCI:	X-chromosome inactivation
XCR:	X-chromosome reactivation
Xi:	Inactive X-chromosome
Xic:	X-chromosome inactivation centre
Xist:	X-inactive specific transcript

X^m: Maternal X-chromosome

X^p: Paternal X-chromosome

Xpr: X-pairing region

Chapter 1
Introduction

1.1 X-chromosome inactivation

In mammals, females have two X-chromosomes and males an X- and a Y-chromosome. Whereas the X-chromosome is large and gene rich, the Y-chromosome has been subject to degradation during mammalian evolution due to its lack of recombination during meiosis (Graves, 2006). As a consequence, the Y-chromosome carries very few functional genes which results in an unequal dosage between males and females for the X-linked genes with no Y partner. In order to equalise X-linked gene expression between the sexes, one of the two X-chromosomes is transcriptionally inactivated in female mammals early in development. This process is called X-chromosome inactivation (XCI) and was observed for the first time by Mary Lyon (Lyon, 1961). Dosage compensation of sex chromosomes is crucial for mammalian development to progress properly, as shown by the fact that ablation of the master regulator of XCI, *Xist*, leads to female-specific lethality early in mouse embryonic development (Marahrens et al., 1997; Penny et al., 1996).

The mouse is the most well characterised XCI model system. During female mouse embryonic development, XCI occurs in two waves (Figure 1.1). A first wave of XCI takes place between 4- to 8- cell stage (Okamoto et al., 2004). This leads to inactivation of the paternally transmitted X-chromosome in all cells of the early embryo in a process known as imprinted XCI (Takagi and Sasaki, 1975; West et al., 1977). At embryonic day (E) 4.5, the paternal X-chromosome is transiently reactivated in cells of the naïve pluripotent epiblast (Mak et al., 2004; Okamoto et al., 2004; Silva et al., 2009; Williams et al., 2011), whereas imprinted XCI persists in the extraembryonic tissues (Harper et al., 1982). Around 24 hours later, shortly after implantation, there is a second wave of XCI which results in random inactivation of either the maternal or the paternal X-chromosome in epiblast cells (Okamoto et al., 2005). Once random XCI is completed, the inactive X-chromosome (Xi) is clonally

propagated throughout cell division, meaning that the same X-chromosome remains inactivated in all daughter cells (Plath et al., 2002).

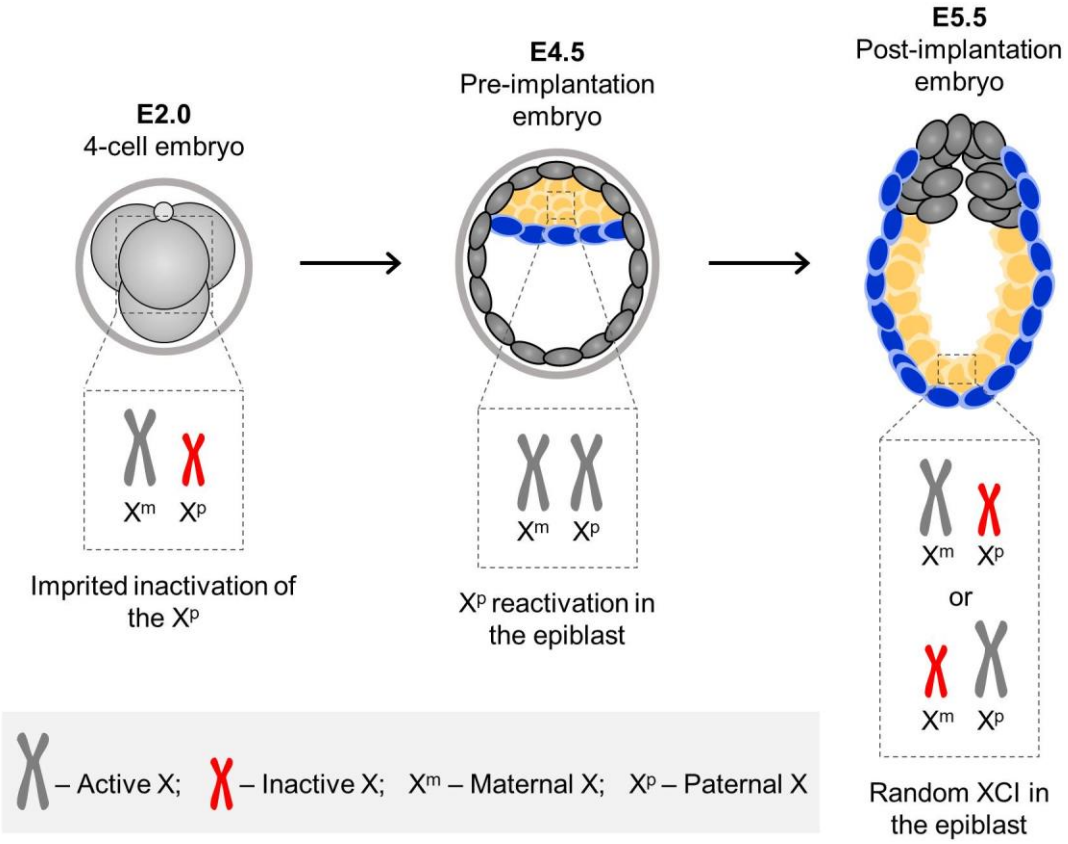

Figure 1.1: XCI during female mouse embryonic development.
Imprinted inactivation of paternal X-chromosome takes place between 4- to 8-cell stage in all cells of female the embryo. The paternal X-chromosome is then reactivated at E4.5 in cells of the pre-implantation epiblast (yellow), whereas extraembryonic tissues, including the primitive endoderm (blue) and the trophectoderm (grey), maintain imprinted inactivation. At E5.5, the post-implantation epiblast undergoes random XCI.

The process of random XCI gives rise to cellular mosaicism in females. Cellular mosaicism confers females with a significant biological advantage by ameliorating the deleterious effects of X-linked mutations. As a consequence, only males are affected by many of the disorders caused by X-linked mutations, such as Wiskott-Aldrich syndrome and Duchenne's muscular dystrophy (Migeon, 2006). Conversely, some X-linked diseases are only observed in females, since in males they are lethal either in utero or in early childhood (e.g., incontinentia pigmenti and Rett syndrome) (Migeon, 2006).

1.1.1 Random XCI in mice

According to the prevailing paradigm, random XCI can be divided into five phases in the following order: counting, choice, initiation, establishment, and maintenance (Avner and Heard, 2001; Boumil and Lee, 2001; Lyon, 1999). With the exception of maintenance, these phases appear to be controlled by the X-chromosome inactivation centre (Xic), a ~500 kb region located on the X-chromosome that harbours *Xist* (Heard et al., 1994; Lee et al., 1996; Rastan, 1983; Rastan and Robertson, 1985). The Xic was first proposed as the master regulatory locus for XCI not long after XCI itself was discovered (Russell, 1963).

During the counting step, a cell determines its X/autosome ratio in order to maintain only one active X-chromosome (Xa) per diploid autosome set. This process was described for the first time by Lyon and Grumbach based on humans with abnormal numbers of X-chromosomes (Grumbach et al., 1963; Lyon, 1962).

During choice, all but one X-chromosome is selected to become inactivated. In the case of diploid female mouse cells, one of the two X-chromosomes is chosen for inactivation. It is hypothesised that the future Xi and Xa are chosen during the process of X-pairing, in which the Xic of both X-chromosomes transiently move into close spatial proximity (Augui et al., 2007; Bacher et al., 2006; Xu et al., 2006). However, a different study reported that heterozygous deletion of the region identified as required for pairing does not affect XCI in mouse embryonic stem cells (ESCs) suggesting that pairing is not required for XCI to occur (Barakat et al., 2014).

Initiation of XCI coincides with the upregulation of *Xist* from the future Xi (Brown et al., 1991). It has been proposed that XCI activators, also contained within the Xic, act in a dose-dependent manner to activate *Xist* (Jonkers et al., 2009; Monkhorst et al., 2009). These activators are predicted to be counteracted by autosomally-encoded XCI inhibitors that are equally expressed between male and female cells. In contrast, as XCI activators are X-encoded, they will be present in a double dose in the epiblast of the female embryo, or in female ESCs, relative to males. This will ensure that only female cells can overcome the threshold for XCI to occur. Moreover, silencing of the X-encoded activators will decrease the probability of the second X-chromosome to initiate XCI ensuring that one of the X-chromosomes remains active (Chureau et al., 2011; Tian et al., 2010). The role of *Xist* and its activators and inhibitors will be further discussed in sections 1.1.3 and 1.1.4.

In the establishment phase, *Xist* spreads and coats the entire future Xi in *cis* in order to silence it. *Xist* spreading is accompanied by depletion of basic transcriptional machinery and of active chromatin marks, such as histone H3 lysine 4 dimethylation and trimethylation (H3K4me2/me3) and histone H3 and histone H4 acetylation (H3/H4Ac) (Goto et al., 2002; Heard et al., 2001; O'Neill et al., 2008). After the loss of euchromatin marks, Polycomb

complex 1 and 2 (PRC1 and PRC2) are recruited (de Napoles et al., 2004; Plath et al., 2004; Schoeftner et al., 2006; Zhao et al., 2008) and catalyse the accumulation of the repressive chromatin marks histone H3 lysine 27 trimethylation (H3K27me3) (Plath et al., 2003; Silva et al., 2003) and monoubiquitylation of lysine 119 of histone H2A (H2A119ub) (de Napoles et al., 2004). These epigenetic changes are followed by incorporation of the histone variant macroH2A (Costanzi et al., 2000; Mermoud et al., 1999; Mietton et al., 2009), DNA methylation at CpG islands of X-linked genes (Grant et al., 1992; Kaslow and Migeon, 1987) and, finally, accumulation of histone H3 lysine 9 dimethylation (H3K9me2) (Heard et al., 2001; Rougeulle et al., 2004). All these features of the Xi are important to ensure that the silenced state of the X-chromosome is permanently locked in.

Once XCI is complete, the Xi is maintained in an inactive state and clonally propagated throughout cell divisions. As previously mentioned, the initiation of XCI relies on *Xist* expression, but once silencing is established, maintenance of the inactive state appears to be independent of further Xic and *Xist* activity (Brown and Willard, 1994; Csankovszki et al., 1999).

1.1.2 *Xist*, the master regulator of XCI

The *Xist* (X-inactive specific transcript) gene was first identified in the early 1990s as a candidate for the master regulatory switch locus required in *cis* for XCI to occur (Borsani et al., 1991; Brockdorff et al., 1991; Brown et al., 1991). *Xist* is located in the Xic (Figure 1.2) and encodes a long non-coding RNA that is around 17 kb in length and that is retained in the nucleus (Borsani et al., 1991; Brockdorff et al., 1992; Brown et al., 1992). There are two major *Xist* isoforms which are produced through use of different termination signals (Ma and Strauss, 2005).

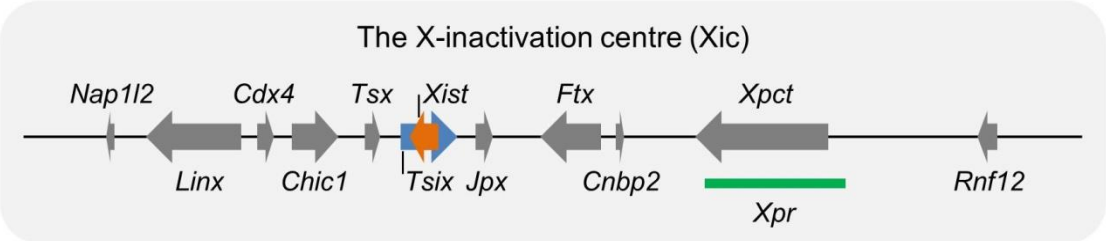

Figure 1.2: The mouse Xic.
Schematic overview of the mouse Xic. The Xic encompasses not only *Xist* but also its regulatory elements. Adapted from Galupa and Heard, 2015.

It has been reported that *Xist* is expressed at low levels in undifferentiated female and male ESCs (Panning et al., 1997; Sheardown et al., 1997). In the female, *Xist* is monoallelically upregulated at the onset of XCI and coats the future Xi in *cis* triggering a cascade of chromosome-wide events that result in transcriptional silencing and heterochromatinization of that X-chromosome (Escamilla-Del-Arenal et al., 2011; Splinter et al., 2011).

Several studies demonstrated that *Xist* is both necessary and sufficient for initiation of XCI. The requirement of *Xist* for XCI has been demonstrated by experiments on female ESCs harbouring a heterozygous *Xist* deletion, which exhibit skewed inactivation towards the wild-type X-chromosome (Penny et al., 1996). On the other hand, ectopic expression of *Xist* from multicopy transgenes causes autosomes to display features of XCI, showing that *Xist* is sufficient for initiation of chromosome inactivation (Herzing et al., 1997; Lee and Jaenisch, 1997). Furthermore, Wutz and Jaenisch demonstrated that, during the early stages of differentiation, X-linked gene silencing is dependent on continued *Xist* expression and is reversible. However, by day 3 of ESC differentiation, XCI becomes permanent and independent of *Xist* (Wutz and Jaenisch, 2000).

Xist RNA is poorly conserved between placental mammals, except for a series of unique tandem repeats termed A-F, which vary in size and number among species (Brown, 1991; Hendrich et al., 1993; Nesterova et al., 2001; Yen et al., 2007). The most conserved sequence in the *Xist* gene is an A-repeat region that is close to the 5' end. Molecular genetics studies have shown that this is required for *Xist*-mediated silencing, but not for coating of the X-chromosome (Wutz et al., 2002). Other regions have been shown to be critical to *Xist* localization to the X-chromosome (Beletskii et al., 2001; Sarma et al., 2010) and to the ability of *Xist* to recruit chromatin-modifying factors such as PRC2 (da Rocha et al., 2014; Kohlmaier et al., 2004; Zhao et al., 2008).

1.1.3 *Cis*-regulation of XCI

The Xic encompasses not only *Xist* but also its known and putative *cis*-regulatory elements (Figure 1.2). *Tsix* is one of these regulatory factors and is transcribed antisense to *Xist* (Lee et al., 1999). It has been proposed that *Tsix* transcription is required to repress *Xist* on the future Xa (Lee, 2000; Lee and Lu, 1999; Luikenhuis et al., 2001; Navarro et al., 2005; Sado et al., 2005; Sado et al., 2001; Stavropoulos et al., 2001). *Tsix* also plays a role in determining which X-chromosome will be silenced as shown by its heterozygous deletion leading to skewed *Xist* expression and non-random inactivation of the mutated chromosome (Lee and Lu, 1999). Moreover, it has been shown that *Tsix* is one of the elements involved in the process of X-pairing (Masui et al., 2011).

The non-protein-coding gene *Ftx*, which is located in close proximity to *Xist*, has been reported to participate in activation of *Xist* (Chureau et al., 2011). *Ftx* deletion in male ESCs results in decreased expression of *Xist* as well as other *loci* across Xic (Chureau et al., 2011). However, deleting *Ftx* in female pre-implantation embryos had no impact on *Xist* expression (Soma et al., 2014).

The *Jpx* locus also produces a non-coding RNA that has been described to positively regulate *Xist* (Tian et al., 2010), even though there is no agreement on whether it acts in *cis* or in *trans*. A heterozygous deletion of *Jpx* in female ESCs has been reported to decrease *Xist* upregulation in both alleles, which could be rescued by an autosomal transgene, suggesting *Jpx* to act in *trans* (Tian et al., 2010). The *trans* activity of *Jpx* has been proposed to occur by dose-dependent eviction of CTCF at the *Xist* promoter (Sun et al., 2013). However, in a more recent study, a large deletion encompassing *Jpx* locus in female ESCs affected XCI and this could not be rescued by random integration of *Jpx* transgene, indicating only a *cis* mechanism of action (Barakat et al., 2014).

The X-pairing region (*Xpr*), previously implicated in Xic pairing, was also proposed to induce *Xist* expression in *trans* (Augui et al., 2007). However, Barakat and colleagues reported that *Xpr* does not seem to act in *trans*, but instead enhances *Xist* expression through a *cis*-mediated mechanism (Barakat et al., 2014).

1.1.4 *Trans*-regulation of XCI

Rnf12, which is located within the Xic (Figure 1.2), has been proposed to upregulate *Xist* in *trans* in a dose-dependent manner (Jonkers et al., 2009). It encodes an E3 ubiquitin ligase that promotes the degradation of the *Xist* repressor REX1. In male ESCs, extra copies of *Rnf12* lead to activation of *Xist* expression (Gontan et al., 2012). Homozygous knockout of *Rnf12* resulted in lack of XCI in differentiating female ESCs (Gontan et al., 2012). In contrast, Shin and colleagues reported that, although *Rnf12* seems to be required for imprinted XCI *in vivo*, its knockout did not impact on random XCI (Shin et al., 2010; Shin et al., 2014). This discrepancy might be explained by the fact that RNF12 protein was not entirely abrogated and the sequences deleted were not the same in both studies.

XCI occurs during a specific developmental time window and has been linked to the pluripotency network. Some of the pluripotency-associated factors have been proposed to repress XCI either by stimulation of *Tsix* or by suppression of *Xist* expression (Galupa and Heard, 2015). The regulation of XCI by pluripotency factors will be further discussed in section 1.3.

1.2 Pluripotency in the embryo and in culture

The dynamics of XCI are tightly coupled with the progression of embryonic development. Remarkably, the link between XCI and differentiation was first proposed in the late 1970s using mouse embryos as a model system (Monk and Harper, 1979). A few years later, it became possible to culture mouse ESCs (Evans and Kaufman, 1981; Martin, 1981), which, if female, retain the XaXa status of the pre-implantation epiblast cells from which they are derived and undergo random XCI upon differentiation (Rastan and Robertson, 1985). Since then, mouse ESCs have become the prevailing *in vitro* model system to study the process of random XCI. Furthermore, there has been a growing interest in how XCI and pluripotency are related. In the study conducted here, I attempted to further explore the link between XCI and naïve pluripotency and, for that purpose, used ESCs as a model system. Therefore, I will now introduce relevant aspects of pluripotency that will be important for this dissertation.

Pluripotency is the potential of a single cell to give rise to all somatic lineages that constitute an organism, comprising mesoderm, endoderm and ectoderm derivatives, as well as the germ cells. Cells within the epiblast of the early mammalian embryo are pluripotent and represent the founding cell population of the embryo proper (Arnold and Robertson, 2009). In the mouse embryo, pluripotent cells emerge in the inner cell mass (ICM) at E3.5 and persist until the onset of somitogenesis at E8.5 (Morgani et al., 2017; Smith, 2017). During this period, the pluripotent population undergoes dynamic transcriptional and epigenetic changes, including changes in the X-chromosome status.

The study of pluripotency began with the observation that mice of the 129 strain spontaneously developed teratocarcinoma, which is a malignant tumour composed of differentiated derivatives of all three germ layers and an undifferentiated proliferative component (Stevens and Little, 1954). Pluripotent stem cells isolated from these tumours, known as embryonal carcinoma cells (ECCs), could be clonally expanded in culture, while retaining their pluripotency, but their tumourigenicity and karyotypic abnormality was problematic (Kahan and Ephrussi, 1970; Martin and Evans, 1975). ECC-conditioned medium subsequently allowed derivation of the so-called ESCs from pre-implantation mouse embryos (Evans and Kaufman, 1981; Martin, 1981). ESCs exhibited a normal karyotype and could be incorporated into chimeric mice without forming tumours (Bradley et al., 1984). Post-implantation epiblast cells, however, cannot be maintained in any of the culture systems used for ESC propagation. Instead, an alternative type of pluripotent stem cell line, termed epiblast stem cells (EpiSCs), can be derived from post-implantation embryos using different growth conditions (Brons et al., 2007; Tesar et al., 2007). EpiSCs are very different from ESCs transcriptionally, epigenetically, metabolically and functionally (Morgani et al., 2017). The terminology “naïve” and “primed” was introduced to describe the early and late phases,

respectively, of pluripotency *in utero*, and the corresponding ESC and EpiSC states *in vitro* (Nichols and Smith, 2009).

1.2.1 Naïve pluripotency

1.2.1.1 Derivation and culture of embryonic stem cells

Mouse ESCs can be isolated from and resemble the naïve epiblast of E3.5-4.5 pre-implantation embryos (Boroviak et al., 2014; Brook and Gardner, 1997; Evans and Kaufman, 1981; Martin, 1981). ESCs were first derived by co-culture with a feeder layer of mitotically inactivated fibroblasts in poorly defined medium containing fetal calf serum (Evans and Kaufman, 1981; Martin, 1981). However, the efficiency of these culture conditions was highly dependent on the genetic background of mice (Brook and Gardner, 1997). In fact, almost all ESC lines efficiently derived using serum and feeders are from the 129 strain of mice. The first step towards a defined culture system was the identification of leukaemia inhibitory factor (LIF) as the cytokine produced by feeders to support ESC self-renewal (Smith et al., 1988; Williams et al., 1988). By adding LIF to the culture medium (Serum/LIF, SL), ESCs could be propagated on gelatin-coated dishes without feeders, making ESC culture simpler while maintaining the capacity to contribute to chimeras.

LIF signals through a bipartite receptor complex composed of LIF receptor α (LIFR) and gp130 to activate Janus-associated kinases (JAKs). In response to JAK activation, STAT3 is recruited to the LIF receptor complex and activated through phosphorylation by JAK. STAT3 activation was demonstrated to be critical for LIF-mediated ESC self-renewal (Boeuf et al., 1997; Matsuda et al., 1999; Niwa et al., 1998). The main downstream targets of STAT3 activation in ESCs are the pluripotency-related genes *Klf4*, *Klf5*, *Tfcp2l1* and *Nanog* (Bourillot et al., 2009; Martello et al., 2013; Niwa et al., 2009; Stuart et al., 2014; Ye et al., 2013). However, ESCs cultured in SL are very heterogeneous, not only morphologically but also in terms of expression of pluripotency genes, and exhibit some degree of spontaneous differentiation (Chambers et al., 2007; Hayashi et al., 2008; Niwa et al., 2009; Toyooka et al., 2008; van den Berg et al., 2008). Therefore, there was a need to develop alternative culture conditions that could allow these limitations to be overcome. Serum-free culture of ESCs was made possible by combining BMP4 and LIF (Ying et al., 2003). Even though this finding provided a defined culture condition, neither maintenance of homogeneous cultures nor derivation of ESCs from different mouse strains were achieved.

Differentiation of ESCs involves activation of MAPK/ERK pathway in an autocrine manner via FGF4 (Kunath et al., 2007; Stavridis et al., 2007). Although BMP and LIF suppress differentiation, they do not block the activation of MAPK/ERK pathway. Therefore,

ways of suppressing this signalling pathway were investigated. Propagation of ESCs without BMP or LIF was achieved by combining selective inhibitors of both MEK/ERK and GSK3 pathways, PD0325901 and CH99021 respectively (Ying et al., 2008). These two small-molecule inhibitors are now widely used to culture ESCs in defined serum-free medium (N2B27) and this culture system is known as 2i medium. Inhibition of MEK/ERK signalling pathway blocks ESC differentiation into all three lineages (Kunath et al., 2007), whereas GSK3 inhibition promotes self-renewal, mainly through activation of canonical Wnt/β-catenin signalling, which leads to the inhibition of the transcriptional repressor TFC3, therefore abrogating its inhibitory effect on the pluripotency network (Shy et al., 2013; Wray et al., 2011; Yi et al., 2011).

2i together with LIF (2i/LIF, 2iL) yields an optimal culture of naïve ESCs. ESCs in 2iL form compact, dome-shaped colonies, morphologically distinct from SL ESCs. Importantly, 2iL medium eliminates the heterogeneity and spontaneous differentiation characteristic of ESCs maintained in SL and maximises the efficiency of ESC clonal expansion (Wray et al., 2011; Wray et al., 2010). Unlike in pairwise combinations, provision of all three 2iL components fully suppresses lineage marker expression and differentiation biases (Hackett et al., 2017). Moreover, 2iL culture conditions allowed the derivation of stable ESCs from mice with different genetic backgrounds (Kiyonari et al., 2010; Nichols et al., 2009) and also from the rat (Buehr et al., 2008; Li et al., 2008) demonstrating that ESC derivation is not an artefact of the 129 mouse strain. Finally, the efficiency of molecular reprogramming of mouse somatic cells into induced pluripotent stem cells (iPSCs) (Takahashi and Yamanaka, 2006) is improved by 2iL (Silva et al., 2008).

1.2.1.2 Transcriptional and epigenetic profiles

The core circuitry of the pluripotency gene regulatory network consists of three transcription factors: OCT4, SOX2 and NANOG (Li and Izpisua Belmonte, 2018; Ng and Surani, 2011; Young, 2011). OCT4, also known as POU5F1, belongs to the Pit-Oct-Unc (POU) family of transcription factors. *Oct4* expression starts very early during mouse embryonic development and, at E4.5, it is highly expressed in the naïve epiblast and is also detected in the primitive endoderm layer (Nichols et al., 1998; Rosner et al., 1990; Yeom et al., 1996). *In vitro*, *Oct4* is essential for the maintenance of pluripotency in a dose-dependent manner. Deletion of *Oct4* leads to trophectoderm differentiation, whereas its overexpression induces differentiation into a mixture of lineages (Niwa et al., 2000). Both in ESCs and in the E4.5 embryo, *Oct4* expression is regulated by its distal enhancer element (Yeom et al., 1996). Furthermore, OCT4 is widely used as one of the components of the transcription factor cocktails used to generate iPSCs (Li and Izpisua Belmonte, 2016; Takahashi and Yamanaka, 2016). *Sox2* is a

SRY-related HMG box transcription factor. SOX2 and OCT4 form heterodimers and act synergistically in the regulation of several downstream targets, including *Sox2* and *Oct4* themselves as well as *Nanog* (Chew et al., 2005; Kuroda et al., 2005; Nakatake et al., 2006; Nishimoto et al., 1999; Rodda et al., 2005; Tokuzawa et al., 2003; Tomioka et al., 2002; Yuan et al., 1995). At E4.5, SOX2 expression is confined to the naïve epiblast (Avilion et al., 2003). Similarly to *Oct4*, *Sox2* is essential for pluripotency maintenance and its abrogation in ESCs induces differentiation towards trophectoderm lineage (Masui et al., 2007). NANOG is a homeodomain-containing transcription factor. *In vivo*, its expression is heterogeneous in the ICM at E3.5, but becomes homogeneous and exclusive to the epiblast at E4.25 (Chambers et al., 2003; Silva et al., 2009). *Nanog* is required for the formation of the naïve pluripotent epiblast (Mitsui et al., 2003; Silva et al., 2009), even though *Nanog*-null ESCs can be generated *in vitro* (Chambers et al., 2007).

In addition to the core pluripotency factors, ESCs express a set of transcriptions factors that are characteristic of the pre-implantation epiblast but are downregulated in the primed epiblast. *Esrrb*, *Tfcp2l1*, *Klf2*, *Klf4*, *Gbx2* and *Tbx3* are among those factors and have all been demonstrated to play a role in functionally maintaining ESC self-renewal (Ivanova et al., 2006; Martello et al., 2013; Martello et al., 2012; Niwa et al., 2009; Tai and Ying, 2013; Ye et al., 2013). Furthermore, they are all part of a highly interconnected network (Dunn et al., 2014; Martello and Smith, 2014).

Notably, ESCs cultured in SL or 2i display distinct transcriptome profiles. SL ESCs exhibit greater heterogeneity in expression of pluripotency factors and increased expression levels of lineage markers (Marks et al., 2012). Moreover, ESCs in 2iL more closely resemble the transcriptome profile of the pre-implantation epiblast from which they are derived (Boroviak et al., 2014).

The nPSC state is characterised by an open chromatin structure that allows transcriptional programmes to switch rapidly during lineage allocation (Meshorer and Misteli, 2006). This means that ESC chromatin is less condensed (Efroni et al., 2008) and exhibits fewer heterochromatin foci (Park et al., 2004) than somatic cells. Importantly, the mouse pre-implantation epiblast shares the same open chromatin conformation as ESCs (Ahmed et al., 2010). Global DNA hypomethylation is also an epigenetic feature of the naïve epiblast (Smith et al., 2012). Although DNA methylation in SL ESCs is comparable to somatic cells, ESCs maintained in 2iL exhibit DNA methylation levels similar to the pre-implantation epiblast (Ficz et al., 2013; Habibi et al., 2013; Leitch et al., 2013).

As previously mentioned, the presence of two Xa in females is another epigenetic hallmark shared between ESCs and the naïve pluripotent epiblast (Mak et al., 2004; Okamoto et al., 2004; Silva et al., 2009; Williams et al., 2011). In fact, this characteristic is used as a measure of the true naïve pluripotent nature of ESCs.

1.2.2 Primed pluripotency

1.2.2.1 Derivation and culture of epiblast stem cells

EpiSCs can be derived from the post-implantation epiblast from E5.5 until E7.5 (Brons et al., 2007; Osorno et al., 2012; Tesar et al., 2007) and are routinely maintained in N2B27 medium supplemented with FGF2 and Activin A (FA) (Brons et al., 2007; Tesar et al., 2007). Notably, the culture conditions applied to derive EpiSCs are essentially the same as those used for propagating human ESCs (Thomson et al., 1998). Even though human ESCs are derived from pre-implantation embryos, they share more features with mouse EpiSCs than mouse ESCs (Bates and Silva, 2017).

EpiSCs are morphologically distinct from ESCs, presenting a flattened epithelial morphology. ESCs can be differentiated *in vitro* into cells resembling EpiSCs by prolonged culture in EpiSC culture conditions (Guo et al., 2009; Tosolini and Jouneau, 2016). Importantly, ESC-derived EpiSCs are transcriptionally similar to EpiSC lines derived from embryos (Hayashi et al., 2011). Conversely, embryo-derived EpiSCs can be reprogrammed to naïve pluripotency by transfection with just a single factor, such as *Klf4*, together with a switch to 2iL culture conditions (Guo et al., 2009).

EpiSCs are heterogeneous within and among cell lines. This heterogeneity can be reduced to some extent through inhibition of WNT stimulation (Kim et al., 2013; Kurek et al., 2015; Sugimoto et al., 2015; Sumi et al., 2013). XAV 939 is a tankyrase inhibitor that can be added to the EpiSC culture resulting in suppression of canonical WNT signalling pathway and consequent increased EpiSC homogeneity (Huang et al., 2009; Sumi et al., 2013).

Contrary to ESCs, EpiSCs contribute poorly to chimeras when injected into E3.5 embryos (Brons et al., 2007; Tesar et al., 2007). However, when introduced into post-implantation embryos up to E8.5, they are able to integrate and contribute to development, which indicates functional equivalence between EpiSCs and post-implantation epiblast cells from the embryo (Huang et al., 2012).

1.2.2.2 Transcriptional and epigenetic profiles

EpiSCs also express the core pluripotency factors, *Oct4*, *Sox2* and *Nanog*, although they have gene expression and epigenetic patterns that are distinct from ESCs (Nichols and Smith, 2009). In EpiSCs, *Oct4* expression is controlled via its proximal enhancer (Yeom et al., 1996) and *Nanog* expression is decreased in comparison to ESCs (Gillich et al., 2012; Guo et al., 2009; Han et al., 2010). Consistent with *in vivo* development, expression of naïve state markers, such as *Rex1*, *Stella*, *Nr0b1*, *Gbx2* and *Klf4*, is reduced or not detected in

EpiSCs, while the early post-implantation epiblast markers *Fgf5*, *Otx2* and *Oct6* are expressed (Brons et al., 2007; Tesar et al., 2007).

Compared to 2iL ESCs, EpiSCs exhibit a more closed chromatin conformation (Hassan-Zadeh et al., 2017) and higher levels of DNA methylation (Auclair et al., 2014; Hackett et al., 2013; Veillard et al., 2014; Zylicz et al., 2015).

Finally, random inactivation of one of the X-chromosomes occurs shortly after implantation in female epiblast cells and, correspondingly, female EpiSCs harbour one Xi (Bao et al., 2009; Guo et al., 2009).

1.3 Pluripotency and the status of X-chromosome

The fact that XCI is absolutely required for proper development of the mouse embryo, makes the presence of two Xa in female naïve pluripotent cells a striking feature. A link between XCI and cell differentiation has long been established and was first described based on biochemical analysis of X-linked enzymatic activities in early mouse embryonic stages (Monk and Harper, 1979). Cell culture studies corroborated this finding through observation of XCI during differentiation of both ECCs and ESCs (Martin et al., 1978; Rastan and Robertson, 1985). The idea that XCI is coupled with cell differentiation was further reinforced by reprogramming experiments. Regardless of the method employed, reprogramming to the naïve pluripotent state is accompanied by reactivation of the X-chromosome and the resulting iPSCs display two Xa (Eggan et al., 2000; Maherali et al., 2007; Silva et al., 2009; Tada et al., 2001; Takagi et al., 1983). Remarkably, a study describing the sequence of epigenetic events of X-chromosome reactivation (XCR) during iPSC generation has reported that the reactivation of genes on the Xi is tightly correlated with the sequential activation of pluripotency-associated factors (Pasque et al., 2014). It has also been demonstrated that *Nanog* knockdown or *Prdm14* knockout reduces the formation of iPSC colonies that display XCR (Pasque et al., 2014; Payer et al., 2013).

The tight link of differentiation with XCI and acquisition of pluripotency with XCR was suggestive of a regulatory interaction between the pluripotency factor network and the genes at the Xic. Indeed, direct repression of *Xist* was proposed to occur through binding of pluripotency-associated factors OCT4, NANOG, SOX2 and PRDM14 to *Xist* intron 1 (Navarro et al., 2008; Payer et al., 2013). The binding of the pluripotency-associated factors was found to be sharply reduced in differentiating ESCs and undetectable in fully differentiated mouse embryonic fibroblasts (Navarro et al., 2008). Moreover, downregulation of *Oct4* and *Nanog* was found to induce moderate upregulation of *Xist* in male ESCs (Navarro et al., 2008) and the same effect was observed when the pluripotency factor binding site in *Xist* intron 1 was deleted in ESCs (Barakat et al., 2011; Nesterova et al.,

2011). However, another study reported that deletion of intron 1 region both in ESCs and in mice did not impact *Xist* expression or XCI (Minkovsky et al., 2013), suggesting that there might be other elements ensuring that *Xist* is repressed in the context of naïve pluripotency. Therefore, it seems that *Xist* intron 1 is not required or that this region acts redundantly with other elements in the Xic. Furthermore, *Xist* was proposed to be directly repressed by REX1, which binds to the *Xist* promoter in ESCs and which is degraded during differentiation by the ubiquitin ligase RNF12 (Gontan et al., 2012). The *Xist* activator RNF12 is also bound by the pluripotency factors NANOG, OCT4, SOX2, KLF4 and PRDM14 (Navarro et al., 2011; Payer et al., 2013). PRDM14 was demonstrated to recruit PRC2 to repress *Rnf12* in ESCs (Payer et al., 2013). *Tsix* also seems to be directly regulated by the naïve pluripotency network as shown by the stimulating effect that OCT4, REX1, KLF4 and c-MYC have on *Tsix* transcription through binding to the *DXPas34* mini-satellite enhancer region associated with the *Tsix* promoter (Donohoe et al., 2009; Navarro et al., 2010).

A further link between differentiation and XCI came from the finding that female ESCs with two Xa show a lower propensity for differentiation when compared to XY or XO ESCs, and that this can be overcome by inducing XCI (Schulz et al., 2014). Transcriptome analyses revealed that the two Xa stabilize the naïve pluripotent state via inhibition of the MAPK and GSK3 signalling pathways (Schulz et al., 2014). The authors suggested that this provides a likely explanation for the observation that in certain mammalian species female embryos develop more slowly than males. This suggests that the two Xa in epiblast cells of the pre-implantation embryo interfere with differentiation, thus ensuring that development does not proceed without dosage compensation.

1.4 Scope of the study

In this study, I aimed to elucidate the relationship between naïve pluripotency and random XCI, using 2iL-cultured ESCs as the *in vitro* counterpart of the relevant developmental stage.

Most studies investigating XCI have been performed using ESCs cultured in SL conditions which are known to be suboptimal (Chambers et al., 2007; Ficz et al., 2013; Habibi et al., 2013; Leitch et al., 2013; Marks et al., 2012; Martello and Smith, 2014). 2iL-cultured ESCs display transcriptional and epigenetic signatures that resemble that of the naïve epiblast (Boroviak et al., 2014; Ficz et al., 2013; Hackett et al., 2017), meaning that they represent the cellular state of relevance for random XCI. According to the prevailing paradigm, ESCs express *Xist* at low levels, and after induction of differentiation, females upregulate *Xist* whereas males display repression of *Xist* (Sheardown et al., 1997).

In Chapter 3, I evaluated the levels of *Xist* in 2iL-cutured ESCs. Using both male and female 2iL-cultured ESCs as a model system, I explored the effect on *Xist* expression following the ablation of key components of the naïve pluripotency network. The experiments revealed that *Xist* is indeed not expressed in ESCs cultured in 2iL and that *Xist* expression is highly upregulated in the presence of a compromised naïve network, not only in females but also in males. These results prompted me to revisit the kinetics of *Xist* expression during male nPSC differentiation. In Chapter 4, I demonstrated that *Xist* is transiently and rapidly upregulated in early differentiating male cells. The data presented here indicate that downregulation of the naïve transcription factor network leads to upregulation of *Xist* and that this is independent of the gender. In Chapter 5, I characterised the nuclear pattern of *Xist* both *in vitro* and *in vivo* at different stages of embryonic development. I observed that early differentiating nPSCs accumulate *Xist* on the single male X-chromosome and on both female X-chromosomes, and that this is accompanied by appearance of a repressive chromatin signature and partial X-linked gene silencing. In the embryo, *Xist* is transiently expressed in males from the single X-chromosome and in females from both X-chromosomes at the onset of naïve epiblast differentiation. Altogether, these findings demonstrate that XCI initiation is gender-independent and is triggered by weakening of the naïve pluripotency network.

Chapter 2
Materials and methods

2.1 Cell culture

2.1.1 Cell lines

Male wild-type ESC lines included E14tg2a and EFC. Female wild-type ESC lines included LF1, LF2 and C6. The cell sorting experiment was performed in male *Nanog*-GFP ESCs. Female *Nanog*-GFP EpiSCs were used as control in *Xist* RNA FISH. Nanog deletion was performed in male and female *Nanog*$^{flox/-}$, *Rosa26*$^{CreERT2/+}$ ESC lines. *Oct4* deletion was performed in male and female *Oct4*$^{flox/-}$, *Rosa26*$^{CreERT2/+}$ ESC lines. The male iPSC line used was derived from *Rex1*-dGFP NSCs. Reprogramming was performed in male *Rex1*-dGFP EpiSCs.

2.1.2 Culture media

Mouse ESCs and iPSCs were cultured in 2iL, 2i, or SL as indicated. 2iL medium was composed of N2B27, 3 μM CHIR99021, 1 μM PD0325901 (Stewart lab, Dresden), and 20 ng ml^{-1} of murine LIF (Hyvonen lab, Cambridge). N2B27 medium comprised 1:1 DMEM/F-12 and Neurobasal (ThermoFisher Scientific), 2 mM L-glutamine (ThermoFisher Scientific), 1X penicillin-streptomycin (Sigma-Aldrich), 0.1 mM 2-mercaptoethanol (ThermoFisher Scientific), 1% B27 (ThermoFisher Scientific) and 0.5% N2 (Stem Cell Institute, University of Cambridge). SL medium contained GMEM (Sigma-Aldrich), 10% FBS (Labtech), 1X NEAA (ThermoFisher Scientific), 1 mM sodium pyruvate (Sigma-Aldrich), 2 mM L-glutamine, 1X penicillin-streptomycin, 0.1 mM 2-mercaptoethanol and 20 ng ml^{-1} of LIF. EpiSCs were cultured in FAX medium composed of N2B27 supplemented with 12.5 ng ml^{-1} Fgf2, 20 ng ml^{-1} Activin A (Hyvonen lab, Cambridge) and 6.25 μg ml^{-1} XAV 939 (Bio-Techne). NSCs

were maintained in DMEM/F-12, 1x NEAA, 0.1 mM 2-mercaptoethanol, 1X penicillin-streptomycin, 1% B27, 0.5% N2, 4.5 µM HEPES (ThermoFisher Scientific), 0.03 M glucose (Sigma-Aldrich), 120 µg ml^{-1} BSA (ThermoFisher Scientific),10 ng ml^{-1} Egf (Peprotech) and 20 ng ml^{-1} Fgf2 (Department of Biochemistry, University of Cambridge). 4-OHT (Sigma-Aldrich) was used at a concentration of 500 nM and InSolution JAKi I (Merck Millipore) at a concentration of 1 µM. During expansion of $Nanog^{flox/-}$ cell lines, selection with 200 µg ml^{-1} G418 (ThermoFisher Scientific) was applied to select for pluripotent cells based on Nanog promoter activity at the null allele.

2.1.3 Routine cell culture manipulations

All cell lines were cultured in a humidified incubator at 37 °C and 7% CO_2. ESCs and iPSCs were cultured on plastic pre-coated with 0.1% gelatin (Sigma-Aldrich) in PBS (Sigma-Aldrich). EpiSCs were cultured on plastic pre-coated with 10 µg ml^{-1} fibronectin (Merck Millipore) in PBS (Sigma-Aldrich). NSCs were cultured on plastic pre-coated with 10 µg ml^{-1} laminin (Sigma-Aldrich) in PBS (Sigma-Aldrich). PLAT-E cells were cultured on plastic without additional substrate. For passaging, cells were dissociated with TrypLE Express (ThermoFisher Scientific) if they were cultured in serum-containing medium or accutase (PAA Laboratories) if they were cultured in serum-free medium. After dissociation cells were centrifuged at 0.5 g for 3 minutes to remove the dissociating agent and replated at a required density in fresh media. All cell types were frozen in 10% DMSO (Santa Cruz Biotechnology) in serum-containing medium in a -80 ºC freezer. After 2 to 30 days, cryovials were transferred to a liquid nitrogen tank.

2.1.4 Cell differentiation

For embryoid body differentiation, 1.5 x 10^6 cells were plated on 10 cm low-attachment dishes in serum-containing medium without LIF. For differentiation in adherent monolayer culture, 6 x 10^5 cells were plated on gelatin-coated 10 cm dishes in serum-free (N2B27) or N2B27 supplemented with FA. SL-derived ESCs (E14tg2a, EFC, LF1 and LF2) were not passaged more than 3 times in 2iL prior to the differentiation assays.

2.1.5 NSC reprogramming

Retroviruses were produced by transfection of PLAT-E cells with pMXs-Klf4 and pMXs-cMyc plasmids (Addgene) using FuGENE 6 (Roche) according to manufacturer's instructions. On day 2, virus-containing supernatants were filtered through 0.45 µm cellulose acetate filters

and mixed with Polybrene (Sigma-Aldrich) to a final concentration of 4 µg ml^{-1}. Polybrene/virus mixture was applied to NSCs for 24 hours. Medium was switched to SL to generate reprogramming intermediates, followed by 2iL to obtain iPSCs.

2.1.6 EpiSC reprogramming

Embryo-derived male EpiSCs with *Rex1*-dGFP reporter (Kalkan et al., 2017) were used that constitutively express the GY118F receptor transgene (Burdon et al., 1999), known to drive EpiSC reprogramming via STAT3 activation (van Oosten et al., 2012; Yang et al., 2010). For reprogramming, EpiSCs were plated at 10,000 cells per fibronectin-coated 6-well in FAX maintenance medium. The following day, reprogramming was induced by medium change to 2iL supplemented with 30 ng ml^{-1} human GCSF (Peprotech). On days 2, 3, 4, 5 and 6, multiple reprogramming wells were harvested using accutase, stained with DAPI (Sigma-Aldrich) to eliminate nonviable cells, and sorted by flow cytometry to isolate the *Rex1*-dGFP-positive subpopulation for further analysis. Parental EpiSCs and male *Rex1*-dGFP ESCs were used as negative and positive gating controls respectively.

2.2 ESC derivation

$Nanog^{flox/flox}$, $Rosa26^{CreERT2/CreERT2}$ mice were crossed with $Nanog^{+/-}$ and ESCs were derived from resultant E4.5 embryos. Embryos were removed from the uteri and plated on gelatin-coated plates in 2iL medium. After 5-7 days of culture, the explants were passaged with accutase (PAA Laboratories) to a fresh plate.

2.3 NSC derivation

For derivation of *Rex1*-dGFP NSCs, brains of E13.5 embryos were dissected and mechanically dissociated by resuspending in NSC medium. Obtained single-cell suspension was plated onto laminin-coated cell culture dishes.

2.4 RNA isolation, cDNA synthesis and qRT-PCR

Total RNA was isolated from cells using the RNeasy mini kit (Qiagen) with DNAse treatment (Qiagen) in accordance with the manufacturer's protocol. After purification, 1 µg of total RNA was reverse-transcribed using SuperScript III First-Strand Synthesis SuperMix (ThermoFisher Scientific). Reverse Transcription Quantitative Real-Time PCR (qRT-PCR)

reactions were set up in triplicate using TaqMan Universal PCR Master Mix (ThermoFisher Scientific) and TaqMan gene expression assays (ThermoFisher Scientific) (Table 2.1). qRT-PCR experiments were performed in mircoAmp qPCR plates (ThermoFisher Scientific) on a StepOnePlus Real-Time PCR System (ThermoFisher Scientific). Each well contained 5 µL of cDNA, 6 µL TaqMan Fast Universal MasterMix (ThermoFisher Scientific), 0.6 µL VIC-labelled *Gapdh* probe for normalisation and 0.6 µL FAM-labelled probe of interest. Delta Ct (ΔCt) values compared to *Gapdh* were calculated and relative quantities calculated as 2 to the power of -ΔCt. The means of three values were calculated and normalised as indicated.

Table 2.1 TaqMan qRT-PCR standard assays used in the study.

Gene	Probe ID
Gapdh	4352339E
Esrrb	Mm00442411_m1
Ftx	Mm03455830_m1
Klf2	Mm01244979_g1
Klf4	Mm00516104_m1
Klf5	Mm00456521_m1
Nanog	Mm02384862_g1
Nexmif	Mm01239465_g1
Oct4	Mm00658129_gH
Rex1	Mm03053975_g1
Rnf12	Mm00488044_m1
Socs3	Mm01249143_g1
Sox2	Mm03053810_s1
Tfcp2l1	Mm00470119_m1
Xist	Mm01232884_m1

2.5 Flow cytometry

Nanog-GFP ESCs were resuspended in PBS containing 3.5% BSA (ThermoFisher Scientific) and sorting was performed using a MoFlo high-speed cell sorter (Beckman Coulter). A 514/10BP filter was used for GFP and a 580/30BP filter was used for autofluorescence. *Rex1*-dGFP positive reprogramming intermediates were sorted using a BD Influx 5 cell sorter (BD Biosciences). A 460/50 filter was used for DAPI and a 530/40 filter was used for GFP.

2.6 DNA extraction

In the case of the cell lines, DNA was isolated using the DNeasy Blood & Tissue Kit (Qiagen) in accordance with the manufacturer's protocol. In the case of the embryos, these were collected from the slides after RNA FISH and imaging and then lysed in 0.2% Triton X-100 and Proteinase K at 56 ˚C for 10 minutes followed by 95 ˚C for 15 minutes.

2.7 Genotyping PCR

To determine whether ESCs were *Nanog*$^{flox/-}$ or *Nanog*$^{flox/+}$, genotyping PCR was conducted in a final volume of 15 µL with 100 ng of DNA, 1X CoralLoad buffer, 0.2 mM dNTPs, 0.2 µM primers and 0.75 units Taq DNA Polymerase (Qiagen) per reaction and run on a thermal cycler with the following conditions: 94 ˚C for 5 minutes, 35 cycles of 94 ˚C for 10 seconds, 60 ˚C for 20 seconds, and 72˚ C for 60 seconds, followed by 72 ˚C for 3 minutes. An equal mix of 3 primers was used: βgeo, S5, and A53 (Table 2.2). An 800 bp product is amplified from Flox and wild-type Nanog alleles, whereas the βgeo allele yields a 600 bp product. Products were electrophoresed on 2% agarose gel stained with 1:25,000 Midori Green (Nippon Genetics). The gel was run at 120 V using a Bio-Rad gel tank and bands were visualised using a UV light cabinet and GeneSnap software.

2.8 Gender PCR

Cell lines were sexed by PCR using primers Ube1XA and Ube1XB (Table 2.2) that results in two products of 217 bp and 198 bp from the Ube1x and Ube1y genes on the X- and Y-chromosome respectively (Chuma and Nakatsuji, 2001). PCR reactions were performed in a final volume of 20 µL with 100 ng of DNA, 1X CoralLoad buffer, 0.2 mM dNTPs, 0.35 µM primers and 0.5 units Taq DNA Polymerase (Qiagen) per reaction and run on a thermal cycler with the following conditions: 94 ˚C for 3 minutes, 30 cycles of 94 ˚C for 30 seconds, 66 ˚C for 30 seconds, and 72˚ C for 30 seconds, followed by 72 ˚C for 10 minutes. In the

case of the embryos, 4 µL per embryo lysate were added to the PCR reaction. Products were electrophoresed on 2% agarose gel stained with 1:25,000 Midori Green (Nippon Genetics). The gel was run at 120 V using a Bio-Rad gel tank and bands were visualised using a UV light cabinet and GeneSnap software.

Table 2.2 Primers used in this study.

Primer ID	Sequence
βgeo	5'-AATGGGCTGACCGCTTCCTC-3'
S5	5'-ACCTCAGCCTCCAGCAGATG-3'
A53	5'-CAGAATGCAGACAGGTCTACAGCCCG-3'
Ube1XA	5'-TGGTCTGGACCCAAACGCTGTCCACA-3'
Ube1XB	5'- GGCAGCAGCCATCACATAATCCAGATG-3'

2.9 Western blot

Dissociated cells were washed in PBS and resuspended in RIPA buffer containing 0.1% SDS, 1% Triton X-100, 1 mM EDTA, 1X Complete mini protease inhibitors (Roche) and 1X PhosSTOP phosphatase-inhibitors (Roche) in PBS. The suspension was incubated on ice for 30 minutes and then sonicated with a Bioruptor200 sonicator (Diagenode) at high frequency for 3 minutes with alternating cycles of 30 seconds on and 30 sec off.

Proteins were denatured by boiling for 10 minutes at 90 °C in 1X Bolt LDS sample buffer (ThermoFisher Scientific) with Bolt reducing agent (ThermoFisher Scientific). Denatured proteins were loaded onto a Bolt 10% Bis-Tris Plus gels (ThermoFisher Scientific) and SDS-PAGE electrophoresis was carried out by the application of 165 V at constant voltage in a Novex MiniCell (ThermoFisher Scientific) with 1X Bolt MOPS SDS running buffer (ThermoFisher Scientific).

Protein transfer was performed using iBlot 2 dry blotting system (ThermoFisher Scientific) and iBlot Transfer Stacks (ThermoFisher Scientific) in accordance with the manufacturer's protocol. The membrane was blocked for 1 hour in 5% skim milk (Sigma-Aldrich) in 0.1% Tween 20/PBS. Primary antibody (Table 2.3) was diluted in 5% skim milk (Sigma-Aldrich) in 0.1% Tween 20/PBS and applied overnight at 4 °C. The membrane was washed three times in 0.1% Tween 20/PBS. In the case of p-Y705-STAT3, antibody dilutions were performed in 5% BSA (Sigma-Aldrich) in 0.1% Tween 20/TBS and washed in 0.1% Tween 20/TBS.

Table 2.3: Primary antibodies used for western blot.

Against	Species	Clonality	Dilution	Cat number	Company
α-TUBULIN	mouse	monoclonal	1:5,000	AB7291	Abcam
NANOG	rabbit	polyclonal	1:5,000	A300-397A	Bethyl Laboratories
p-Y705-STAT3	rabbit	monoclonal	1:1,000	9145	Cell Signalling Technology
OCT4	goat	polyclonal	1:1,000	SC-8628	Santa Cruz Biotechnology
RNF12	rabbit	polyclonal	1:1,000	ABE1949	Merck Millipore

Horseradish peroxidase (HRP)-conjugated secondary antibodies (Table 2.4) were diluted at a concentration of 1:10,000 in 5% skim milk in 0.1% Tween 20/PBS and then applied for 1 hour at room temperature. The membrane was washed three times in 0.1% Tween 20/PBS and once in PBS before being treated with ECL Plus Western Blotting Detection System (GE Healthcare) and used to expose photographic film in a darkroom.

Table 2.4: Secondary antibodies used for western blot.

Against	Species	Cat number	Company
Mouse	sheep	NA931	GE Healthcare
Rabbit	donkey	NA934	GE Healthcare
Goat	donkey	sc-2020	Santa Cruz Biotechnology

2.10 RNA FISH with double-strand probe

Cells were plated on SuperFrost Plus Adhesion slides (ThermoFisher Scientific) and permeabilised in cytoskeletal buffer (100 mM NaCl, 300 mM sucrose, 3 mM MgCl2, 10 mM PIPES) containing 0.5% Triton X-100 (Sigma-Aldrich), 1 mM EGTA pH 8 and vanadyl ribonucleoside (New England Biolabs) for 5 minutes on ice. They were subsequently fixed in 4% paraformaldehyde (Sigma-Aldrich) for 10 minutes, briefly washed in 1X PBS and dehydrated through 70%, 80%, 95% and 100% ethanol, after which the slides were air-dried. At this stage, a denatured *Xist* probe was applied onto the slides and these were incubated overnight at 37 °C.

The probe was prepared by labelling plasmid DNA containing a mouse *Xist* exon 1 fragment sequence (provided by Professor Neil Brockdorff, University of Oxford, UK) with a

biotin-nick translation mix (Roche) according to manufacturer's instructions. Non-incorporated nucleotides were removed using with an S-300HR Illustra microspin column (GE Healthcare). To 20 ng of probe, 10 µg of sheared salmon sperm DNA (Ambion) and 3 µg of mouse Cot-1 DNA (ThermoFisher Scientific) were added. Finally, the probe was dehydrated by vacuum and resuspended in deionized formamide (VWR). Before applying onto the slide, the probe was denatured at 80 °C and 2X hybridization buffer (4X SSC, 20% dextran sulphate, 2 mg ml^{-1} BSA, 2 mM vanadyl ribonucleoside) was added.

The following day, the slides were washed at 42 °C in 2X SSC/50% formamide for 15 minutes, then three times in 2X SSC for 5 minutes each. They were then transferred to 4X SSC/0.1% Tween 20 at room temperature and blocked in 4 mg ml^{-1} BSA in 4X SSC/0.1%Tween 20 at 37 °C for 30 minutes. Probe detection was performed by first applying Avidin conjugated to Texas Red (1:500, Vector Laboratories), then a biotinylated anti-avidin antibody (1:200, Vector Laboratories), followed by a second layer of Avidin-Texas Red. All detection reagents were diluted in 4 mg ml^{-1} BSA in 4X SSC/0.1%Tween 20 and incubated at 37 °C for 30 minutes followed by three washes in 4X SSC/0.1% Tween20 in between each step. Finally, the slides were mounted in Vectashield Mounting Medium containing DAPI (Vector Laboratories).

2.11 RNA FISH with single-strand probe

RNA FISH protocol was modified from the Stellaris (Biosearch Technologies) protocol for adherent mammalian cells. Cells were plated on SuperFrost Plus Adhesion slides (ThermoFisher Scientific) and fixed in 4% PFA (Sigma-Aldrich) at room temperature for 10 minutes. They were subsequently washed in 1X PBS and permeabilised in cytoskeletal buffer (100 mM NaCl, 300 mM sucrose, 3 mM MgCl2, 10 mM PIPES) containing 0.5% Triton X-100, 1 mM EGTA pH 8 and vanadyl ribonucleoside (New England Biolabs) for 5 minutes on ice. Following washing in 1X PBS, they were incubated in 70% ethanol at 4 °C overnight. Cells were incubated in 10% formamide (VWR) in 2X SSC (Sigma-Aldrich) for 10 minutes and then overnight in 250 nM Stellaris Probes diluted in 100 mg mL^{-1} dextran sulfate (MP Biomedicals) and 10% formamide in 2X SSC at 37 °C. *Xist* was recognised using Stellaris FISH Probes labelled with either Quasar 570 or Quasar 670 (BioSearch Technologies). *Rnf12*, *Nexmif*, *Huwe1*, *Nsdhl* and *Wbp5* were recognised using Custom Stellaris FISH Probes labelled with Quasar 570 (BioSearch Technologies). The sequences of 48 oligonucleotides were designed against unique intronic sequences using the online Stellaris Probe Designer tool (BioSearch Technologies). The *Rnf12* and *Huwe1* probes sequences were kindly provided by Prof. Neil Brockdorff and Dr. Tatyana Nesterova (University of Oxford, UK). After hybridisation, cells were incubated in 10% formamide in 2X

SSC at 37 °C for 30 minutes followed by a wash in 2X SSC at room temperature for 5 minutes. Cells were mounted with Vectashield Antifade Mounting Medium with DAPI (Vector Laboratories).

2.12 RNA FISH on mouse embryos

Mouse embryos were collected from CD1 mice and fixed in 4% paraformaldehyde at room temperature for 15 minutes. Embryos were further processed for RNA FISH using Stellaris probes (BioSearch Technologies) according to the procedure described above.

2.13 Immunofluorescence

Immunofluorescence was always performed in combination with RNA FISH using Stellaris probes. Sequential immunofluorescence and RNA FISH protocol was modified from the Stellaris (BioSearch Technologies) protocol for adherent mammalian cells. Cells were fixed and permeabilised as for RNA FISH only. They were then washed in 1X PBS and incubated with primary antibody (Table 2.5) diluted in 1X PBS at 37 °C for 2 hours. Following washing three times in 1X PBS, cells were incubated with secondary antibody (Table 2.6) diluted at 1:5,000 in 1X PBS at 37 °C for 1 hour. An appropriate Alexa Fluor conjugated secondary antibody (ThermoFisher Scientific) was used. Cells were then washed three times in 1X PBS and fixed again in 4% PFA at room temperature for 10 minutes. Following washing with 1X PBS, RNA FISH protocol was carried out as described above, starting from the incubation in 10% formamide in 2X SSC.

Table 2.5: Primary antobodies used for immunofluorescence.

Against	Species	Clonality	Dilution	Cat number	Company
H3K27me3	rabbit	polyclonal	1:500	07-449	Merck Millipore
H3K27ac	rabbit	polyclonal	1:500	ab4729	Abcam
NANOG	rat	monoclonal	1:300	14-5761-80	ThermoFisher Scientific
OCT4	rabbit	monoclonal	1:300	83932	Cell Signalling Technology
Cleaved CASPASE-3	rabbit	monoclonal	1:100	9664	Cell Signalling Technology

Table 2.6: Secondary antibodies used for immunofluorescence.

Against	Species	Wavelength	Cat number	Company
Rabbit	Donkey	488 nm	A-21206	ThermoFisher Scientific
Rabbit	Donkey	647 nm	A-31573	ThermoFisher Scientific
Rat	Donkey	488 nm	A-21208	ThermoFisher Scientific

2.14 Metaphase spread

ESCs were plated onto a gelatinised 6-well two days prior preparation of the chromosome spreads. Cultures were then arrested in metaphase by addition of 0.5 µg mL^{-1} KaryoMAX colcemid (ThermoFisher Scientific) and incubation at 37 °C for 3 hours. Cells were then washed in PBS, harvested with accutase and centrifuged at 300 g for 5 minutes. Following aspiration of the supernatant, the pellet was resuspended in 5 mL of 0.075 M KCl solution and incubated at 37 °C for 15 minutes. Then 100 µL of ice cold methanol:glacial acetic acid (3:1) fixative solution were added drop-wise followed by a 10-minute incubation on ice. Following incubation, cells were centrifuged at 300 g for 5 minutes, supernatant was aspirated leaving 500 µL in the tube and 5 mL of fixative solution were added to the cells. After centrifugation, 500 µL of the supernatant were kept in the tube and then spread onto a glass slide. After at least 3 hours at room temperature, the slide was stained or stored at -20 °C for further analysis.

2.15 DNA FISH chromosome painting

Prior to X- and Y-chromosome painting, immunofluorescence was performed in combination with RNA FISH, slides were imaged and x-y coordinates were marked for future reference. After removal of the coverslip, slides were then washed in 2X SSC at room temperature. X- and Y-chromosome painting was also performed on metaphase spreads. Slides were dehydrated through an ice-cold ethanol series (70%, 80%, 95% and 100%) for 3 minutes each and then allowed to air dry. X- and/or Y-chromosome paint probe (Metasystems) was added to the slide, denaturation was carried out at 75 °C for 2 minutes and slides were incubated at 37 ˚C overnight. After hybridisation, slides were incubated in 0.4X SSC at 72 ˚C for 2 minutes followed by a wash with 0.05% Tween 20 in 2X SSC at room temperature for 30 seconds. Slides were rinsed in water, allowed to air dry and mounted with Vectashield Antifade Mounting Medium with DAPI (Vector Laboratories).

2.16 Microscopy and image analysis

Images were taken with an Eclipse Ti Spinning Disk confocal microscope (Nikon) equipped with an Andor Revolution XD System using either 40X or 60X objectives. Images were processed and analysed with ImageJ. Presented images are maximum intensity projections of Z-stack slices. Scoring of RNA FISH signals was done by eye from images.

2.17 RNA-seq

RNA integrity was assessed on a Qubit Fluorometer (ThermoFisher Scientific) and Agilent Bioanalyzer Nano Chips (Agilent Technologies). Depletion of ribosomal RNA was performed on 2-5 µg of total RNA using the Ribo-Zero rRNA Removal Kit (Illumina) and libraries were produced from 10-100ng of ribosomal-depleted RNA using NextFlex Rapid Directional RNA-seq Kit (Bioo Scientific) with 12 cycles of PCR amplification. Libraries were pooled in equimolar quantities and sequenced on the HiSeq4000 platform (Illumina) at CRUK.

2.18 Bioinformatic analysis of RNA-seq

RNA-seq reads were adapter-trimmed with *TrimGalore* (http://www.bioinformatics.babraham.ac.uk/projects/trim_galore) and mapped to the mouse reference genome (GRCm38/mm10) with *TopHat2* (https://ccb.jhu.edu/software/tophat) allowing for one mismatch and alignments guided by Ensembl gene models (Ensembl release 82). Strand-specific read counts were obtained with *featureCounts* (http://b*ioinf.wehi.edu.au/featureCounts)*. Transcript counts were normalised, and the statistical significance of differential expression between samples was assessed using the R Bioconductor *DESeq2* package *(https://bioconductor.org/packages /release/bioc/html/DESeq2.html).* Transcript counts normalised by DESeq2 size factors were subsequently normalised by their length/1000. Principal component analysis (PCA) was performed by singular value composition using the R prcomp() function on scaled expression values.

Chapter 3
Understanding the link between naïve pluripotency and *Xist* status

3.1 Introduction

According to the literature, both female and male SL-cultured ESCs express *Xist* at low levels, which can be detected by RNA FISH as two pinpoint signals in the case of female cells or one in male cells (Panning et al., 1997; Sheardown et al., 1997). As female ESCs differentiate, *Xist* is upregulated monoallelically and coats the inactivating X-chromosome (Panning et al., 1997; Sheardown et al., 1997). This temporal correlation between differentiation and XCI led to the idea that pluripotency factors may play a role in the regulation of this process. Indeed, there have been several reports describing the regulation of *Xist* and other members of the Xic by pluripotency factors (Donohoe et al., 2009; Navarro et al., 2008; Navarro et al., 2011; Navarro et al., 2010; Nesterova et al., 2011; Payer et al., 2013; Silva et al., 2009). However, these studies have largely been conducted *in vitro* and using ESCs cultured in SL conditions, an environment in which repression of any of the naïve pluripotency factors would induce collapse of the naïve network and consequent differentiation. Moreover, SL conditions are known to be suboptimal. SL-cultured ESCs exhibit transcriptional heterogeneity of pluripotency factors (Chambers et al., 2007), increased expression of lineage markers (Marks et al., 2012), reduced strength of the naïve network (Martello and Smith, 2014), and high DNA methylation levels that are comparable to those observed in somatic cells (Ficz et al., 2013; Habibi et al., 2013; Leitch et al., 2013). Remarkably, using defined serum-free 2iL medium these limitations have been overcome (Silva et al., 2008; Silva et al., 2009; Ying et al., 2008). In addition, ESCs cultured in 2iL exhibit transcriptional and epigenetic signatures that resemble that of E4.5 epiblast (Boroviak et al., 2015; Ficz et al., 2013; Hackett et al., 2017). Importantly, this means that, unlike SL

ESCs, 2iL ESCs are the appropriate epigenetic counterpart to the naïve epiblast, the starting identity from which random XCI occurs.

3.1.1 Aims of the chapter

It is unknown whether increased transcriptional homogeneity and naïve pluripotency network robustness have an impact on *Xist* status. Moreover, the effect of the repression of naïve pluripotency factors on *Xist* expression in the context of naïve pluripotency is still unclear. Therefore, I aimed to characterise the status of *Xist* expression in nPSCs and to study the relationship of naïve cell identity and *Xist* status by making use of nPSC culture conditions that increase the strength of the naïve transcriptional network and allow the removal of key components of the naïve network without induction of differentiation.

3.2 Results

3.2.1 Robust nPSC self-renewal abolishes *Xist* expression

To evaluate the impact of increased naïve pluripotency gene expression homogeneity and robustness on the levels of *Xist*, I used two female and two male ESC lines as a model. First, the gender of these cell lines was confirmed by genomic PCR (Figure 3.1A). Additionally, DNA FISH with X- and Y-chromosome painting probes was performed on metaphase spreads of one female and one male ESC line. The male cell line revealed a normal 40, XY karyotype in virtually all cells analysed, whereas the female cell line presented a 40, XX karyotype in a very high proportion of the cells (Figure 3.1B). The four ESC lines, which had been previously derived in SL conditions, were transferred to 2iL conditions and analysed before and after passaging in 2iL (Figure 3.1C). As a consequence of transferring the cells from SL to 2iL, upregulation of naïve pluripotency factors was observed (Figure 3.1D). This is in agreement with previous studies showing that exogenous 2iL signals actively interact with the internal transcription factor network leading to augmented expression of its members (Martello and Smith, 2014).

Concomitantly with the upregulation of naïve pluripotency factors, 2iL conditions led to repression of *Xist* in both male and female ESCs (Figure 3.1D). Remarkably, only one passage in 2iL was required for *Xist* expression to be extinguished.

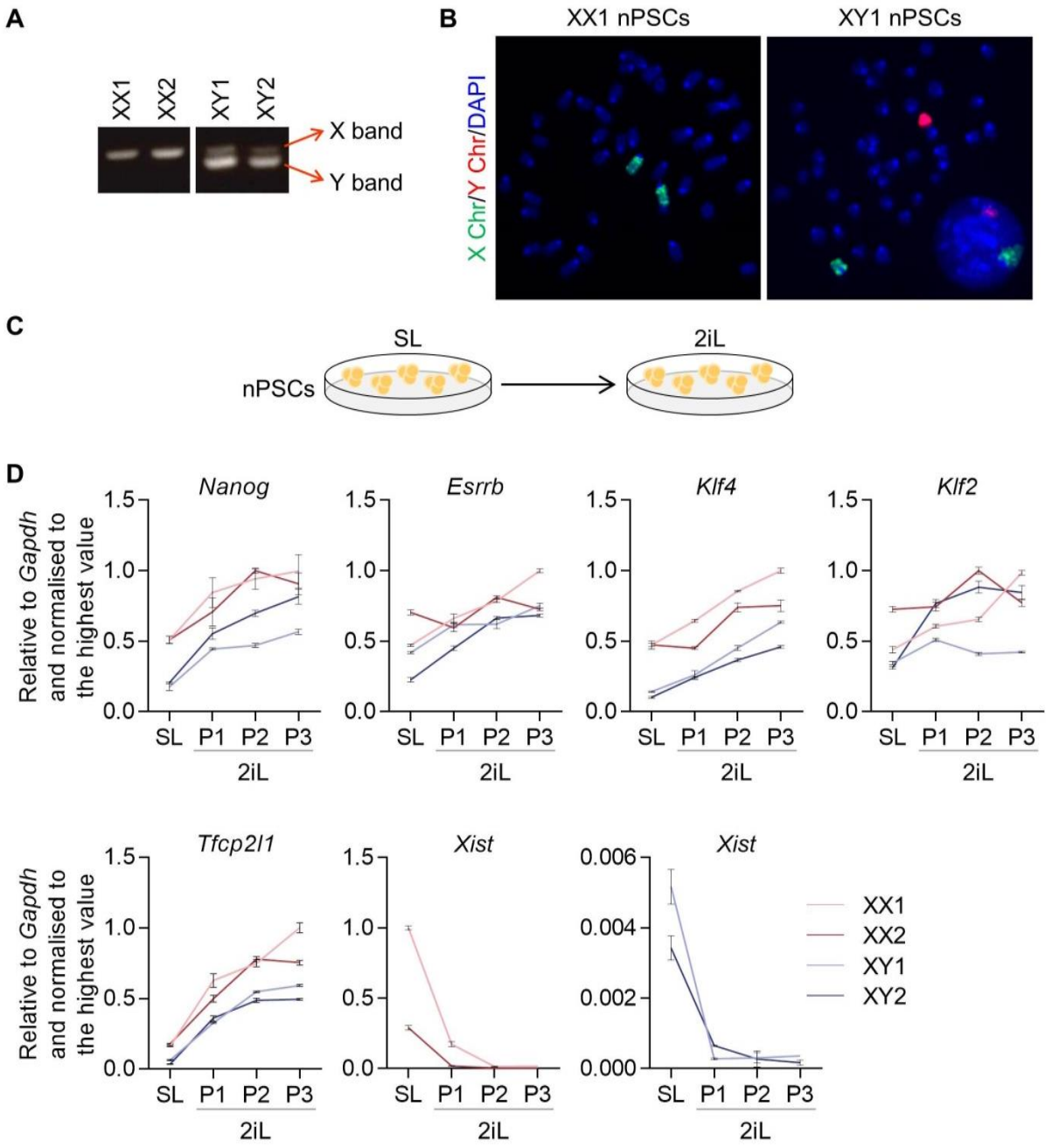

Figure 3.1: *Xist* expression is repressed by a robust naïve pluripotency network.
(A) PCR-based sex determination of the cell lines LF1 (XX1), LF2 (XX2), E14tg2a (XY1), and EFC (XY2).
(B) DNA FISH with X (green) and Y (red) chromosome painting probes of metaphase spreads of the ESC lines XX1 and XY1.
(C) Schematic illustrating the experiment performed to evaluate the impact of the nPSC culture conditions on *Xist* expression.
(D) qRT-PCR analysis of naïve pluripotency factors (*Nanog*, *Esrrb*, *Klf4*, *Klf2*, and *Tfcp2l1*) and *Xist* in XX1, XX2, XY1, and XY2 ESC lines in SL versus 2iL conditions. P indicates the number of passages in 2iL. Data shown are the mean of three technical replicates. Error bars represent ± SD.

ESCs in SL present heterogeneous levels of naïve pluripotency factors (Chambers et al., 2007) rendering these cells a useful tool to study the relationship between naïve network status and *Xist* expression. Male SL ESCs harbouring a *Nanog*-GFP reporter were FACS-sorted into low, medium, and high GFP populations (Figures 3.2A and 3.2B). The correlation between the levels of GFP and *Nanog* expression was confirmed by qRT-PCR (Figure 3.2C). Importantly, *Oct4* was expressed at high levels in all the three fractions showing that these cells do not seem to be exiting pluripotency despite the heterogeneity of *Nanog* expression levels. As expected, the pluripotency factor *Klf4*, which has been shown to be regulated by *Nanog* (Stuart et al., 2014), positively correlated with *Nanog* expression. Interestingly, *Nanog*-high cells exhibited 28-fold lower *Xist* expression levels than *Nanog*-low cells (Figure 3.2C). These results suggest that the increased *Xist* expression observed when the cells are cultured in SL are a consequence of the pluripotency-associated transcriptional heterogeneity observed in these culture conditions.

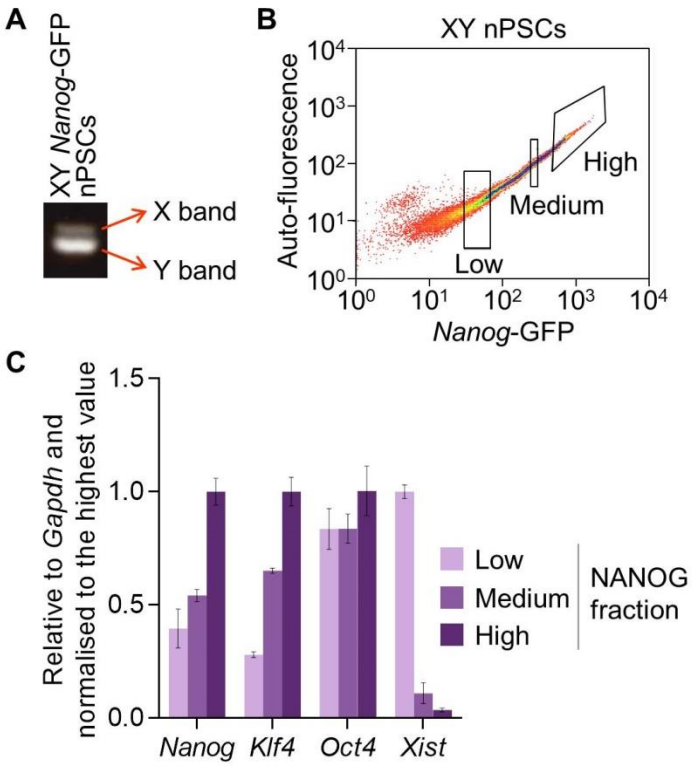

Figure 3.2: *Xist* expression is heterogeneous in SL-cultured nPSCs.
(A) PCR-based sex determination of the *Nanog*-GFP ESC line.
(B) Flow cytometry analysis of male SL *Nanog*-GFP ESCs and subsequent sorting into three *Nanog*-GFP populations: low, medium, and high.
(C) qRT-PCR analysis of *Nanog*, *Klf4*, *Oct4*, and *Xist* in low, medium and high *Nanog*-GFP ESCs. Data shown are the mean of three technical replicates. Error bars represent ± SD.

To validate the qRT-PCR data showing that *Xist* is not expressed in nPSCs, RNA-seq was performed in male 2iL-cultured nPSCs. I would like to highlight that RNA-seq was strand-specific so expression of *Xist* could be distinguished from expression of its antisense RNA *Tsix*. Importantly, RNA-seq data corroborated the qRT-PCR results showing that *Xist* is repressed in male 2iL nPSCs (Figure 3.3A). The results clearly demonstrate that expression at the *Xist* locus is exclusively antisense (Figure 3.3A).

I then analysed the pattern of *Xist* RNA using both a single-strand *Xist*-specific probe and a conventional double-strand probe detecting *Xist* exon 1 and also *Xist* antisense transcript. When using the double-strand probe, most male and female cells analysed exhibited one or two pinpoint signals, respectively (Figure 3.3B). This is in agreement with previous studies in which *Xist* double-strand probe was used (Panning et al., 1997; Sheardown et al., 1997). In contrast, *Xist* was detected in less than 2% of the cells when the strand-specific probe was used. These results indicate that the pinpoint signals observed with the double-strand probe correspond to expression antisense to *Xist* (Figure 3.3B). To confirm that the single-strand probe successfully detects *Xist* expression, a female EpiSC line was analysed. Female EpiSCs have one Xi and, therefore, one *Xist* cloud per cell was observed (Figures 3.3B and 3.3C).

Altogether, these data demonstrate that *Xist* is not expressed in robust self-renewing nPSCs. It also highlights that previous publications reporting *Xist* expression in nPSCs must be considered with caution, due to the confounding detection of *Tsix* with the conventionally used double-strand probe.

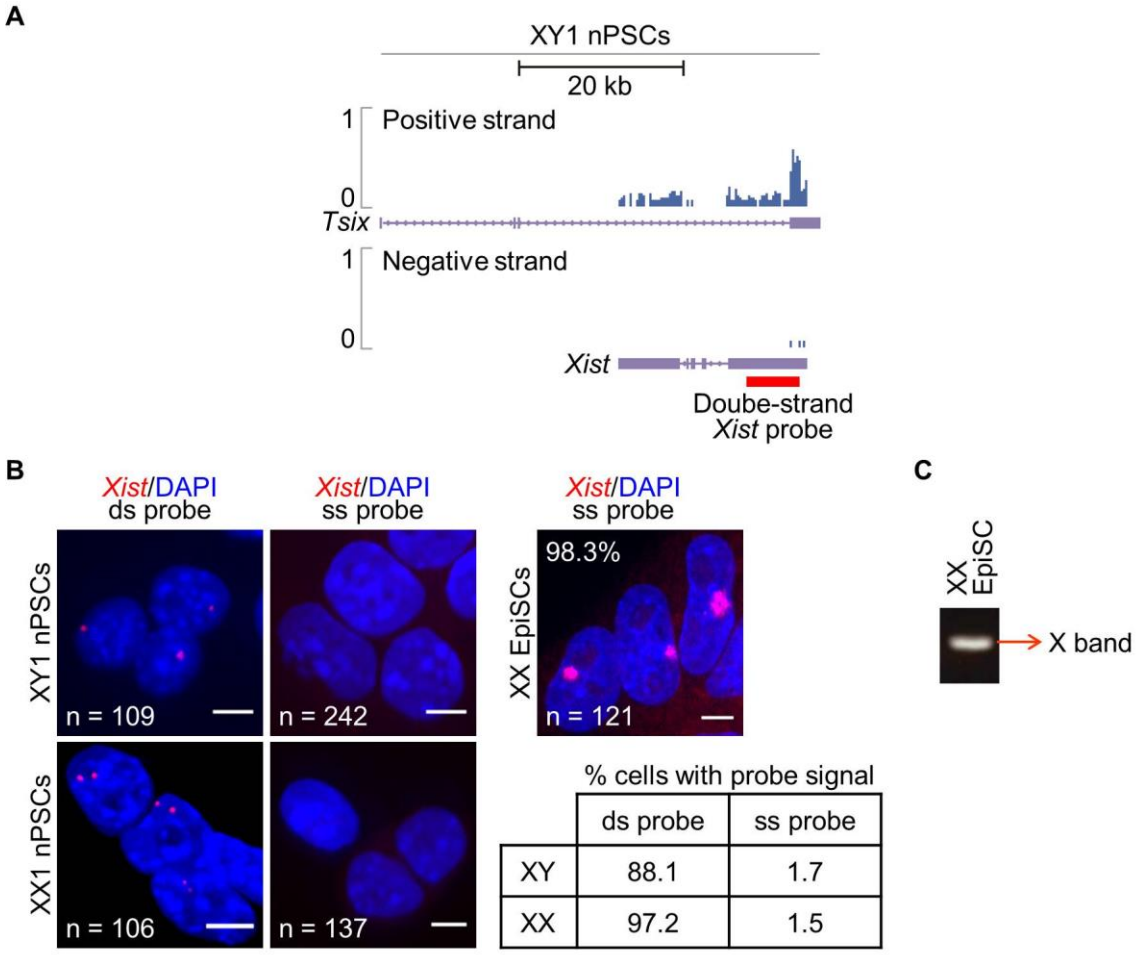

Figure 3.3: *Xist* is undetectable in nPSCs by either strand-specific RNA-seq or RNA FISH.

(A) Strand-specific RNA-seq showing expression of *Tsix* (positive strand) and *Xist* (negative strand) in male (XY1) 2iL ESCs. The double-strand *Xist* probe used in (B) is represented in red. The RNA-seq analysis was performed by Dr. Sabine Dietmann and Dr. Mohammadmersad Ghorbani.

(B) RNA FISH in male (XY1) and female (XX1) 2iL ESCs with a double-strand probe (indicated as ds) detecting both *Xist* and *Tsix* (left) or with a single-strand probe (indicated as ss) detecting only *Xist* (right). Nuclei are shown in blue (DAPI staining). The percentage of cells with *Xist* signal is indicated. Female EpiSCs were used as a control for the single-strand probe. The scale bar represents 5 µm.

(C) PCR-based sex determination of the control EpiSC line.

3.2.2 Analysis of *Xist* status in nPSCs upon *Nanog* deletion

Having established by different methods that *Xist* is not expressed in 2iL nPSCs, I decided to further investigate the relationship between naïve pluripotency network and *Xist* status using 2iL conditions. It has been reported that 2iL culture medium allows the removal of components of the naïve transcription factor network that otherwise would be essential (Ying et al., 2008). Therefore, I aimed to analyse *Xist* expression following withdrawal of some of these factors in the context of pluripotency. Navarro and colleagues used SL-cultured ESCs to show that *Nanog*, one of the core components of the naïve network, was implicated in the regulation of *Xist* (Navarro et al., 2008). In order to revisit this finding, we first derived ESCs in 2iL that would allow us to perform *Nanog* conditional knockout. Mice homozygous for a *Nanog* conditional allele ($Nanog^{flox/flox}$) (Chambers et al., 2007) and expressing CreERT2 ubiquitously from the *Rosa26* locus were crossed with *Nanog* heterozygous mice ($Nanog^{+/-}$) (Mitsui et al., 2003) (Figure 3.4A). ESCs were derived from the resulting $Nanog^{flox/+}$, $Rosa26^{CreERT2/+}$ and $Nanog^{flox/-}$, $Rosa26^{CreERT2/+}$ E4.5 embryos (Figure 3.4A). After determining the genotype and sex of each cell line, two of the $Nanog^{flox/-}$ lines, one female (number 15) and one male (number 10), were selected for subsequent experiments (Figures 3.4B and 3.4C). The $Nanog^{flox/-}$, $Rosa26^{CreERT2/+}$ ESCs were then treated with 4-hydroxytamoxifen (4-OHT) to excise LoxP-flanked exons and bring GFP under control of the *Nanog* promoter. This resulted in $Nanog^{-/-}$ GFP-expressing ESCs that were harvested at different time points for analysis (Figures 3.4D and 3.4E).

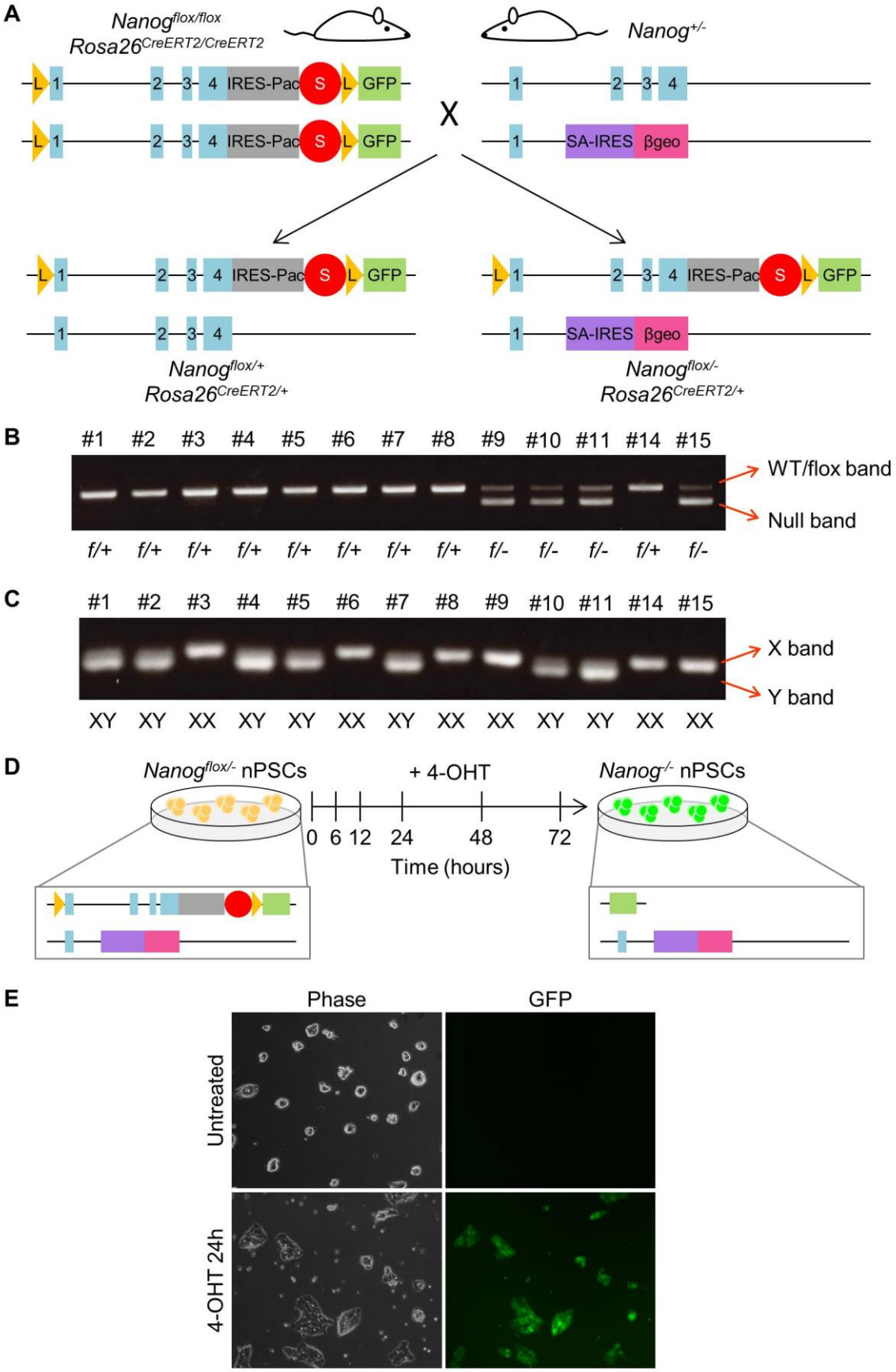

Figure 3.4: Strategy for *Nanog* conditional knockout.
Legend continues on next page.

Deletion of *Nanog* was confirmed at the protein level by western blot. NANOG levels were already diminished after 6 hours of treatment and barely detectable 48 hours post-treatment (Figure 3.5A). Strikingly, *Xist* was highly upregulated at 72 hours post-treatment with 4-OHT in both female and male cells (Figure 3.5B). As expected, *Nanog* deletion also had an effect on the expression of its downstream targets, such as *Klf4* (Stuart et al., 2014) and *Esrrb* (Festuccia et al., 2012), but not on *Oct4* or other naïve pluripotency genes (Figure 3.5C). The fact that the levels of pluripotency markers, like *Oct4* and *Sox2*, remain unchanged shows that despite *Nanog* deletion these cells remain naïve pluripotent, consistent with the ability of Nanog$^{-/-}$ ESCs to be generated and maintained (Chambers et al., 2007).

Figure 3.4: Strategy for *Nanog* conditional knockout.
(A) Simplified schematic of the strategy used to generate *Nanog*$^{flox/+}$ and *Nanog*$^{flox/-}$ ESCs, not to scale. All alleles are under control of the endogenous *Nanog* promoter, and the *Nanog* 5' UTR is unchanged. *Nanog*$^{flox/flox}$, *Rosa26*$^{CreERT2/CreERT2}$ mice were crossed with *Nanog*$^{+/-}$ and the resulting E4.5 embryos were derived into ESCs. Key: endogenous *Nanog* exons (1, 2, 3, 4); splice-acceptor (SA); internal ribosome entry site (IRES); geneticin resistance (βgeo); stop codon (S); LoxP site (L); puromycin resistance (Pac); GFP coding sequence without a promoter (GFP). These cell lines were derived in collaboration with Prof. Jennifer Nichols.
(B) Genotyping of the ESC lines obtained from the cross represented in (A).
(C) PCR-based sex determination of the ESC lines obtained from the cross represented in (A). Cell lines number 10 and number 15 were used to carry out the subsequent experiments.
(D) Schematic illustrating the approach employed to delete *Nanog* from ESCs. *Nanog*$^{flox/-}$, *Rosa26*$^{CreERT2/+}$ were treated with 4-OHT to excise LoxP-flanked Nanog exons and bring GFP under control of the *Nanog* promoter. This resulted in *Nanog*$^{-/-}$ GFP-expressing ESCs that were harvested at the indicated time points for analysis.
(E) Phase and GFP images of the *Nanog*$^{flox/-}$, *Rosa26*$^{CreERT2/+}$ ESCs before and after 24 hours (h) of treatment with 4-OHT. The 4-OHT-treated cells express GFP indicating that the deletion was successful.

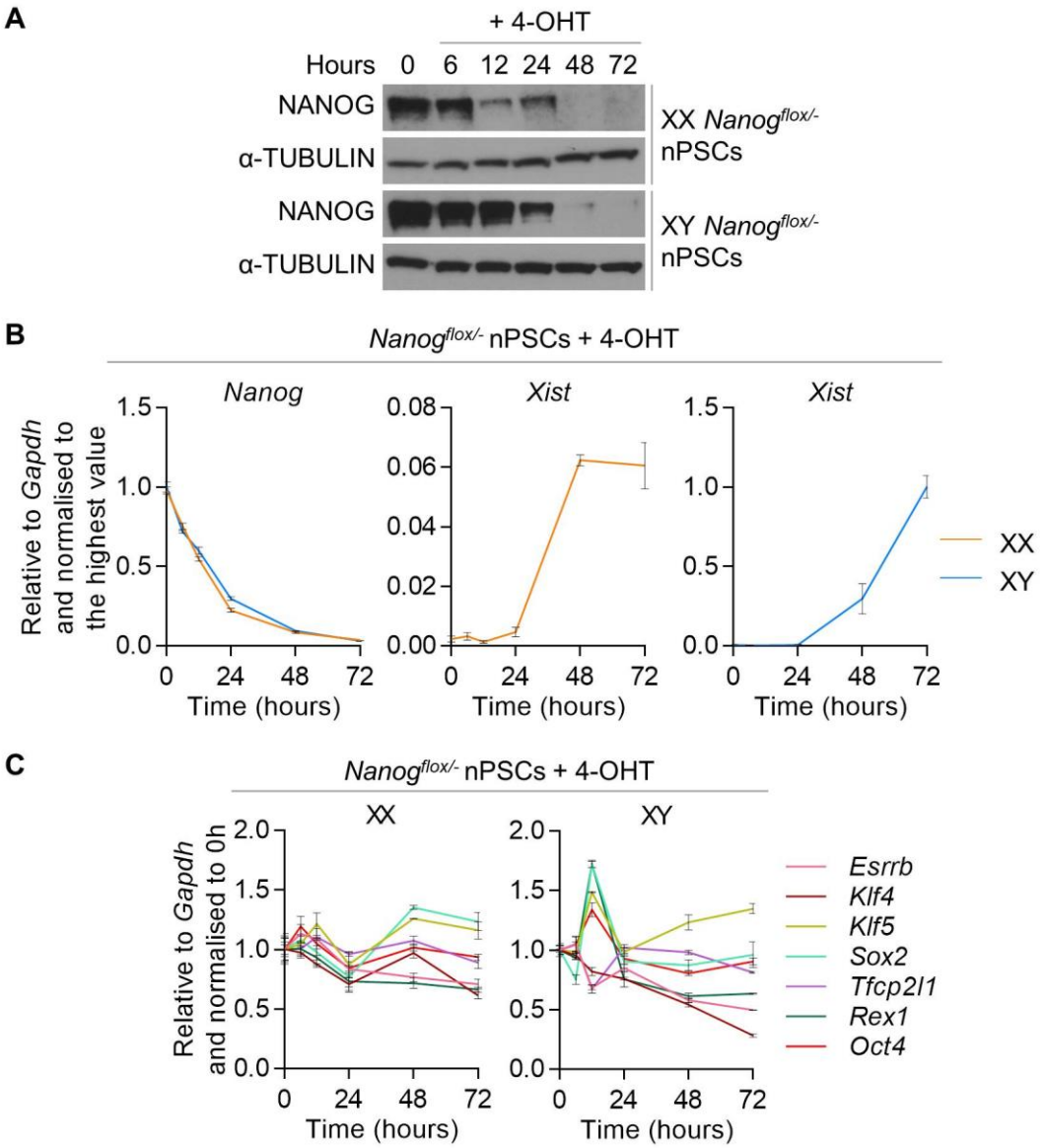

Figure 3.5: *Nanog* deletion leads to *Xist* upregulation in the context of naïve pluripotency.

(A) Western blot analysis of NANOG in female and male *Nanog*$^{flox/-}$, *Rosa26*$^{CreERT2/+}$ ESCs in 2iL (0 hours) and at different time points following treatment with 4-OHT.

(B) qRT-PCR analysis of *Nanog* and *Xist* in female and male *Nanog*$^{flox/-}$, *Rosa26*$^{CreERT2/+}$ ESCs in 2iL (0 hours) and at different time points following treatment with 4-OHT. Data shown are the mean of three technical replicates. Error bars represent ± SD.

(C) qRT-PCR analysis of naïve markers (*Esrrb*, *Klf4*, *Klf5*, *Sox2*, *Tfcp2l1*, *Rex1*, and *Oct4*) in female and male *Nanog*$^{flox/-}$, *Rosa26*$^{CreERT2/+}$ ESCs in 2iL (0 hours) and at different time points following treatment with 4-OHT. Data shown are the mean of three technical replicates. Error bars represent ± SD.

3.2.3 Impact of JAK/STAT3 signalling inhibition on the expression of *Xist*

JAK/STAT3 signalling plays an important role in the maintenance of pluripotency (Burdon et al., 1999; Matsuda et al., 1999). Moreover, activated STAT3 (p-STAT3) and its downstream target genes have binding sites within the XIC that harbours *Xist* and other genes involved in its regulation (Sanchez-Castillo et al., 2015). Thus, I examined the impact of JAK/STAT3 signalling inhibition on *Xist* expression in nPSCs. Inhibition of JAK/STAT3 signalling was achieved by treatment of ESCs with a JAK inhibitor (JAKi) that has inhibitory activity against all members of the JAK family – JAK1, JAK2, JAK3, and TYK2. Since LIF signals via JAKs and induces activation of STAT3 (Niwa et al., 1998), treatment with JAKi was performed in the absence of LIF. Treated ESCs (1μM JAKi + 2i) were compared with ESCs cultured in either 2iL or 2i, both of which maintain naïve pluripotency (Dunn et al., 2014). Cells were analysed at 0, 3, and 5 days post-treatment (Figure 3.6A). This experiment was carried out in both female and male ESCs (Figures 3.1A and 3.6B). JAK/STAT3 inhibition was confirmed through depletion of p-STAT3 (Figure 3.6C) and downregulation of its downstream target *Socs3* (Figure 3.6D).

Interestingly, treatment with 1 μM JAKi induced a striking upregulation of *Xist* in both female and male ESC lines (Figure 3.7). However, ESCs treated with JAKi demonstrated diminished expression of certain pluripotency factors, such as *Oct4* (Figure 3.8A), which are known to be required for the integrity of the pluripotency network. Moreover, there were loss of the characteristic ESC morphology and decreased self-renewal capacity of ESCs in the presence of JAKi (Figure 3.8B).

Together, these observations suggest that, when treated with 1 μM JAKi, ESCs appear to initiate exit from naïve pluripotency. This is in agreement with a previous report showing that *Stat3*$^{-/-}$ ESCs can be generated in 2i but are prone to differentiation (Carbognin et al., 2016). The results were particularly surprising in the case of male cells because according to the literature naïve identity loss is accompanied by inhibition of *Xist* in males (Panning et al., 1997; Sheardown et al., 1997). Nevertheless, our data revealed a surprisingly high upregulation of *Xist* not only in females but also in males upon treatment with JAKi and consequent apparent exit from the naïve state.

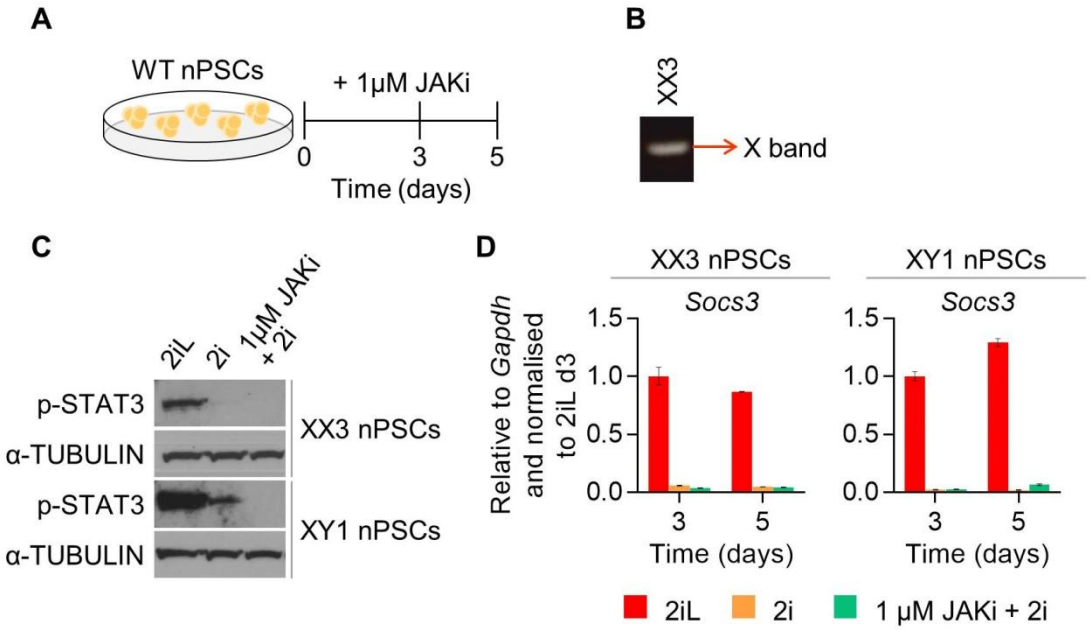

Figure 3.6: Strategy for inhibition of JAK/STAT3 signalling in nPSCs.
(A) Schematic of the time course performed with JAKi to deplete JAK/STAT3 signalling from ESCs.
(B) PCR-based sex determination of the C6 (XX3) ESC line.
(C) Western blot analysis of p-STAT3 in female (XX3) and male (XY1) ESCs in 2iL, 2i or after 3 days in 1μM JAKi + 2i.
(D) qRT-PCR analysis of the STAT3-target *Socs3* in female (XX3) and male (XY1) ESCs in 2iL, 2i or after 3 and 5 days in 1μM JAKi + 2i. Data shown are the mean of three technical replicates. Error bars represent ± SD.

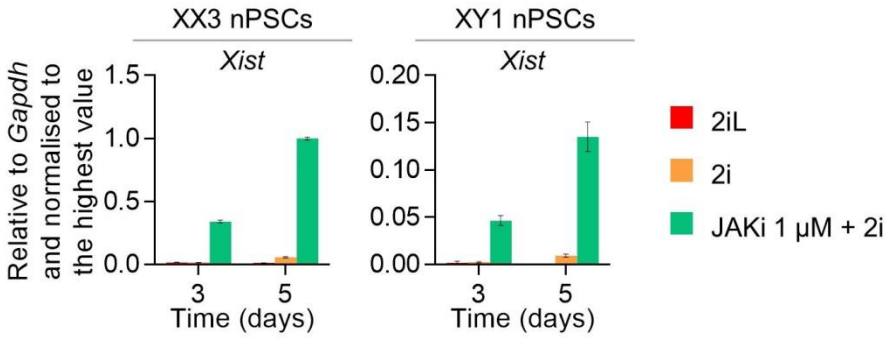

Figure 3.7: Inhibition of JAK/STAT3 induces upregulation of *Xist*.
qRT-PCR analysis of *Xist* in female (XX3) and male (XY1) ESCs in 2iL, 2i or after 3 and 5 days in 1μM JAKi + 2i. Data shown are the mean of three technical replicates. Error bars represent ± SD.

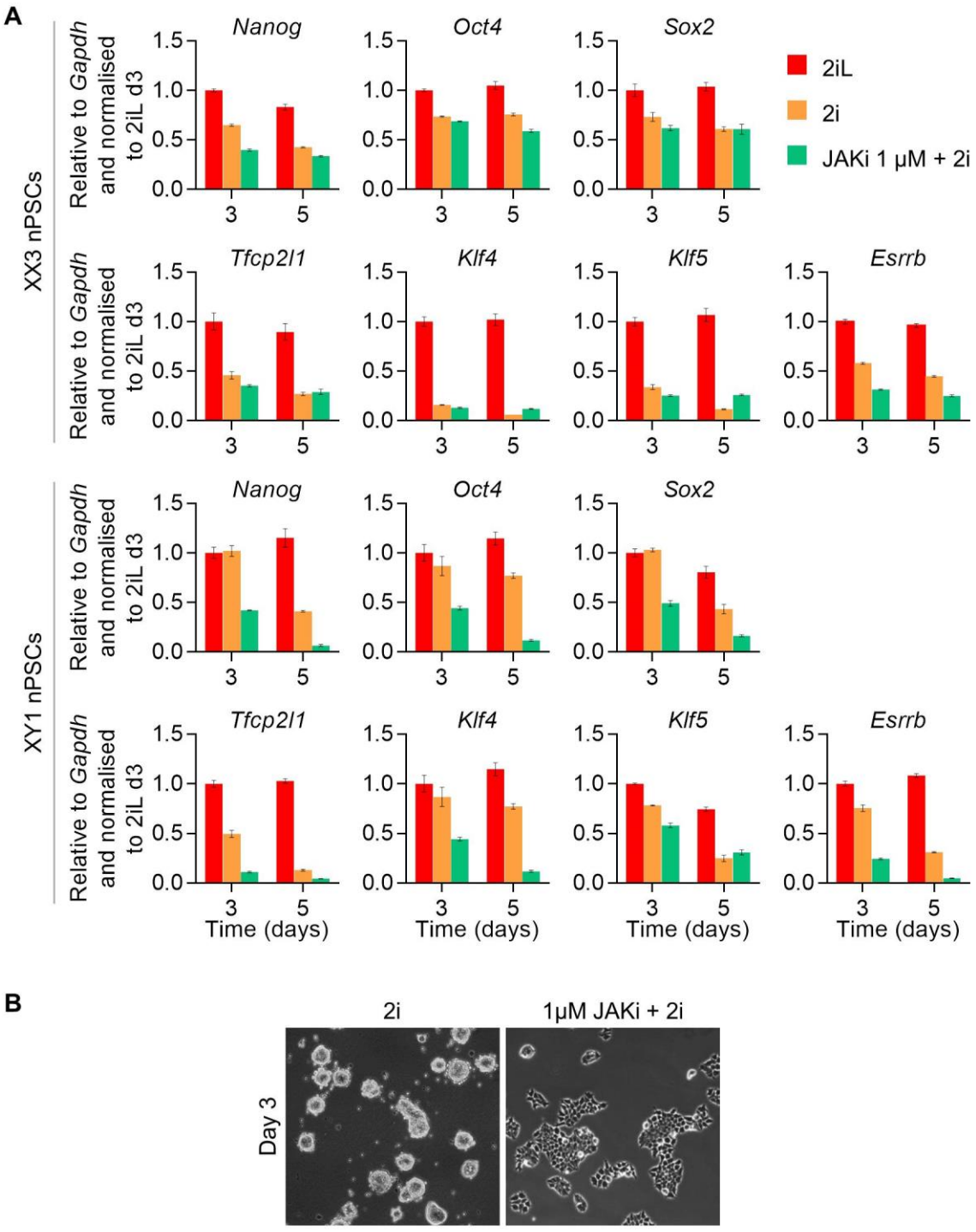

Figure 3.8: ESCs treated with JAKi appear to be exiting from naïve pluripotency.
(A) qRT-PCR analysis of the naïve markers (*Nanog*, *Oct4*, *Sox2*, *Tfcp2l1*, *Klf4*, *Klf5*, and *Esrrb*) in female (XX3) and male (XY1) ESCs in 2iL, 2i or after 3 and 5 days in 1μM JAKi + 2i. Data shown are the mean of three technical replicates. Error bars represent ± SD.
(B) Phase images of ESCs in 2i before and after treatment with 1μM JAKi.

3.3 Discussion

In this chapter, I reported that *Xist* is fully repressed in both male and female nPSCs provided they have a robust naïve transcription factor network. This can be achieved through the use of optimal nPSC culture conditions, like 2iL medium. It had been previously shown that *Xist* expression is decreased in 2i conditions when compared to SL (Marks et al., 2015). However, using strand-specific RNA-seq and RNA FISH allowed me to find that *Xist* is indeed not expressed in 2iL-cultured nPSCs. I speculate that the RNA antisense to *Xist* was responsible for the expression levels detected in nPSCs in previous studies employing methods that do not enable the distinction between the two strands. Given the resemblance between 2iL nPSCs and the E4.5 mouse naïve pluripotent epiblast (Boroviak et al., 2015), I hypothesise that *Xist* is also not expressed in the epiblast at this stage. This will be investigated further in this dissertation.

Repression of *Xist* in nPSCs may be the result of a combination of direct and indirect mechanisms taking place at the Xic. It has been reported that *Xist* and other non-coding and coding genes involved in its regulation harbour multiple genomic binding sites that are occupied by naïve pluripotency-associated transcriptions factors (Sanchez-Castillo et al., 2015). Moreover, there have been some studies reporting the regulation of members of the Xic, including *Xist*, by pluripotency factors (Donohoe et al., 2009; Navarro et al., 2008; Navarro et al., 2011; Nesterova et al., 2011; Payer et al., 2013; Silva et al., 2009). Regulation of *Xist* by both NANOG and OCT4 was proposed to occur through binding to *Xist* intron 1 and spatial association with the *Xist* promoter (Navarro et al., 2008). Additionally, deletion of *Xist* intron 1 in female or male ESCs induced a moderate upregulation of *Xist* expression (Nesterova et al., 2011). However, in a different study deletion of intron 1 region both in ESCs and in mice did not significantly impact *Xist* expression (Minkovsky et al., 2013). Therefore, although there is strong evidence that the pluripotency network plays a role in the regulation of *Xist*, it seems that this relationship does not rely on *Xist* inton 1.

Here, I made use of 2iL-cultured nPSCs to achieve deletion of *Nanog* without losing the naïve pluripotent identity of the cells and then study the impact of *Nanog* deletion on *Xist* status. Upregulation of *Xist* in this context was much more striking than that observed when the cells were cultured in SL (Navarro et al., 2008). This may be explained by the homogeneity of the nPSCs cultured in 2iL and also by the fact that *Xist* is repressed in these culture conditions. As expected, deletion of *Nanog* in 2iL conditions did not promote exit from naïve pluripotency. The effect of JAK/STAT3 inhibition on *Xist* expression was similar to that observed when *Nanog* was deleted: striking upregulation of *Xist* in both male and female cells. However, treatment with JAKi induced exit of nPSCs from the naïve state as indicated by changes in cell morphology and downregulation of pluripotency markers, like *Oct4*.

According to the literature, differentiation of male ESCs is accompanied by inhibition of *Xist* (Panning et al., 1997; Sheardown et al., 1997). Therefore, it was very surprising to observe increased expression of *Xist* in male cells that seem to be exiting the naïve pluripotent state. These results prompted me to revisit the kinetics of *Xist* expression during male nPSC differentiation.

Chapter 4
Investigating the relationship between loss of naïve cell identity and *Xist* expression

4.1 Introduction

Female mouse nPSCs contain two Xa and undergo random XCI upon induction of differentiation (Penny et al., 1996), making these cells a very useful tool to study this process. During differentiation of female nPSCs, one of the two X-chromosomes is randomly chosen for inactivation and *Xist* is upregulated from the future Xi. In contrast, *Xist* is thought to be repressed as male nPSCs exit from naïve pluripotency and undergo differentiation (Panning et al., 1997; Sheardown et al., 1997). Intriguingly, the results from Chapter 3 show that, in the presence of a naïve network that appears to have been compromised, *Xist* is highly upregulated not only in female but also in male cells. However, it remained to be elucidated whether *Xist* upregulation in males is due to a weaker but nonetheless naïve identity or a consequence of naïve cell differentiation.

Although several models have been proposed, it is still a mystery how the cell ensures that there is always one Xa per diploid genome (Goodrich et al., 2016). Moreover, it is not clear yet how the cell distinguishes whether it is male or female and whether or not XCI should be triggered. Therefore, I hypothesised that the rapid collapse of the naïve pluripotency network may impact the expression of *Xist* in both male and female cells before gender-specific mechanisms take place.

4.1.1 Aims of the chapter

In the previous chapter, I have demonstrated that the nPSC culture conditions impact on the expression and nuclear pattern of *Xist*. Moreover, the results showed that male cells that seem to be exiting from the naïve state display highly increased *Xist* expression. Therefore, I

aimed to study the kinetics of *Xist* expression during differentiation of both male and female 2iL-cultured nPSCs.

4.2 Results

4.2.1 Analysis of *Xist* expression upon *Oct4* deletion

The data shown in the previous section raised the need to investigate whether the observed sharp upregulation of *Xist* in males is indeed associated with a weaker but nonetheless naïve identity or a consequence of naïve cell differentiation. To examine this, I first analysed *Xist* expression kinetics upon *Oct4* deletion. *Oct4* is considered a master regulator of pluripotency and its expression is required to sustain stem cell self-renewal (Niwa et al., 2000). Here, *Oct4* deletion was achieved through the treatment of female and male *Oct4*$^{flox/-}$, *Rosa26*$^{CreERT2/+}$ ESCs with 4-OHT (Figure 4.1A). The gender of the ESC lines used for this experiment was confirmed by PCR (Figure 4.1B). Deletion of *Oct4* was confirmed by both western blot and qRT-PCR (Figures 4.1C and 4.2A).

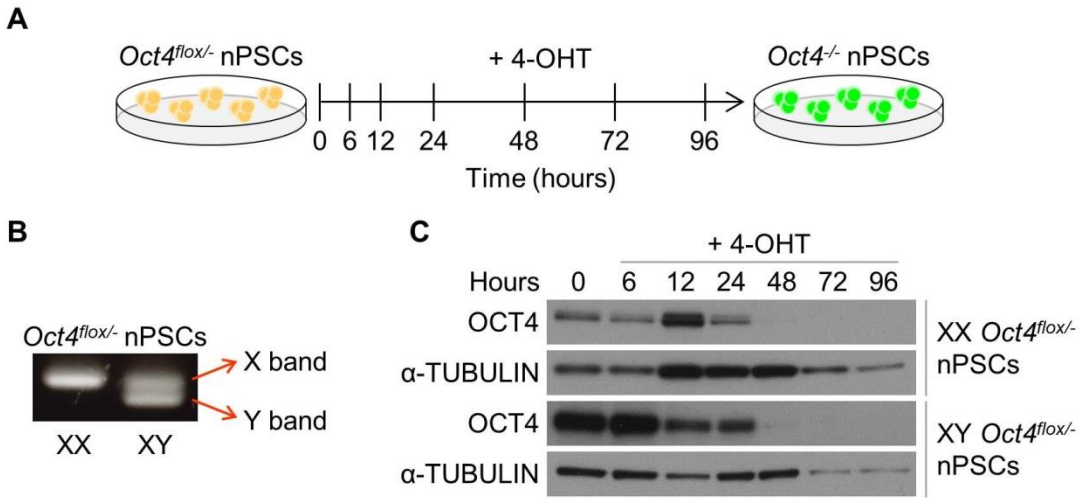

Figure 4.1: Strategy for *Oct4* conditional knockout.
(A) Schematic of the strategy used to delete *Oct4* from ESCs. *Oct4*$^{flox/-}$, *Rosa26*$^{CreERT2/+}$ were treated with 4-OHT which gave rise to *Oct4*$^{-/-}$ ESCs that were harvested at the indicated time points for analysis. These cell lines had been previously derived by Prof. Jennifer Nichols.
(B) PCR-based sex determination of the *Oct4*$^{flox/-}$, *Rosa26*$^{CreERT2/+}$ ESC lines.
(C) Western blot analysis of OCT4 in female and male *Oct4*$^{flox/-}$, *Rosa26*$^{CreERT2/+}$ ESCs in 2iL (0 hours) and at different time points following treatment with 4-OHT.
These experiments were performed by Lawrence Bates and analysed by me.

In this context, the naïve network collapses as shown by a striking reduction in the expression of naïve markers (Figure 4.2A). Concomitantly with *Oct4* deletion and exit from naïve pluripotency, both male and female cells exhibited a marked increase in the expression of *Xist* (Figure 4.2B). Strikingly, *Xist* expression in males reached 16% of the levels observed in female somatic cells (Figure 4.2B).

These data, together with the results shown in section 3.2.3, link the loss of naïve gene expression and identity to the upregulation of *Xist* in male cells.

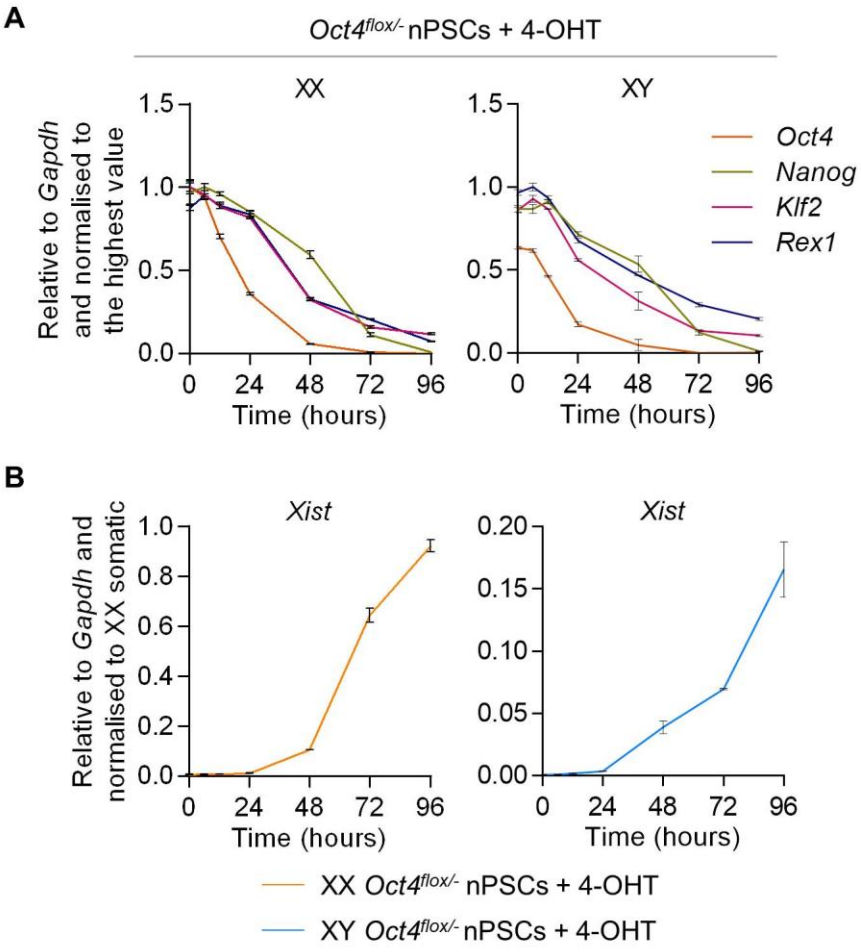

Figure 4.2: *Oct4* deletion leads to the collapse of the naïve network and *Xist* upregulation.

(A and B) qRT-PCR analysis of (A) *Oct4*, other naïve markers (*Nanog*, *Klf2*, and *Rex1*) and (B) *Xist* in female and male *Oct4*$^{flox/-}$, *Rosa26*$^{CreERT2/+}$ ESCs in 2iL (0 hours) and at different time points following treatment with 4-OHT. Data shown are the mean of three technical replicates. Error bars represent ± SD. Female somatic cells (neural stem cells) were used as control for *Xist* expression.

These experiments were performed by Lawrence Bates and analysed by me.

4.2.2 *Xist* is transiently and rapidly upregulated at the onset of male nPSC differentiation

To study the kinetics of *Xist* expression during male differentiation, I induced differentiation of male ESCs that had been previously cultured in traditional SL or optimal 2iL (Figure 4.3). Importantly, three distinct differentiation conditions were employed. ESCs were differentiated in adherent monolayer in serum-free medium supplemented with FA or in serum-free medium only. Differentiation was also achieved by culture of ESCs in suspension in serum-based medium without LIF. When cultured in these conditions, ESCs spontaneously differentiate and form three-dimensional multicellular aggregates called embryoid bodies (EBs) (Doetschman et al., 1985). An EB contains cells that are committed for differentiation into all the three germ lineages and recapitulates many aspects of cell differentiation during early mammalian embryogenesis (Desbaillets et al., 2000; Itskovitz-Eldor et al., 2000).

Surprisingly, a striking upregulation of *Xist* was observed in differentiating male 2iL ESCs (Figure 4.4A). Moreover, this was independent of the differentiation condition applied. *Xist* upregulation was transient and rapid, occurring between 1.5 and 2 days upon induction of differentiation (Figure 4.4A). Although less apparent, this pattern was also observed in differentiating male SL ESCs (Figure 4.4A). Importantly, analysis of a different male 2iL ESC line corroborated these findings (Figure 4.4B).

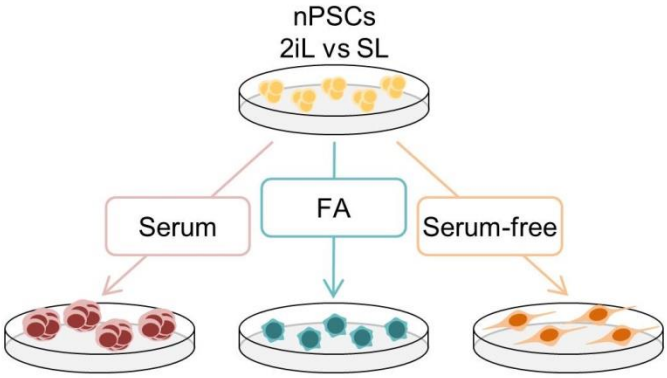

Figure 4.3: Strategy for differentiation of male nPSCs.
Schematic illustrating three conditions employed to differentiate 2iL and SL ESCs: suspension culture in serum-based medium to generate EBs, adherent monolayer culture in serum-free medium supplemented with FA and adherent monolayer culture in serum-free medium only.

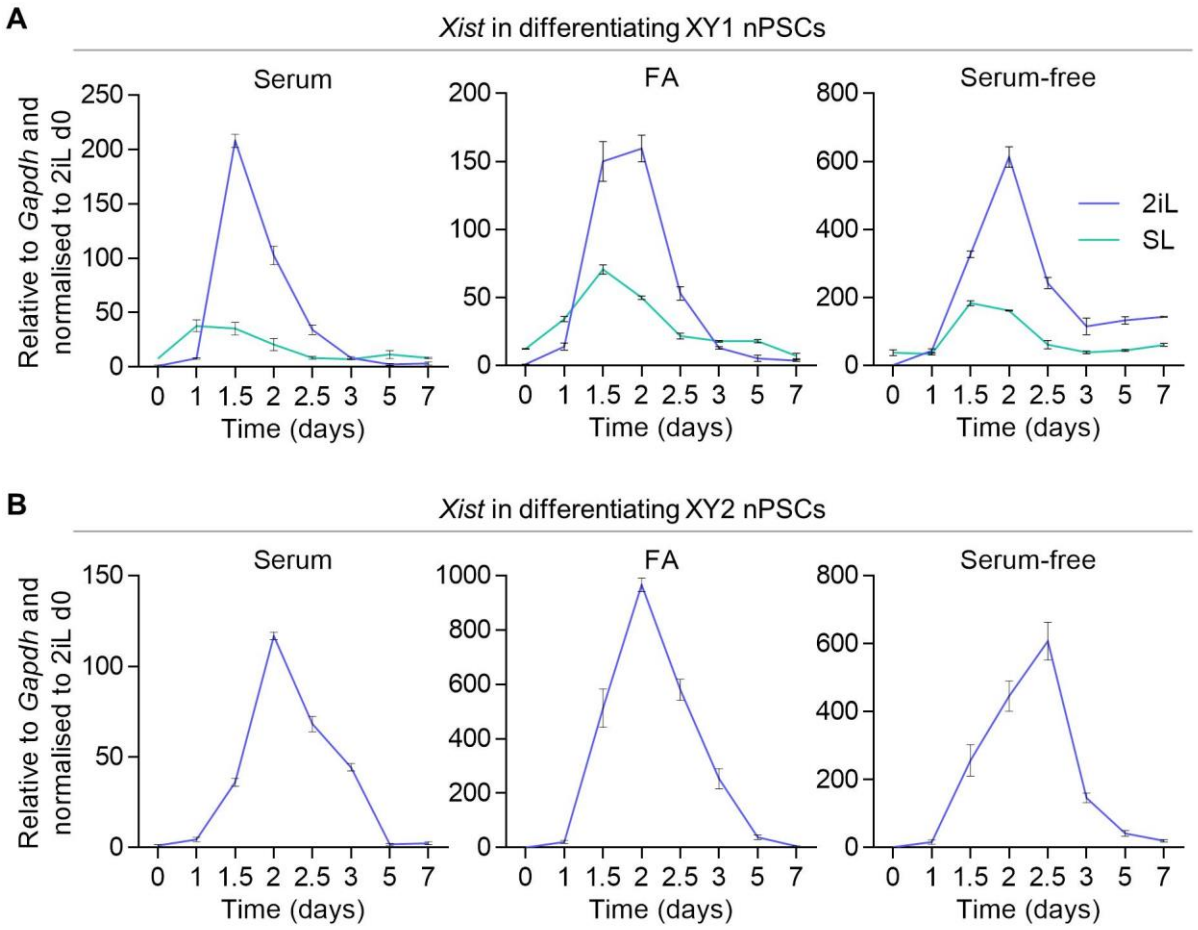

Figure 4.4: *Xist* is transiently upregulated during differentiation of ESCs.
(A) qRT-PCR analysis of *Xist* during differentiation of male (XY1) ESCs in three different conditions. Before differentiation, ESCs were maintained in 2iL or SL conditions, as indicated.
(B) qRT-PCR analysis of *Xist* during differentiation of male (XY2) ESCs in three different conditions. Before differentiation, cells were maintained in 2iL.
(A and B) Data shown are the mean of three technical replicates. Error bars represent ± SD.

To test whether the same pattern could be observed during differentiation of induced pluripotent stem cells (iPSCs), I generated a male iPSC line that could be subsequently induced to differentiate. First, neural stem cells (NSCs) with a *Rex1*-dGFP reporter were derived from brains of E12.5 embryos and then one of the male NSC lines generated was reprogrammed into iPSCs (Figure 4.5A). Reprogramming of male *Rex1*-dGFP NSCs into iPSCs was successful as shown by acquisition of ESC-like morphology, activation of the *Rex1*-dGFP reporter (Figure 4.5B) and upregulation of naïve markers (Figure 4.5C). The iPSC line generated was then subjected to EB differentiation assay. Notably, *Xist* also underwent transient and rapid upregulation during differentiation of male iPSCs (Figure 4.5D).

I also induced a female ESC line to differentiate in order to compare the expression levels of *Xist* with those observed during differentiation of male ESCs. Remarkably, 1.5 days after induction of EB differentiation, *Xist* expression reaches very similar levels in male and female cells (Figure 4.6A). However, while *Xist* expression keeps increasing in differentiating female cells, in male cells it starts declining after 1.5 days of differentiation (Figure 4.6A). These results suggest that XCI may be initiated in both male and female cells upon induction of differentiation, but it is only maintained in female cells.

Moreover, I found that differentiating female 2iL ESCs reach much higher *Xist* expression levels than female ESCs that were culture in SL before differentiation, even though *Xist* expression is lower at day 0 in 2iL conditions (Figure 4.6B). I hypothesise that this may be due to the transcriptional homogeneity of ESCs in 2iL which results in a more synchronous differentiation of these cells, although it could be due to other features such as signalling differences between 2iL and SL (Martello and Smith, 2014). I would like to reiterate that 2iL ESCs more closely represent *in vivo* naïve pluripotency in terms of their signalling, transcriptome and epigenetic profiles (Ahmed et al., 2010; Boroviak et al., 2014; Ficz et al., 2013; Hackett et al., 2017; Smith et al., 2012).

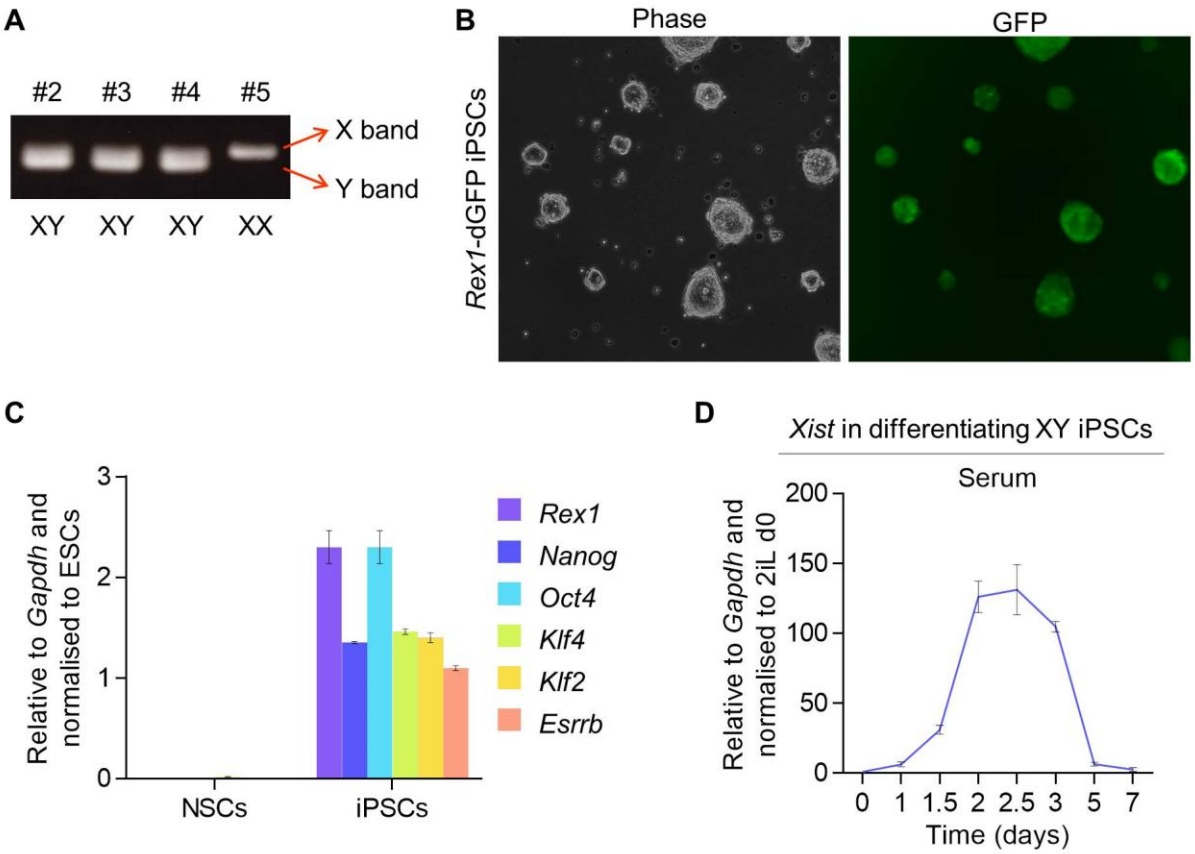

Figure 4.5: *Xist* is transiently upregulated in differentiating iPSCs.
(A) PCR-based sex determination of the *Rex1*-dGFP NSC lines derived. Cell line number 2 was used to perform the subsequent experiments. *Rex1*-dGFP NSC lines were derived in collaboration with Hannah Stuart.
(B) Phase and GFP images of the male iPSC line generated from NSCs. These cells express GFP indicating that reprogramming was successful.
(C) qRT-PCR analysis of naïve markers (*Rex1*, *Nanog*, *Oct4*, *Klf4*, *Klf2*, and *Esrrb*) in *Rex1*-dGFP NSCs before and after reprogramming to iPSCs (2iL-cultured). *Rex1*-dGFP ESCs in 2iL were used as a control.
(D) qRT-PCR analysis of *Xist* during EB differentiation of male iPSCs. Before differentiation, cells were maintained in 2iL.
(C and D) Data shown are the mean of three technical replicates. Error bars represent ± SD.

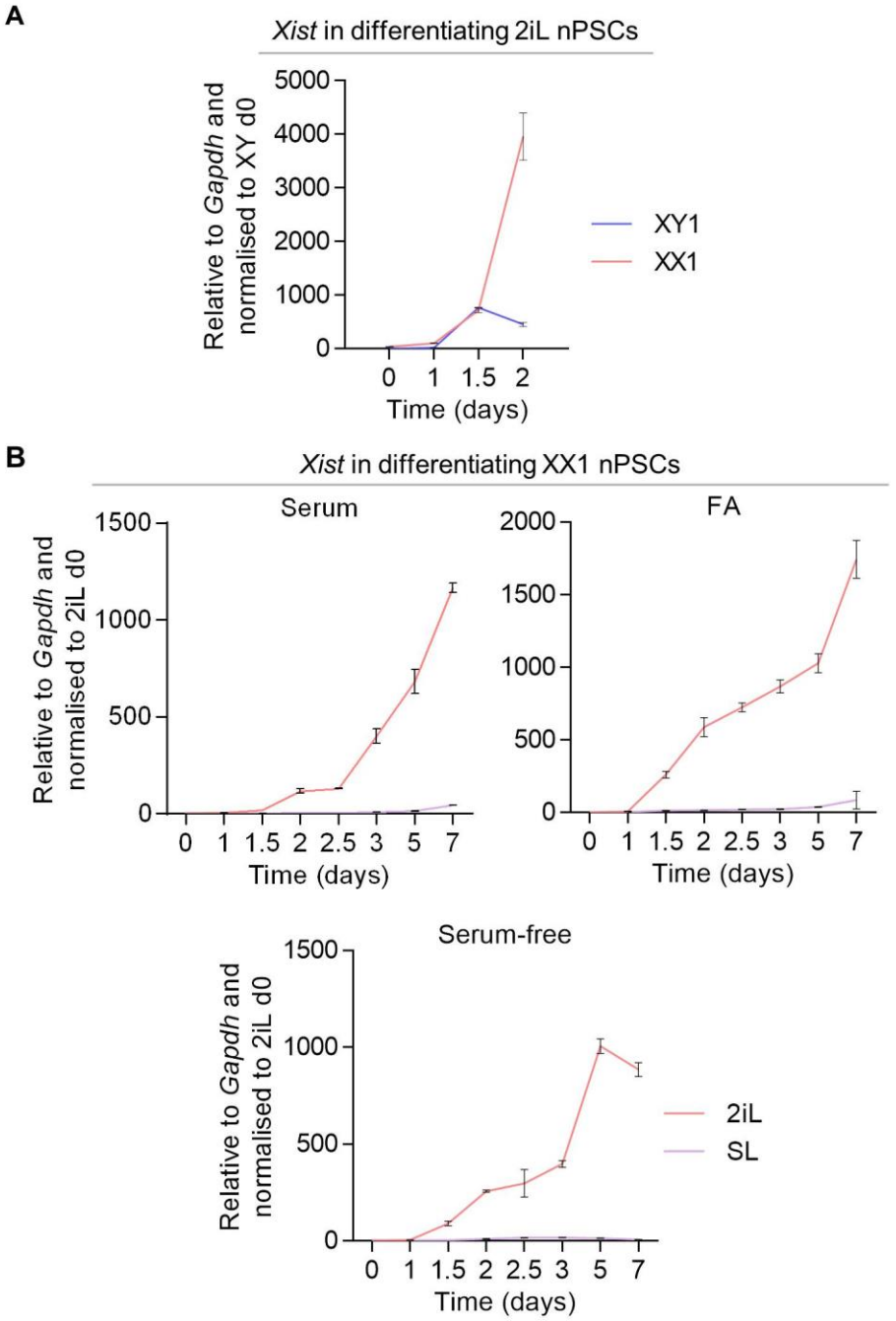

Figure 4.6: At the onset of differentiation, *Xist* expression levels are similar in male and female cells.

(A) qRT-PCR analysis of *Xist* during EB differentiation of male versus female 2iL ESCs.

(B) qRT-PCR analysis of *Xist* during differentiation of female (XX1) ESCs in three different conditions. Before differentiation, ESCs were maintained in 2iL or SL conditions, as indicated.

(A and B) Data shown are the mean of three technical replicates. Error bars represent ± SD.

To further validate the results showing that *Xist* is transiently upregulated during differentiation of male ESCs, differentiation time-courses were analysed by RNA-seq. It is important to highlight that the RNA-seq was strand-specific to ensure that *Xist* could be distinguished from its antisense transcript, *Tsix*. In agreement with the qRT-PCR data, when male 2iL ESCs are differentiated there is a surge of *Xist* expression that starts 1.5 days following induction of differentiation and lasts approximately 12 hours (Figure 4.7).

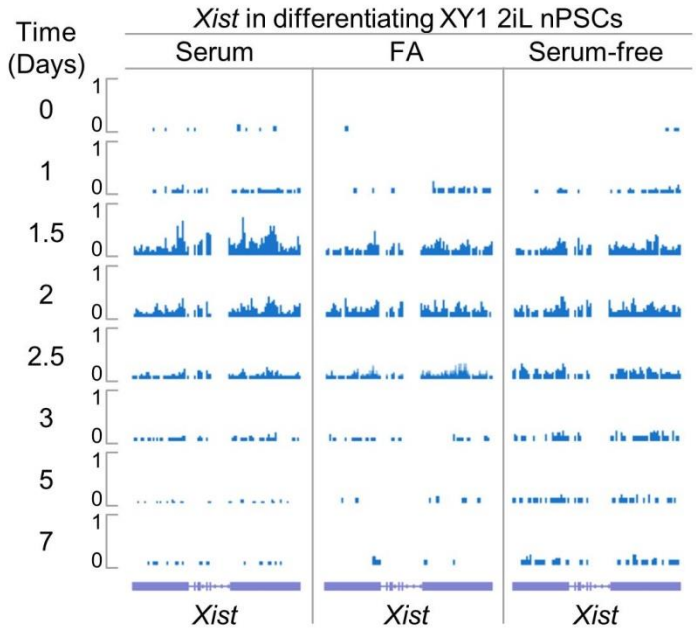

Figure 4.7: Strand-specific RNA-seq shows increased expression of *Xist* in male differentiating cells.
Strand-specific RNA-seq (negative strand only) showing the expression of *Xist* during differentiation of male (XY1) 2iL ESCs in three different conditions. Scale represents reads per million (RPM). The RNA-seq analysis was performed by Dr. Sabine Dietmann and Dr. Mohammadmersad Ghorbani.

Principal component analysis (PCA) based on differentially expressed genes demonstrated that 2iL ESCs exhibit a more undifferentiated profile when compared to SL ESCs (Figure 4.8), which corroborates the qRT-PCR data from section 3.2.1 showing that transferring ESCs from SL to 2iL increases the expression of naïve pluripotency markers and is in agreement with previously published work (Martello and Smith, 2014).

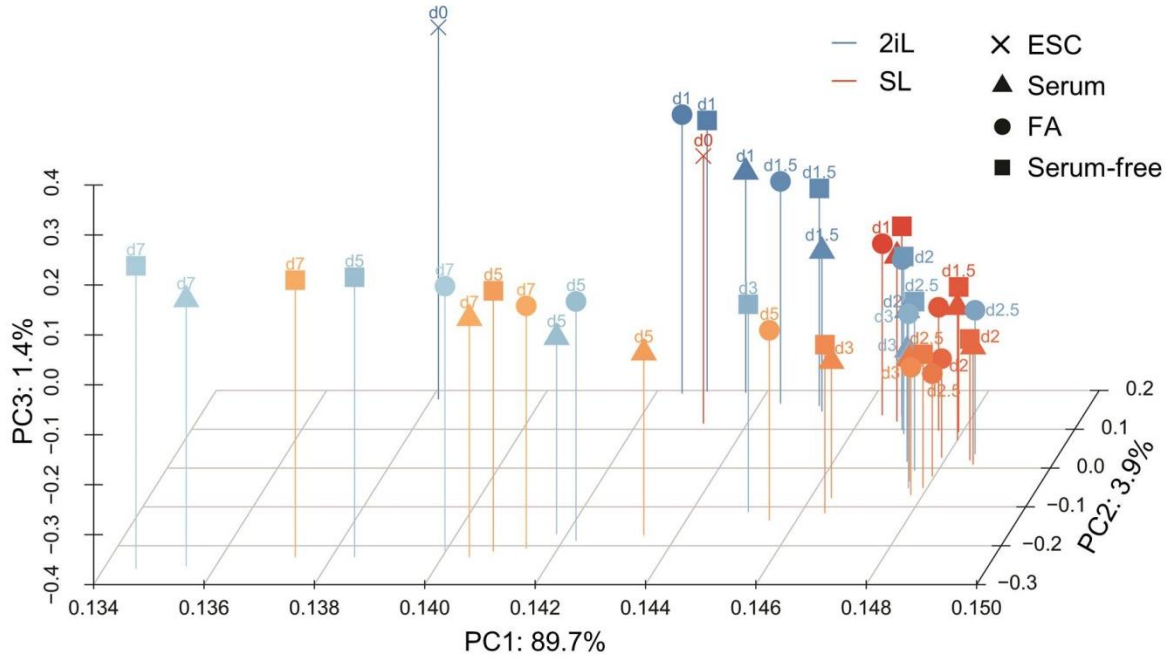

Figure 4.8: nPSCs cultured in 2iL are more undifferentiated when compared to SL cells.

PCA of differentiating male (XY1) cells based on differential expression of genes that had an expression of at least Log_2 (normalized counts) 4.5 in at least one of the samples. Before differentiation, ESCs were maintained in 2iL or SL media, as indicated. Data was obtained by strand-specific RNA-seq. The RNA-seq analysis was performed by Dr. Sabine Dietmann and Dr. Mohammadmersad Ghorbani.

The expression of components of the Xic that have been directly or indirectly implicated in the regulation of *Xist* (Anguera et al., 2011; Barakat et al., 2011; Chureau et al., 2011; Stavropoulos et al., 2001; Tian et al., 2010) was also analysed (Figure 4.9). Interestingly, *Ftx* and *Jpx*, which are putative positive regulators of *Xist* (Chureau et al., 2011; Tian et al., 2010), and *Tsx*, which is a putative positive regulator of *Tsix* (Anguera et al., 2011), also appear to be downregulated by 2iL conditions in comparison to SL at day 0 (Figure 4.9). This suggests that, like *Xist*, they might also be regulated by the naïve pluripotency network. Moreover, I observed that the non-coding RNA *Ftx* was upregulated during differentiation (Figures 4.9 and 4.10A) and may also contribute towards *Xist* upregulation. On the other hand, RNF12, which acts as an activator of *Xist* (Barakat et al., 2011; Gontan et al., 2012), was transiently increased (Figure 4.10B) following an expression pattern similar to that of *Xist* in male differentiation.

Global analysis of the expression pattern of long non-coding RNAs showed that *Xist* follows a pattern during differentiation that is distinct from all the other long non-coding RNAs (Figure 4.11).

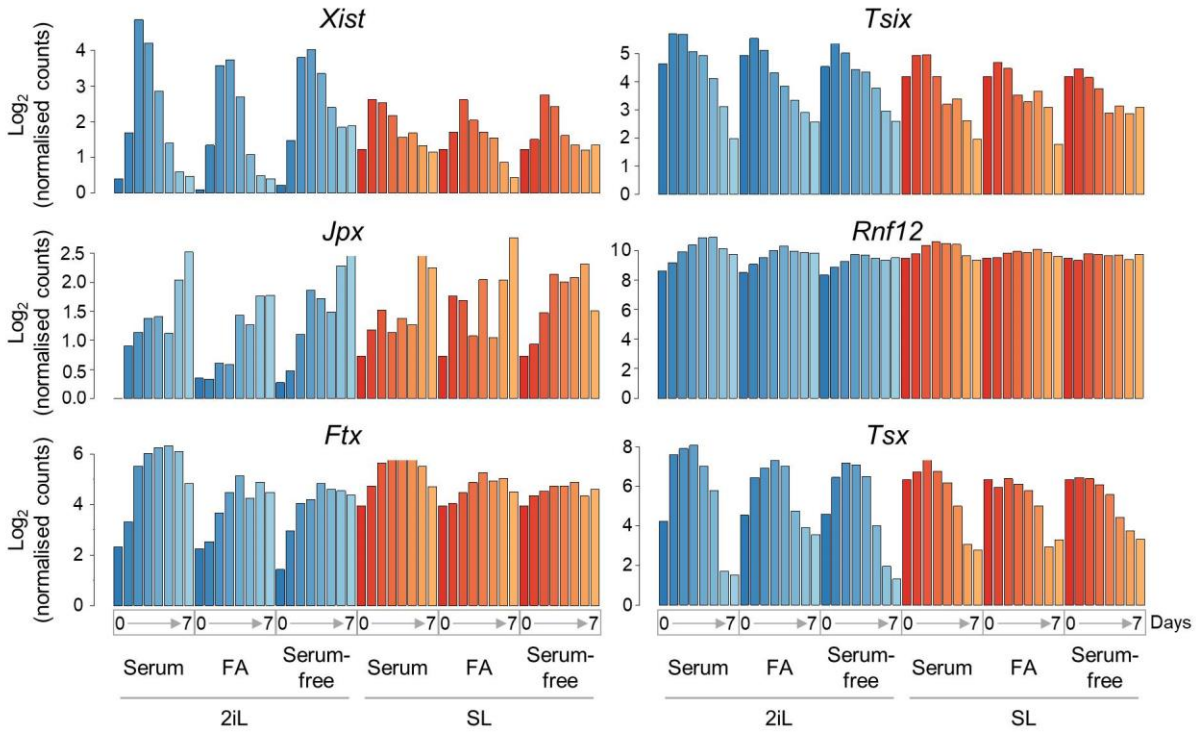

Figure 4.9: Gene expression analysis of *Xist* regulators during differentiation of male nPSCs.

Expression levels observed during differentiation of male (XY1) ESCs for *Xist* and other elements of the Xic that have been implicated in the regulation of *Xist*. Before differentiation, ESCs were maintained in 2iL or SL media, as indicated. Data were obtained by strand-specific RNA-seq. Scale represents Log_2 transformed expression value. The RNA-seq analysis was performed by Dr. Sabine Dietmann and Dr. Mohammadmersad Ghorbani.

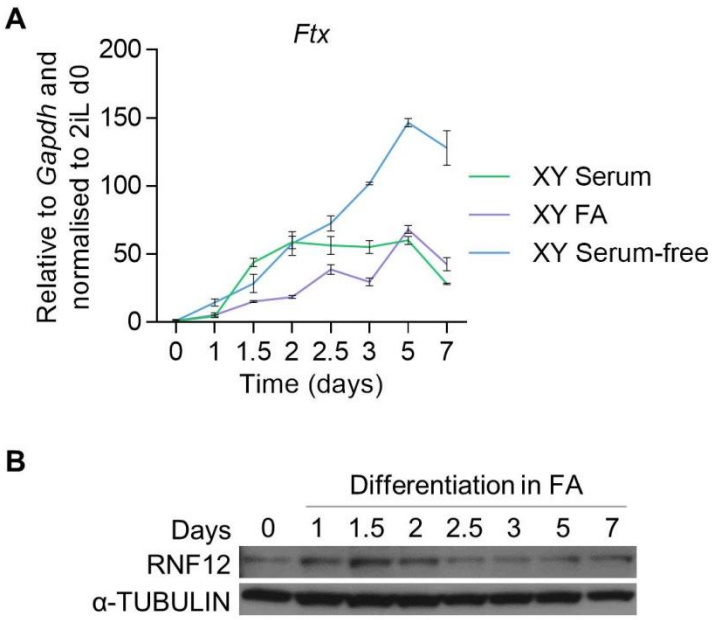

Figure 4.10: Dynamics of *Xist* activators during differentiation of male nPSCs.
(A) qRT-PCR analysis of *Ftx* during differentiation of male (XY1) ESCs in three different conditions. Before differentiation, cells were maintained in 2iL. Data shown are the mean of three technical replicates. Error bars represent ± SD.
(B) Western blot analysis of RNF12 during differentiation of male (XY1) ESCs in FA. Before differentiation, cells were maintained in 2iL.

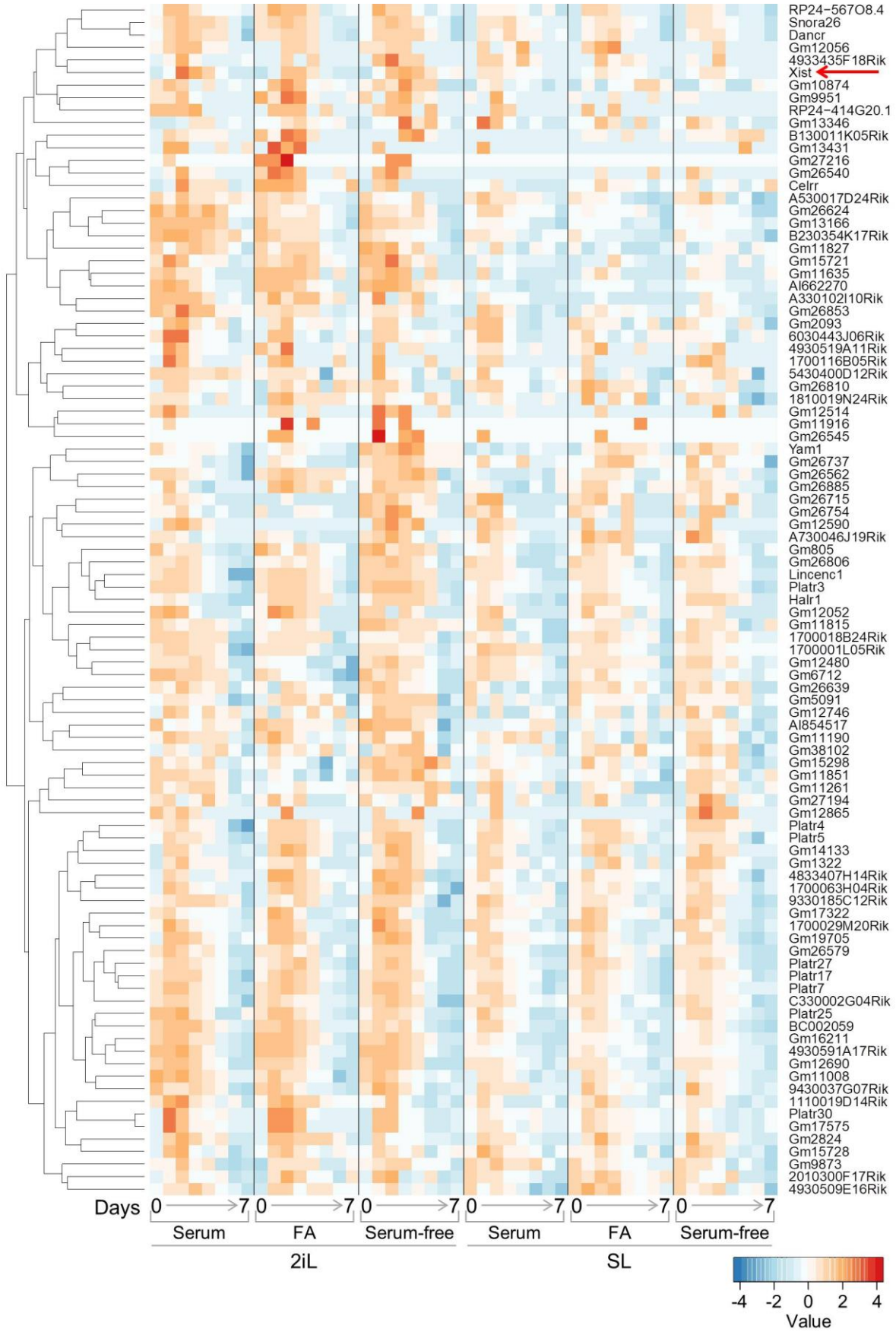

Figure 4.11: Gene expression analysis of long non-coding RNAs in differentiating male nPSCs.

Figure legend continues on next page.

To position *Xist* modulation in the sequence of events taking place during differentiation, we analysed the timing of *Xist* upregulation relative to the expression of naïve pluripotency and lineage markers over time (Figure 4.12). Importantly, downregulation of naïve pluripotency factors, such as *Nanog*, *Rex1*, *Esrrb*, *Klf2*, *Prdm14*, and *Tfcp2l1*, preceded *Xist* upregulation. In contrast, expression of lineage markers was detected only after *Xist* upregulation. These results, together with the effect of naïve network perturbations on *Xist* expression shown in the previous chapter, indicate that the upregulation of *Xist* observed in male cells is a consequence of naïve cell differentiation and is caused by a weakening naïve pluripotency network. It also makes *Xist* a very early marker for male cells exiting naïve pluripotency.

Altogether, these results demonstrate that male nPSCs also upregulate *Xist* upon induction of differentiation, an occurrence associated with initiation of XCI and previously ascribed exclusively to females.

Figure 4.11: Gene expression analysis of long non-coding RNAs in differentiating male nPSCs.

Heatmap depicting the expression profile of long non-coding RNAs during differentiation of male (XY1) ESCs. Before differentiation, ESCs were maintained in 2iL or SL media, as indicated. Data was obtained by strand-specific RNA-seq. Scale represents z-scores of Log_2 transformed expression values. *Xist* is indicated with a red arrow. The RNA-seq analysis was performed by Dr. Sabine Dietmann and Dr. Mohammadmersad Ghorbani.

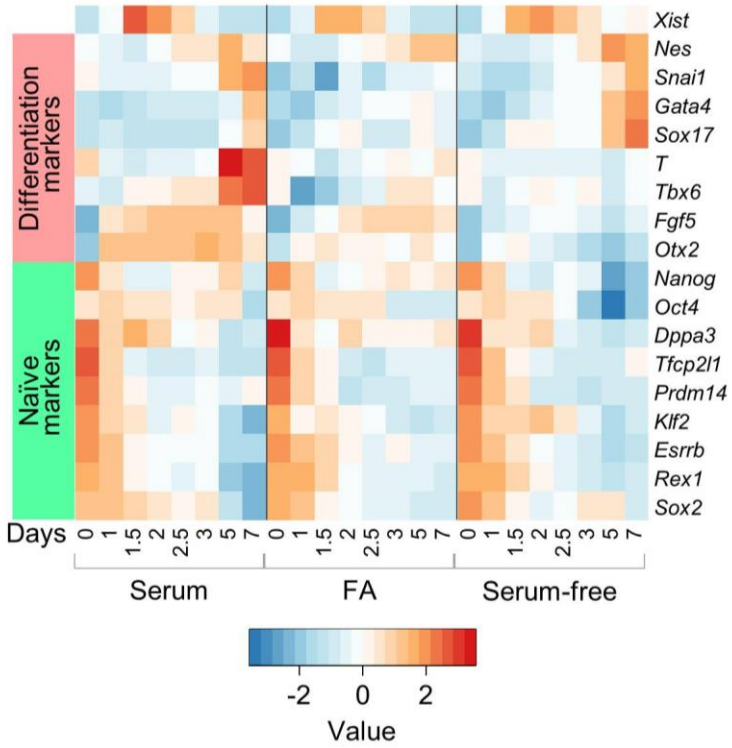

Figure 4.12: Gene expression analysis of differentiation and naïve markers during differentiation of male nPSCs.
Heatmap showing the expression profile of *Xist*, differentiation and naïve markers during differentiation of male (XY1) 2iL ESCs, as indicated. Scale represents z-scores of Log_2 transformed expression values. The RNA-seq analysis was performed by Dr. Sabine Dietmann and Dr. Mohammadmersad Ghorbani.

4.2.3 *Xist* is transiently upregulated during reprogramming of male cells

The aforementioned association between a strong naïve transcription factor network and the repression of *Xist* prompted us to investigate whether these are correlated in the context of reprogramming to naïve pluripotency in 2iL. We analysed the productive reprogramming intermediates from male EpiSCs (Figure 4.13A) using STAT3 activation (Yang et al., 2010) and *Rex1*-dGFP reporter activity (Kalkan et al., 2017) to induce and monitor reprogramming, respectively. STAT3 activation by phosphorylation was elicited by GCSF-stimulation of the GY118F receptor transgene (Yang et al., 2010) since LIF signal transduction of EpiSCs is limited (Burdon et al., 1999). I would like to note that obtained iPSCs were chimera and germline competent (Stuart et al., in preparation), demonstrating true establishment of naïve pluripotency.

Flow cytometry analysis was performed at different time-points to collect the *Rex1*-positive reprogramming intermediates for further analysis (Figure 4.13B). As expected, *Xist* was repressed in both male EpiSCs and control ESCs (Figure 4.13C). However, in

productive reprogramming intermediates, *Xist* was sharply upregulated (Figure 4.13C), prior to establishment of a consolidated nPSC identity.

Overall, this suggests that *Xist* upregulation occurs in the presence of a weak naïve network, whether this be due to network collapse during differentiation initiation, or conversely due to the fragile nature of the nascent network during reprogramming.

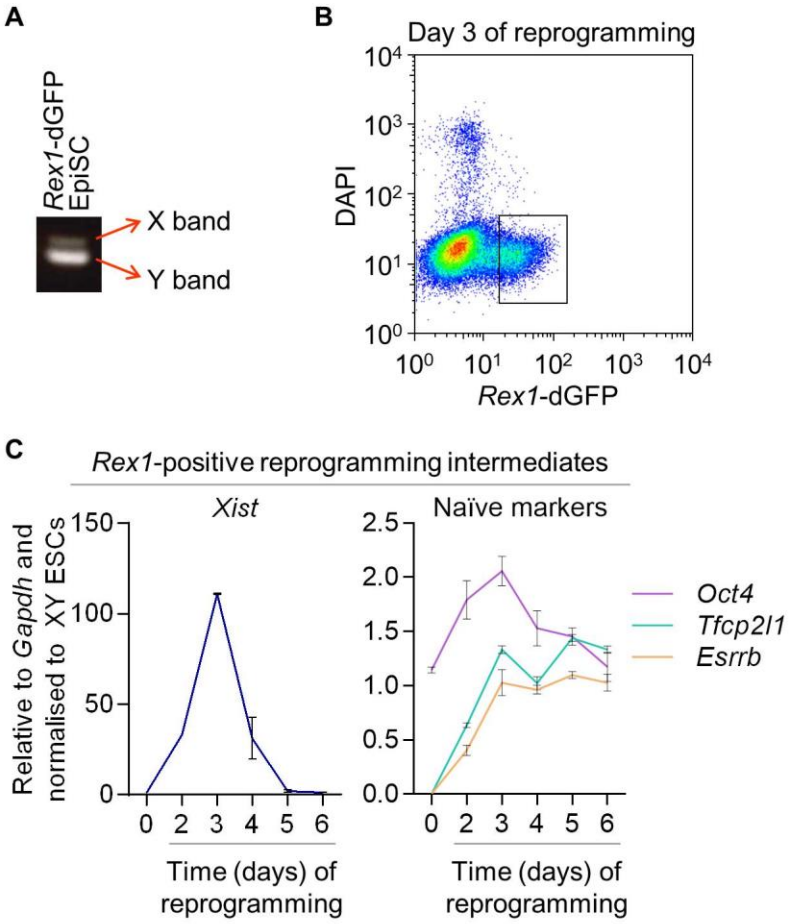

Figure 4.13: *Xist* is transiently upregulated during male EpiSC reprogramming.
(A) PCR-based sex determination of the *Rex1*-dGFP EpiSC line.
(B) Flow cytometry analysis of male GY118F *Rex1*+/GFP EpiSCs following reprogramming induction with GCSF in 2iL. Cells were sorted at different time points, with *Rex1*-dGFP reporter activation indicating the subset of cells successfully transitioning to the naïve identity. A representative plot from day 3 is shown. The reprogramming experiment was performed by Hannah Stuart.
(C) qRT-PCR analysis of *Xist* and naïve markers (*Oct4*, *Tfcp2l1*, and *Esrrb*) in male GY118F *Rex1*-positive reprogramming intermediates at different time points after induction of reprogramming with 2iL+GCSF. Parental EpiSCs (day 0) and ESCs in 2iL were used as controls. Error bars represent ± SD.

4.3 Discussion

In this chapter, I showed that *Xist* is upregulated rapidly and transiently during differentiation of male nPSC. Importantly, 1.5 days after differentiation induction, the levels of *Xist* expression are comparable between male and female cells, indicating that XCI appears to be initiated not only in female but also in male cells.

These results suggest that gender-independent upregulation of *Xist* is linked to the downregulation of naïve pluripotency factors. I hypothesise that, in the context of a compromised naïve transcription factor network, known and putative positive regulators of *Xist*, such as RNF12 (Barakat et al., 2011; Gontan et al., 2012), *Ftx* (Chureau et al., 2011), and *Jpx* (Tian et al., 2010), may transiently gain the upper hand and induce *Xist* upregulation. However, *Xist* is subsequently rapidly suppressed suggesting that other mechanisms of *Xist* silencing are readily available. In agreement with this, deletion of *Tsix*, a known *Xist* repressor, has been previously correlated with the presence of an *Xist* cloud in a proportion of differentiating male nPSCs (Sado et al., 2002). Likewise, male *Dnmt1* mutant nPSCs display *Xist* upregulation and consequent silencing of X-linked genes during differentiation (Beard et al., 1995; Panning and Jaenisch, 1996).

It remained to be elucidated whether upregulation of *Xist* in differentiating male cells is accompanied by other events associated with XCI. I therefore address this in the subsequent chapter.

Chapter 5
Characterisation of X-chromosome silencing state during male and female naïve cell differentiation

5.1 Introduction

In Chapter 4, I showed that *Xist* is rapidly upregulated in a transient manner in early differentiating male cells upon collapse of the naïve pluripotent network. In female differentiating cells, once upregulated at the onset of XCI, *Xist* coats the entire future Xi in *cis* and induces several epigenetic changes, such as the accumulation of the repressive histone mark H3K27me3 (Plath et al., 2003; Silva et al., 2003). Ultimately, this results in silencing of one of the X-chromosomes. I demonstrated that, upon induction of differentiation, male cells appear to initiate XCI by upregulating *Xist* transiently. However, it remained to be elucidated whether this upregulation of *Xist* observed in males is accompanied by the same events that follow upregulation of *Xist* in female differentiating cells.

It has been demonstrated that X-linked gene silencing is reversible during the first 3 days of ESC differentiation (Wutz and Jaenisch, 2000). In the previous chapter, I observed that *Xist* upregulation takes place 1.5 days after induction of differentiation of male ESCs. Hence, I hypothesise that *Xist* upregulation might be inducing silencing of the male X-chromosome given that the silencing state is fully reversible as long as *Xist* expression ceases within 3 days of differentiation.

5.1.1 Aims of the chapter

In the previous chapter, I have demonstrated that male cells transiently and rapidly upregulate *Xist* at the onset of differentiation. In this chapter, I aimed to characterise *Xist* nuclear pattern during male and female naïve cell differentiation both *in vitro* and *in vivo*. Using early differentiating nPSCs, I also aimed to assess the silencing state of the single

male X-chromosome and of both female X-chromosomes, to ascertain the molecular impact of the observed *Xist* expression.

5.2 Results

5.2.1 Male X-chromosome exhibits hallmarks of XCI upon upregulation of *Xist*

In section 4.2.2, I showed that *Xist* is upregulated in a transient manner during differentiation of male nPSCs. Therefore, I wanted to examine whether the observed *Xist* upregulation in males was linked to events associated with the initiation of XCI as described for females. To determine this, I first assessed the nuclear pattern of *Xist* by RNA FISH. In differentiated female cells, *Xist* RNA coats the Xi in *cis*, forming a cloud-like structure that can be visualised by RNA FISH (Panning et al., 1997; Sheardown et al., 1997). Remarkably, 1.5 days after male 2iL ESCs were induced to differentiate in FA, 20% of the cells showed *Xist* RNA expression (Figure 5.1A). Nearly half of the early differentiating male cells expressing *Xist* exhibited RNA clouds with a wide range of sizes (Figure 5.1A). Although in a smaller proportion, differentiating male SL ESCs also displayed expression of *Xist* (Figure 5.1B). I speculate that the percentage of cells expressing *Xist* in the latter case reflects the heterogeneity of the starting population which translates into greater cell differentiation asynchrony and consequently into fewer cells exhibiting *Xist* expression at a given snapshot. Unless stated otherwise, the subsequent differentiation experiments were performed in 2iL-cultured ESCs.

The expression of active CASPASE-3, which is an early marker of apoptosis, was evaluated to assess the viability of the *Xist*-positive male cells at 1.5 days of differentiation. Importantly, all analysed cells with *Xist* RNA upregulation were negative for active CASPASE-3. Moreover, only 1.4% of the cells were positive for this marker, a much lower percentage than that observed for the cells expressing *Xist* (Figure 5.2). Hence, I proceeded to the analysis of other XCI markers.

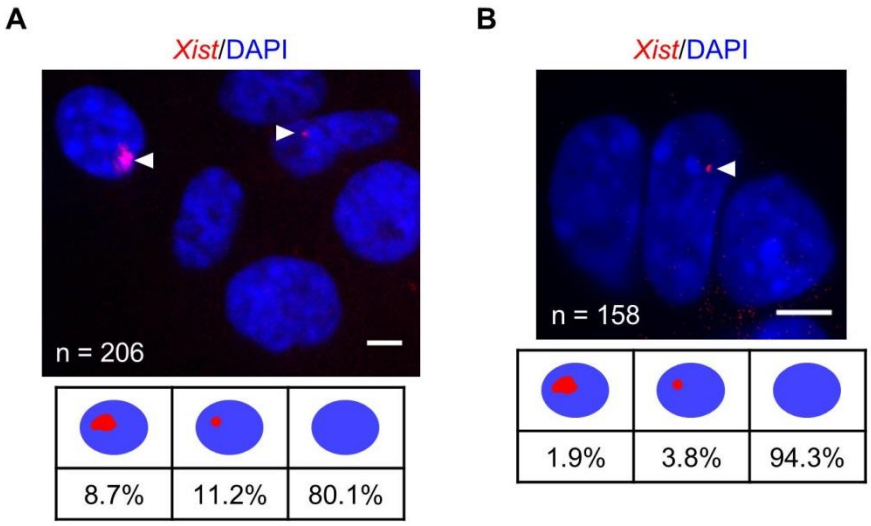

Figure 5.1: Differentiating male nPSCs display formation of *Xist* RNA cloud.
(A and B) RNA FISH for *Xist* (red) in male (A) 2iL and (B) SL ESCs at 1.5 days of differentiation in FA using strand-specific probe. Nuclei are shown in blue (DAPI staining). White arrowheads indicate the location of the *Xist* signals. Quantification of the different *Xist* RNA patterns is shown. The ESC line used was E14tg2a (XY1). The scale bar represents 5 μm.

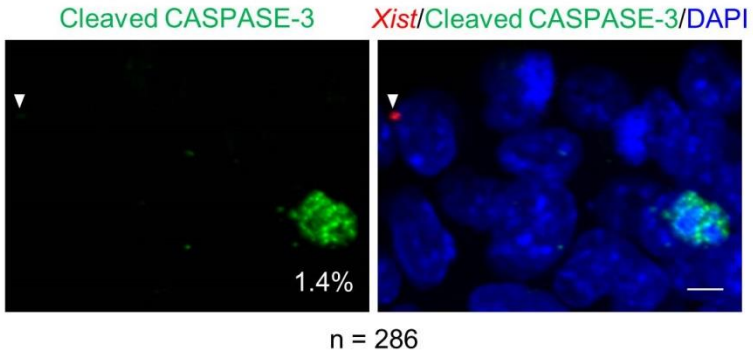

Figure 5.2: Male cells with *Xist* cloud do not express active CASPASE-3.
Immuno RNA FISH for *Xist* (red) and cleaved CASPASE-3 (green) in male (XY1) 2iL ESCs at 1.5 days of differentiation in FA. Nuclei are shown in blue (DAPI staining). White arrowhead indicates the location of an *Xist* RNA cloud. The percentage of cleaved CASPASE-3-positive cells is indicated. None of the cells analysed were positive for both *Xist* and cleaved CASPASE-3. The scale bar represents 5 μm.

Accumulation of the repressive histone mark trimethyl-H3K27 (H3K27me3) on the inactivating X-chromosome is an event associated with XCI in female cells (Plath et al., 2003; Silva et al., 2003). Interestingly, H3K27me3 accumulation on the X-chromosome was observed in 63% of male cells showing *Xist* RNA cloud (Figure 5.3A). I then addressed the status of acetyl-H3K27 (H3K27ac), which is a mark of active enhancers (Creyghton et al., 2010). H3K27 hypoacetylation was found at the male *Xist* RNA cloud (Figure 5.3B). Negative control cells, in which the X-chromosome is marked by DNA FISH but there is lack of H3K27me3 and existence of H3K27ac, are also presented (Figures 5.3C and 5.3D). These results indicate that a silencing epigenetic signature has formed in the *Xist*-coated male X-chromosome.

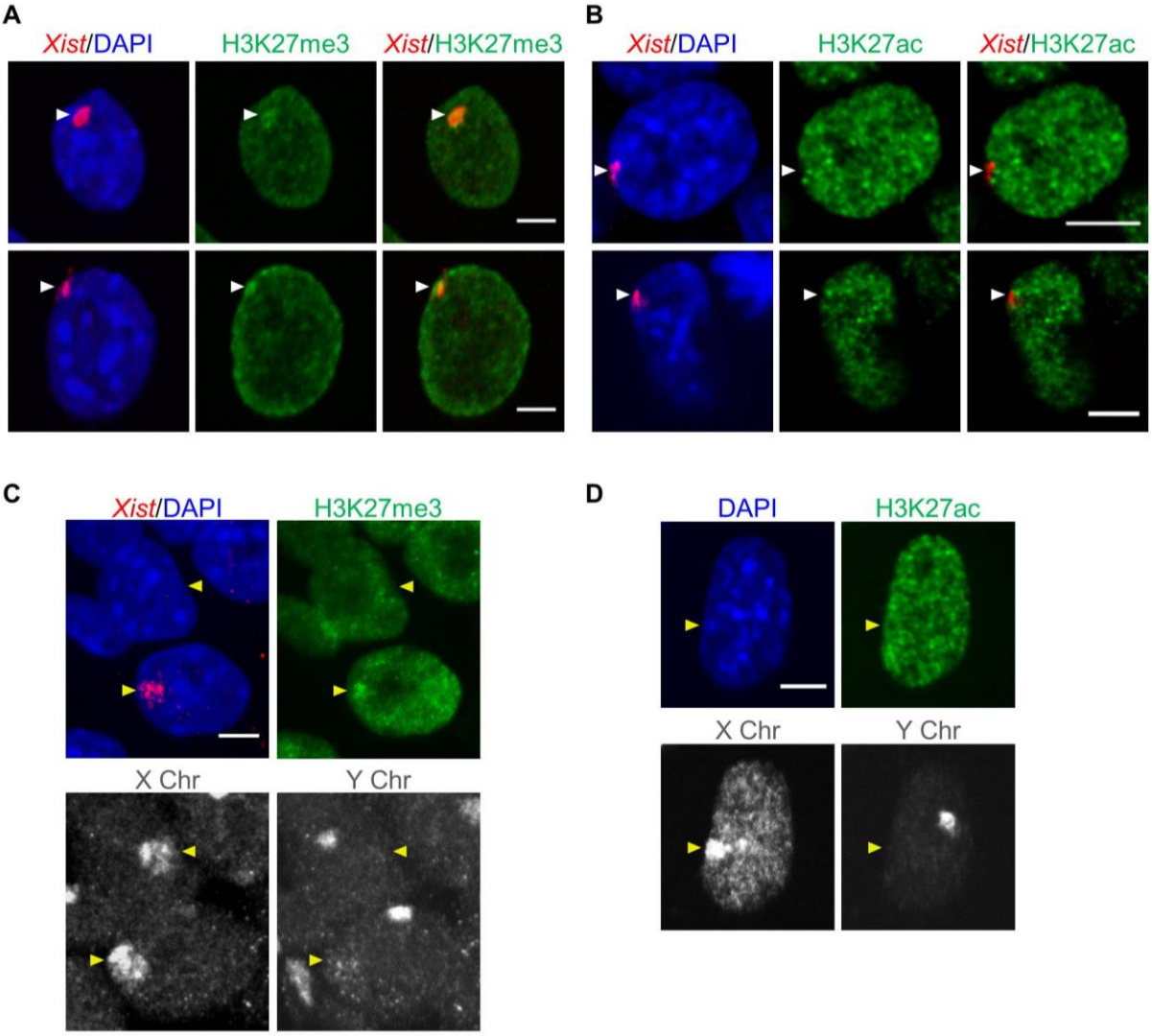

Figure 5.3: Differentiating male cells show accumulation of H3K27me3 and lack of H3K27ac.

(A and B) Immuno RNA FISH for *Xist* (red) and (A) H3K27me3 or (B) H3K27ac (green) in male 2iL ESCs at 1.5 days of differentiation in FA. Nuclei are shown in blue (DAPI staining). White arrowheads indicate the location of the *Xist* cloud.

(C) Immuno RNA FISH for *Xist* (red) and H3K27me3 (green) in male 2iL ESCs at 1.5 days of differentiation in FA with subsequent DNA FISH XY paint (greyscale). Nuclei are shown in blue (DAPI staining). Yellow arrowheads indicate the location of the X-chromosome. A cell lacking H3K27me3 on the X-chromosome is shown as a negative control.

(D) Immunofluorescence for H3K27ac (green) in male 2iL ESCs at 1.5 days of differentiation in FA with subsequent DNA FISH XY paint (greyscale). Nuclei are shown in blue (DAPI staining). Yellow arrowheads indicate the location of the X-chromosome. A cell displaying H3K27ac on the X-chromosome is shown as a negative control.

The ESC line used was E14tg2a (XY1). The scale bar represents 5 µm.

To examine whether *Xist* accumulation was inducing gene silencing, nascent transcripts of five X-linked genes – *Rnf12*, *Nexmif*, *Nsdhl*, *Wbp5*, and *Huwe1* – were analysed by RNA FISH. The choice of X-linked genes was based on their distance to the *Xist* locus, on their expression levels in male early differentiating cells according to our RNA-seq data, and on whether they are silenced at an early or late stage as reported by Marks and colleagues (Marks et al., 2015). *Huwe1* is quite distant from *Xist* (~48Mb), and the distance between the remaining genes and *Xist* ranges between 474kb and 33Mb. Furthermore, it has been reported that *Huwe1* is silenced late during XCI, whilst silencing of the other selected genes occurs at an early stage (Marks et al., 2015). The percentage of cells expressing *Rnf12*, *Nsdhl*, and *Nexmif* was between 3- and 4-fold lower in male cells showing *Xist* cloud than in male cells lacking *Xist* accumulation (Figures 5.4A-C). In the case of *Wbp5*, no examples of gene expression were found at the male X-chromosome coated by *Xist*, while *Wbp5* expression was detected in 9% of cells without *Xist* cloud (Figure 5.4C). In contrast, *Huwe1* showed no difference between cells with or without *Xist* (Figures 5.4A and 5.4B). Moreover, for all X-linked genes analysed no differences were observed between cells with *Xist* pinpoint signal and cells with no *Xist* expression at all (Figures 5.4A and 5.4B). These data are consistent with a rapid transient upregulation of *Xist* in male cells, an upregulation that lasts long enough to have an impact on early silenced genes but not to affect late silenced ones.

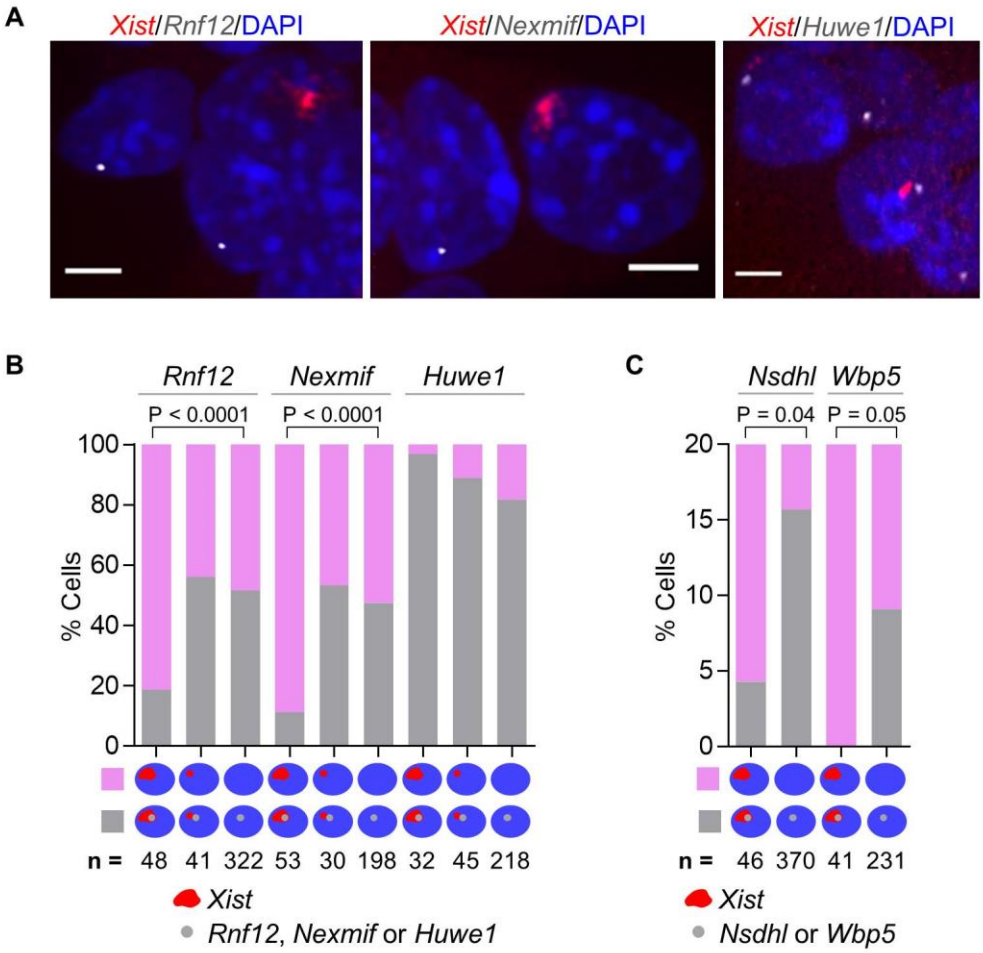

Figure 5.4: Male cells undergo partial X-linked gene silencing during differentiation.
(A) RNA FISH for *Xist* (red) and *Rnf12*, *Nexmif* or *Huwe1* (greyscale) in male (XY1) 2iL ESCs at 1.5 days of differentiation in FA. Nuclei are shown in blue (DAPI staining). The scale bar represents 5 µm.
(B) Quantification of the RNA FISH patterns for the X-linked genes *Rnf12*, *Nexmif* or *Huwe1* and *Xist* as shown in (A). Grey indicates the presence of *Rnf12*/*Nexmif*/*Huwe1* signal and pink indicates the absence of *Rnf12*/*Nexmif*/*Huwe1* signal.
(C) Quantification of the RNA FISH patterns for the X-linked genes *Nsdhl* or *Wbp5* and *Xist* in male 2iL ESCs at 1.5 days of differentiation in FA.
Fisher's exact test was used for statistical analyses.

Rnf12 and *Nexmif*, which were affected by *Xist* accumulation at the single cell level, were also analysed at the cell population level. Although there is some degree of *Rnf12* silencing at the single cell level, global levels of *Rnf12* were not diminished during differentiation of male cells (Figure 5.5). Interestingly, *Nexmif* was transiently upregulated shortly before *Xist* during differentiation of both male and female cells (Figure 5.5). This may be indicative of a role in the regulation of *Xist*. As far as I am aware, *Nexmif* has not been associated with the process of XCI and it would be interesting to address this question in the future.

Altogether, the results presented in this section show that several events associated with the process of XCI in female cells also take place during male differentiation. However, unlike female, male XCI is partial, transient and rapid.

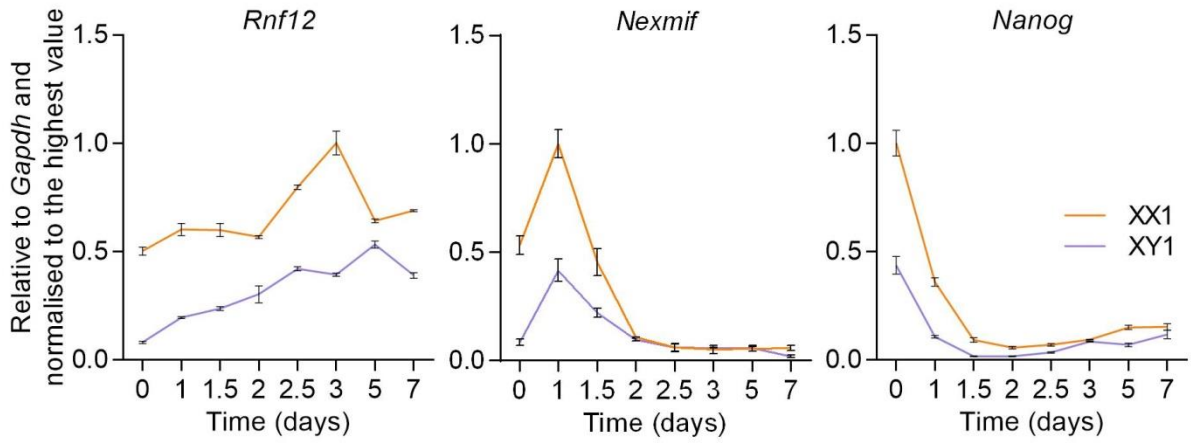

Figure 5.5: Cell population analysis of the genes affected by *Xist* coating of the male X-chromosome.
qRT-PCR analysis of *Rnf12*, *Nexmif*, and *Nanog* during differentiation of female (XX1) and male (XY1) ESCs in FA. Before differentiation, cells were maintained in 2iL. Data shown are the mean of three technical replicates. Error bars represent ± SD.

5.2.2 Female cells undergo transient biallelic *Xist* upregulation at the onset of differentiation

It has been proposed that a mechanism of counting and choice precedes initiation of XCI in female cells (Monkhorst et al., 2008). The observed upregulation of *Xist* in male cells, which possess only one X-chromosome, questions the existence of this mechanism preceding initiation of XCI. To address this, I performed *Xist* RNA FISH in differentiating female nPSCs. In section 3.2.1, I showed that the female ESC line analysed here does not express *Xist* in self-renewing conditions. At 1.5 days of differentiation, I observed that 30% of the female cells expressing *Xist* display RNA accumulation on both X-chromosomes which can be visualized as two clouds (Figure 5.6A). Some of the cells also exhibited one *Xist* pinpoint signal and one cloud or two pinpoint signals (Figure 5.6A). Control experiments revealed that 99% of the cells in this female ESC line have no more than two X-chromosomes (Figure 5.6B) demonstrating that these results cannot be explained by the occurrence of tetraploid cells in culture.

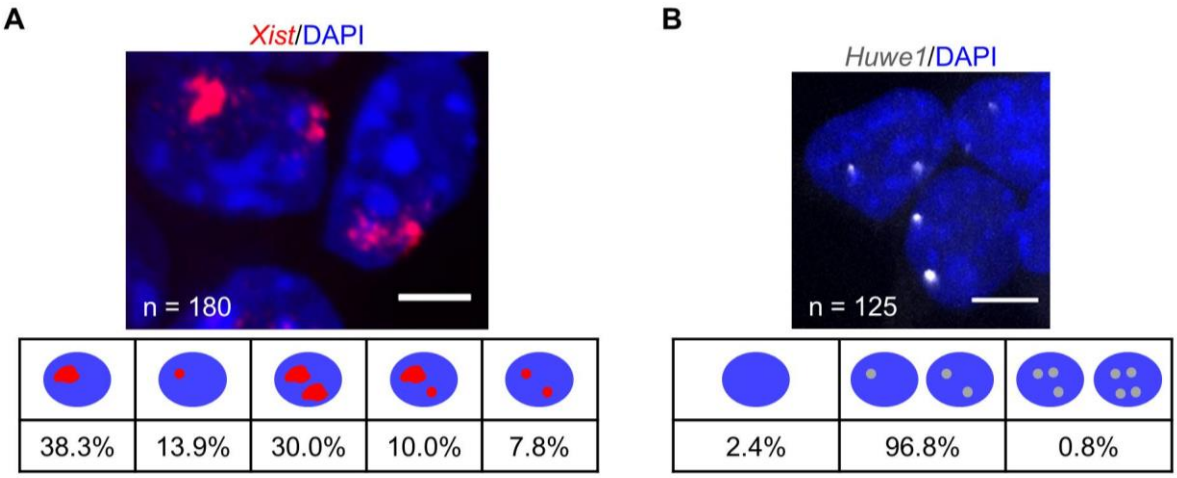

Figure 5.6: Female cells display two *Xist* clouds at the onset of differentiation.
(A) RNA FISH for *Xist* (red) in female (XX1) 2iL ESCs at 1.5 days EpiSC differentiation in FA using strand-specific probe. Nuclei are shown in blue (DAPI staining). Quantification of the different *Xist* RNA patterns is shown.
(B) RNA FISH in female (XX1) 2iL ESCs with a strand-specific probe detecting X-encoded nascent RNA of Huwe1 (greyscale). Nuclei are shown in blue (DAPI staining). Quantification of the different RNA FISH patterns is shown.
The scale bar represents 5 µm.

To assess whether *Xist* accumulation is inducing gene silencing on both X-chromosomes, I carried out RNA FISH analysis of *Rnf12* and *Huwe1* nascent transcripts in female cells after 1.5 days of differentiation (Figures 5.7A and 5.7B). The incidence of biallelic silencing of *Rnf12* was 12-fold greater in female cells exhibiting *Xist* RNA

accumulation on both X-chromosomes than in cells not expressing *Xist* (Figure 5.7B). On the other hand, *Huwe1* showed no difference between the two groups (Figure 5.7B). These results are in agreement with the data shown for male cells in which all X-linked genes analysed except *Huwe1* show some degree of silencing.

These results suggest that the choice of which X-chromosome is going to be irreversibly silenced may follow rather than precede the initiation of XCI.

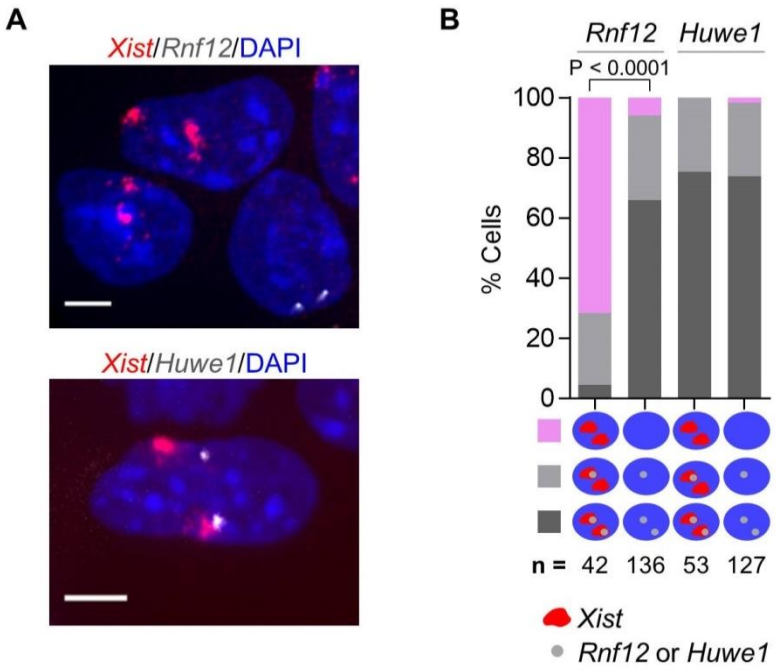

Figure 5.7: Female cells undergo transient biallelic silencing of X-linked genes during differentiation.
(A) RNA FISH for *Xist* (red) and *Rnf12* or *Huwe1* (greyscale) in female (XX1) 2iL ESCs at 1.5 days of differentiation in FA. Nuclei are shown in blue (DAPI staining). The scale bar represents 5 μm.
(B) Quantification of the RNA FISH patterns for the X-linked genes *Rnf12* or *Huwe1* and *Xist* as shown in (A). Dark grey indicates biallelic *Rnf12*/*Huwe1* signal, light grey indicates monoallelic *Rnf12*/*Huwe1* signal and pink indicates absence of *Rnf12*/*Huwe1* signal.

5.2.3 Transient *Xist* upregulation occurs as nPSCs become NANOG-negative

To investigate whether *Xist* upregulation corresponds with a particular differentiation stage, I analysed the expression of NANOG and OCT4 relative to *Xist* at the single cell level in both male and female differentiating cells (Figures 5.8 and 5.9). First, expression profile of NANOG and OCT4 was determined in the bulk population of cells independent of the *Xist* status. In both male and female, most cells remained OCT4-high whereas NANOG expression was variable at 1.5 days of differentiation (Figures 5.8A-B and 5.9A-B). I

hypothesise that this variability was due to asynchronicity in nPSC differentiation, as previously reported in Kalkan and et al., 2017. Expression of NANOG and OCT4 was then analysed focusing only on *Xist*-expressing male differentiating cells. Interestingly, *Xist* upregulation occurred exclusively in male cells that were either NANOG-low or NANOG-negative (Figures 5.8A and 5.8C). Moreover, most *Xist*-expressing male cells were OCT4-high (Figures 5.8A and 5.8C). Expression profiles of NANOG and OCT4 were also examined specifically in differentiating female cells with biallelic expression of *Xist*. Likewise, biallelic *Xist* upregulation was mainly found in female cells that were OCT4-high and NANOG-low or NANOG-negative (Figures 5.9A and 5.9C).

These results indicate that transient *Xist* upregulation occurs in a defined developmental window and in close relationship with a weakening naïve network.

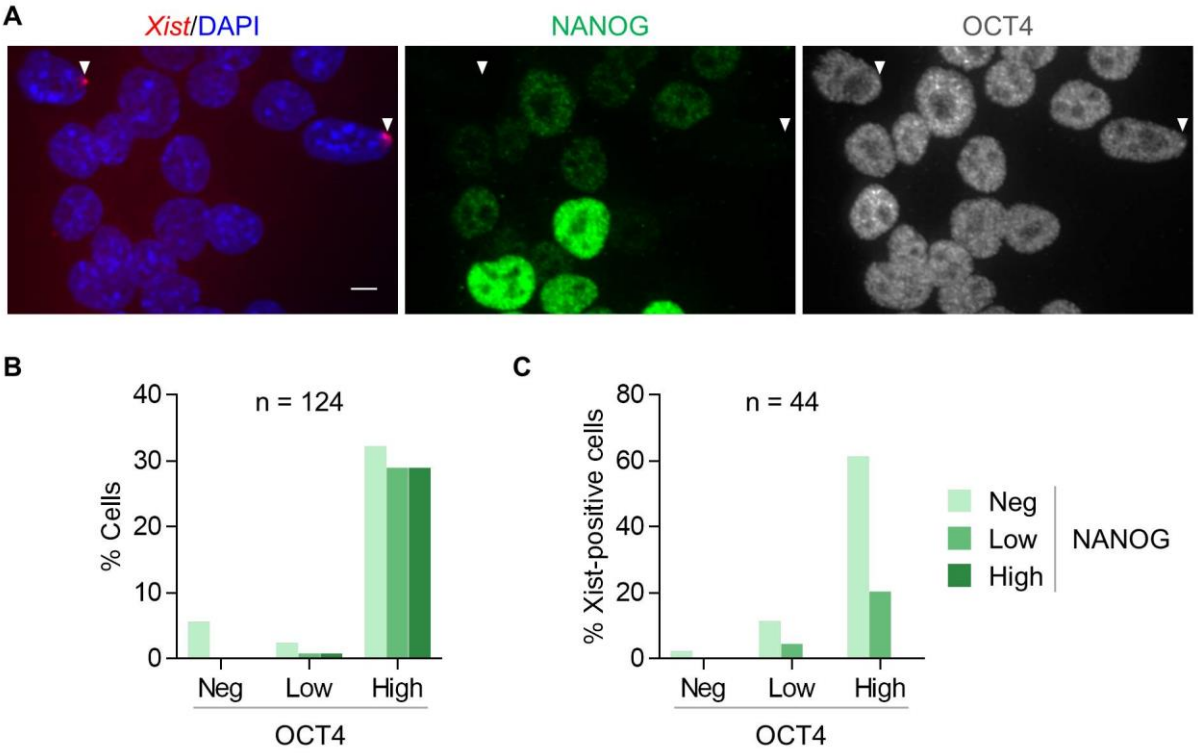

Figure 5.8: Analysis of the expression of NANOG and OCT4 relative to *Xist* at the single cell level in male differentiating cells.
(A) Immuno RNA FISH for *Xist* (red), NANOG (green), and OCT4 (greyscale) in male (XY1) 2iL ESCs at 1.5 days of differentiation in FA. Nuclei are shown in blue (DAPI staining). White arrowheads indicate the location of the *Xist* clouds.
(B and C) Quantification of the NANOG and OCT4 expression profile in (B) the bulk population and in (C) cells with *Xist* cloud as shown in (A).
The scale bar represents 5 μm.

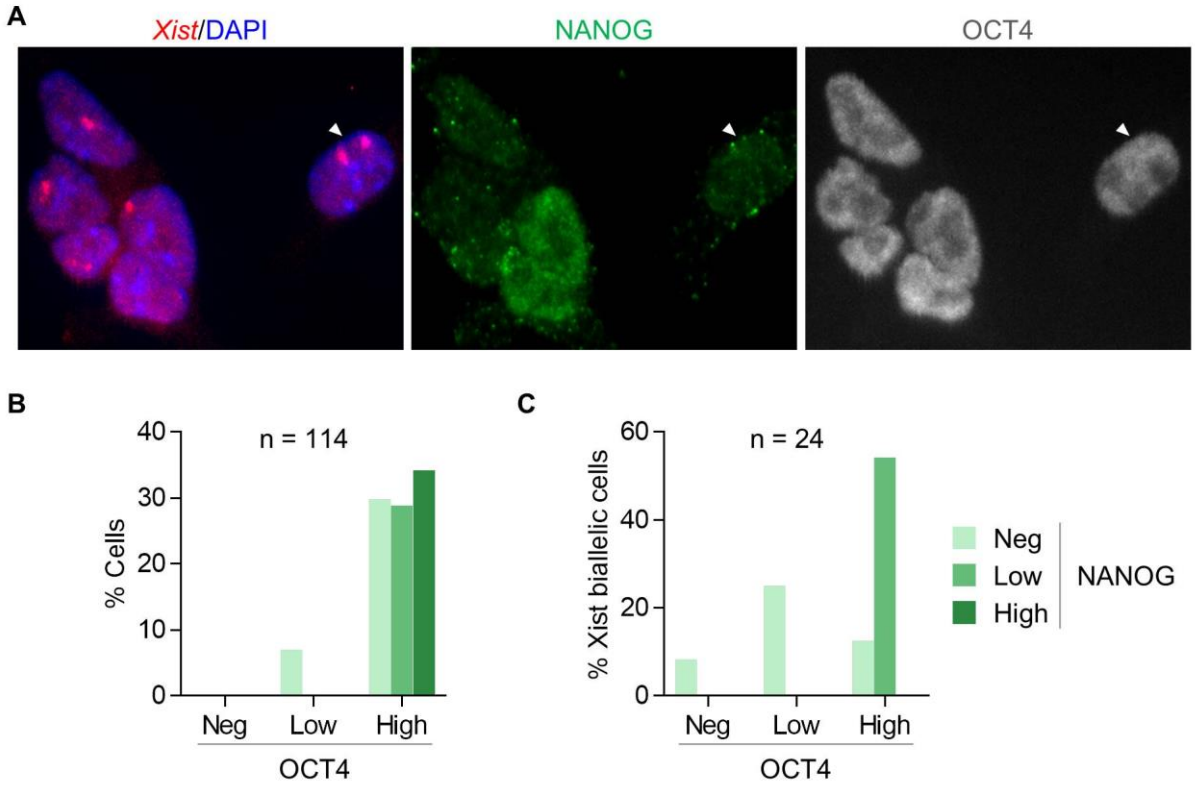

Figure 5.9: Analysis of the expression of NANOG and OCT4 relative to *Xist* at the single cell level in female differentiating cells.
(A) Immuno RNA FISH for *Xist* (red), NANOG (green) and OCT4 (greyscale) in female (XX1) 2iL ESCs at 1.5 days of differentiation in FA. Nuclei are shown in blue (DAPI staining). White arrowhead indicates the location of a cell with biallelic *Xist* upregulation.
(B and C) Quantification of NANOG and OCT4 expression profile in (B) the bulk population and in (C) cells with biallelic *Xist* expression as shown in (A).
The scale bar represents 5 μm.

5.2.4 *Xist* is transiently upregulated monoallelically in males and biallelically in females during embryo implantation

The E4.5 naïve epiblast is molecularly and functionally very similar to *in vitro* 2iL nPSCs (Boroviak et al., 2015; Nichols and Smith, 2009). Given the observed transient upregulation of *Xist* during *in vitro* male nPSC differentiation, I investigated whether this phenomenon also takes place during *in vivo* differentiation of the naïve pluripotent epiblast. Male and female embryos could be readily distinguished based on *Xist* expression patterns as cells of extraembryonic tissues in female embryos, but not male, would display an *Xist* RNA cloud at all developmental stages examined. Sex was confirmed for a number of embryos by PCR analysis (Figure 5.10A). I started by performing *Xist* RNA FISH on E4.5 embryos to assess whether they present the same *Xist* expression pattern as their *in vitro* counterpart nPSCs as shown in section 3.2.1. I observed that E4.5 naïve epiblast cells do not display *Xist* expression in either sex (Figure 5.10B) which is in agreement with the findings in nPSCs. From E4.5, the embryo starts implanting and naïve pluripotent gene expression is rapidly downregulated (Boroviak et al., 2015). Thus, E5.5 male and female post-implantation embryos were analysed in an attempt to find a match between this developmental stage and the differentiation time point analysed *in vitro* – 1.5 days. At E5.5, I also failed to detect *Xist* expression in males whereas female epiblasts already exhibited one *Xist* cloud in nearly all cells (Figure 5.10B), meaning that XCI had already been completed. This prompted me to examine earlier time points. Remarkably, at E4.75-5.0, I found 1 to 3 cells per male epiblast exhibiting *Xist* upregulation (Figure 5.11A and 5.11B). When analysing female epiblast cells for the same time points, I observed that *Xist* was biallelically upregulated in up to 10% of the epiblast cells showing expression of *Xist* (Figures 5.11A-C). Together, these data indicate that at implantation stage, male and female epiblast cells undergo transient and rapid monoallelic and biallelic upregulation of *Xist*, respectively, and this correlates with the downregulation of the naïve epiblast network.

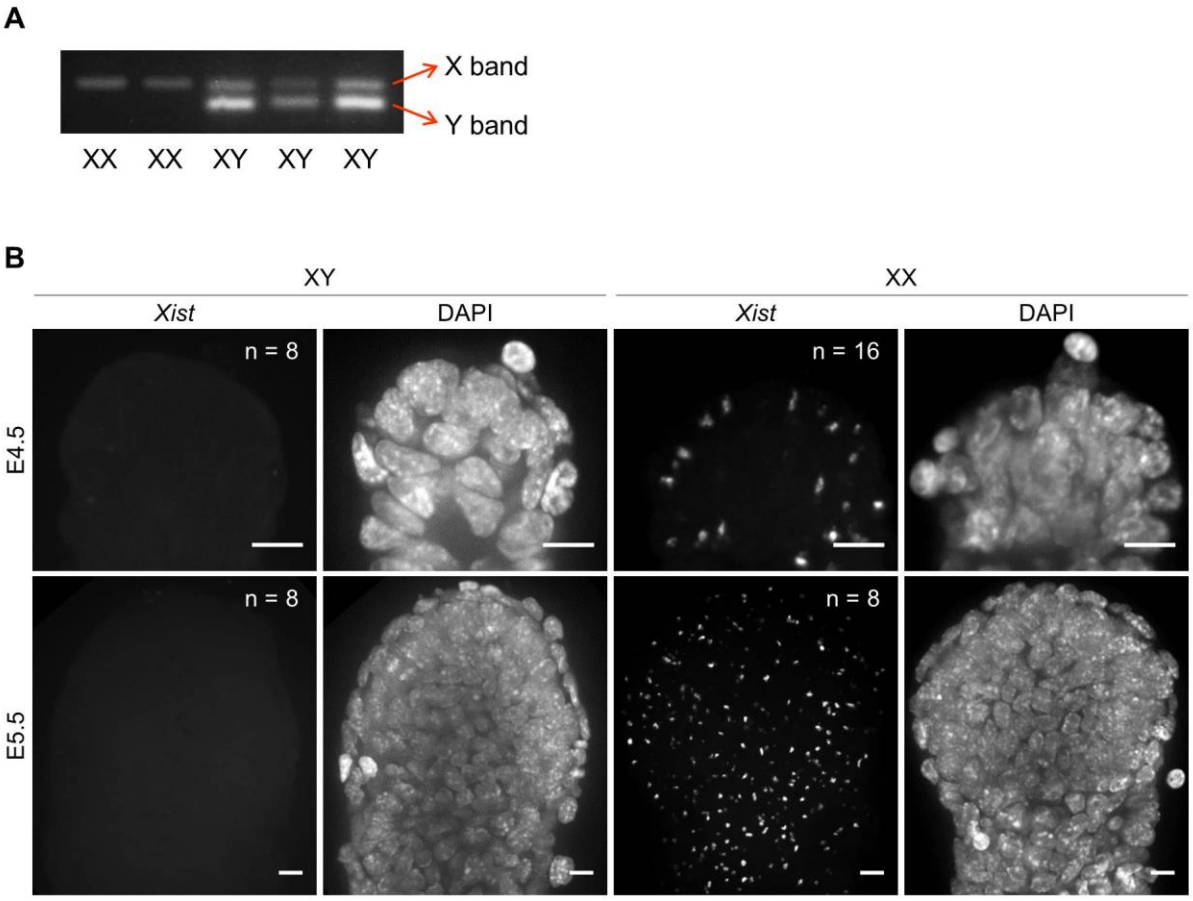

Figure 5.10: *Xist* is not expressed at E4.5 *in vivo*.
(A) PCR-based sex determination of mouse embryos used in this study.
(B) RNA FISH for *Xist* in representative male and female epiblasts of mouse embryos at E4.5 and E5.5. The scale bar represents 10 µm.

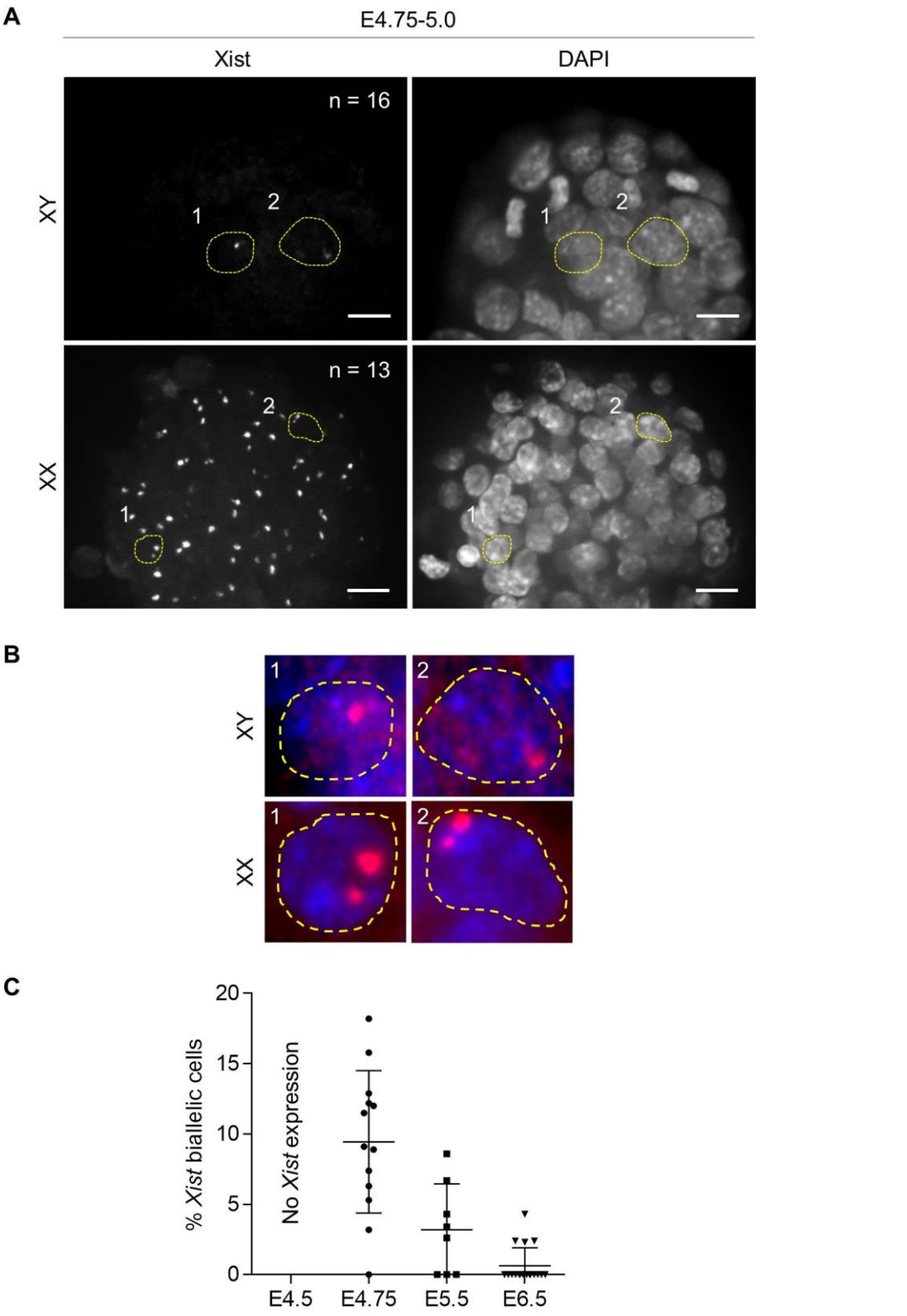

Figure 5.11: *Xist* is transiently upregulated monoallelically in males and biallelically in females *in vivo*.

Figure legend continues on the next page.

Figure 5.11: *Xist* is transiently upregulated monoallelically in males and biallelically in females in vivo.

(A) RNA FISH for *Xist* in representative male and female epiblasts of mouse embryos at E4.75-5.0. Examples of cells with monoallelic *Xist* expression in males and biallelic expression in females are delineated with yellow dashed lines. The scale bar represents 10 μm.

(B) Higher magnifications of the cells delineated with yellow dashed lines in (A) are shown.

(C) Graphical representation of the percentage of cells with biallelic *Xist* over the total number of epiblast cells expressing *Xist* analysed in female embryos at indicated developmental stages.

5.3 Discussion

In this chapter, I demonstrated that *Xist* accumulates transiently on the male X-chromosome and induces partial X-linked transcriptional silencing in early differentiating cells. Additionally, I observed transient biallelic accumulation of *Xist* and partial biallelic X-linked gene silencing in female differentiating cells. I would like to note that the percentages reported here are only representative of a snapshot in time. Due to the asynchronous nature of differentiation and transience of the events described in this study, I hypothesise that the fraction of cells displaying monoallelic *Xist* upregulation in males or biallelic in females at 1.5 days of differentiation may underrepresent the actual percentage of cells undergoing this phenomenon throughout differentiation. It would be interesting to investigate this further by developing an *Xist* reporter system for male and female nPSCs in order to monitor *Xist* expression at the single cell level during differentiation.

It has been previously shown that male E4.5 naïve epiblast cells exhibit one pinpoint *Xist* signal, whereas two *Xist* pinpoint signals could be detected in the majority of female E4.5 naïve epiblast cells (Sheardown et al., 1997). Conversely, I demonstrated that *Xist* is not expressed in E4.5 naïve epiblast cells in either sex. These differences might be explained by the fact that, in previous studies, FISH probes were not strand-specific and thus would also detect the expression of *Xist* antisense RNA, *Tsix*. Here, the embryos were analysed using a strand-specific probe that only detects the expression of *Xist*. Having established that *Xist* is not expressed in pre-implantation male naïve epiblast cells, allowed the detection of an upregulation of *Xist* in a small percentage of male epiblast cells shortly after implantation. Similarly, *Xist* was expressed biallelically in approximately 10% of *Xist* expressing female epiblast cells at E4.75-E5.0. Interestingly, this is the time point *in vivo* when the naïve network is downregulated (Boroviak et al., 2015). As for the nPSCs, the asynchrony of cell differentiation and the transiency of this event need to be taken into consideration.

Chapter 6
General discussion

6.1 Parallels to human XCI

It is well established that female mice undergo X-chromosome dosage compensation via XCI in two waves. At 4- to 8-cell stage, female mouse embryos initiate the first wave of XCI (Okamoto et al., 2004). This results in silencing of the X-chromosome of paternal origin in all cells of the early embryo in a process known as imprinted XCI (Takagi and Sasaki, 1975; West et al., 1977). The paternal X-chromosome is transiently reactivated in cells of the naïve pluripotent epiblast at E4.5 (Mak et al., 2004; Okamoto et al., 2004; Silva et al., 2009; Williams et al., 2011), and around 24 hours later a second wave of random XCI takes place (Okamoto et al., 2005).

Similarly to the mouse, random XCI also occurs after human embryo implantation, leading to inactivation of either the paternal or the maternal X-chromosome. However, in contrast to the mouse, recent reports demonstrated that imprinted XCI does not take place in human pre-implantation embryos (Moreira de Mello et al., 2010; Okamoto et al., 2011; Petropoulos et al., 2016). According to Petropoulos and colleagues, dosage compensation in human pre-implantation embryos is achieved not by inactivation of one of the two X-chromosomes in the female, but rather by reducing X-linked gene expression of both female X-chromosomes (Petropoulos et al., 2016). This X-chromosome dampening (XCD) is thought to be mediated by the long non-coding *XIST* which is transcribed from both alleles throughout this process (Okamoto et al., 2011; Petropoulos et al., 2016; Vallot et al., 2017). Moreover, expression of *XIST*, which starts at the 4-8-cell state of the human embryo, increases over time up to E7.0 and correlates with X-linked dampening (Petropoulos et al., 2016). Interestingly, an expression imbalance between the X-chromosomes was detected from E6.0, suggesting that X-linked gene silencing may initiate in a progressive manner at this developmental stage (Vallot et al., 2017). However, these experiments were performed

with embryos cultured *in vitro* and potential differences with their *in vivo* counterparts cannot be excluded, meaning that caution should be used when interpreting these results.

Accumulation of *XIST* on the single X-chromosome was also observed in human male embryos, even though the proportion of *XIST*-expressing cells was discrepant between studies (Okamoto et al., 2011; Petropoulos et al., 2016; Vallot et al., 2017). I hypothesise that accumulation of *XIST* on the single X-chromosome in human male embryos and on both X-chromosomes in human female embryos might be akin to what I am reporting in this dissertation for the mouse. It remains to be elucidated whether this phenomenon observed in the human is associated with the naïve transcription factor network.

6.2 Progress in understanding XCI

According to the prevailing paradigm, *Xist* is expressed at low levels in both female and male mouse nPSCs (Panning et al., 1997; Sheardown et al., 1997). However, most of the studies investigating XCI have been performed using ESCs cultured in SL, which are known to be suboptimal (Chambers et al., 2007; Ficz et al., 2013; Habibi et al., 2013; Leitch et al., 2013; Marks et al., 2012; Martello and Smith, 2014). Using conditions that enable the culture of mouse nPSCs that closely resemble the naïve pluripotent epiblast both transcriptionally and epigenetically (Boroviak et al., 2014; Ficz et al., 2013; Habibi et al., 2013; Hackett et al., 2017; Leitch et al., 2013), I demonstrated that *Xist* is indeed not expressed in these cells (Chapter 3). As shown in this study and in previous publications (Martello and Smith, 2014), 2iL culture conditions increase the strength of the naïve pluripotent network by augmenting the expression of its members. I observed that, in the presence of a robust naïve network, the expression of *Xist* is repressed (Chapter 3). Importantly, these results were corroborated by *Xist* RNA FISH analysis of male and female E4.5 embryos (Chapter 5). Similarly to nPSCs, *Xist* is not expressed in the naïve epiblast of E4.5 embryos, the starting identity from which random XCI occurs (Chapter 5).

It has been proposed that random XCI has five key phases in the following order: counting, choice, initiation, establishment, and maintenance (Avner and Heard, 2001; Boumil and Lee, 2001; Lyon, 1999). The first step in the process of XCI consists of a recognition step in which the number of X-chromosomes in the cell is counted relative to the number of autosomes in order to ensure that only a single X-chromosome is active per diploid genome, i.e. that XCI occurs for females but not males (Grumbach et al., 1963; Lyon, 1962). A process of choice then occurs, whereby one of the two X-chromosomes in the female cell is selected for inactivation (Cattanach and Williams, 1972). According to the current paradigm, initiation of XCI occurs after these two phases have taken place and coincides with the upregulation of *Xist* from the future Xi (Brown et al., 1991). Here, I showed that *Xist*

accumulates transiently on the single male X-chromosome and on both female X-chromosomes at the onset of naïve cell differentiation (Chapter 4). These findings suggest that the phases of counting and choice are not required for XCI initiation. Moreover, our results indicate that downregulation of the naïve transcription factor network acts as the main trigger for the initiation of XCI regardless of the gender (Figure 6.1).

Therefore, I propose that counting and choice only take place after gender-independent initiation of XCI. This represents a paradigm-shift in our understanding of the XCI process.

I also showed that accumulation of *Xist* on the male X-chromosome triggers the enrichment of repressive epigenetic marks leading to partial X-linked gene silencing (Chapter 5). Importantly, I observed that these steps take place within a defined window of time where the process of XCI is known to be reversible (Wutz and Jaenisch, 2000), meaning that as long as *Xist* expression ceases within 3 days of differentiation any induced changes on the X-chromosome are fully reversible. Indeed, our data show that *Xist* expression is already downregulated by day 3 of differentiation of male nPSCs. Therefore, I hypothesise that in the mouse species a counting mechanism occurs only after XCI initiation, but still during the reversible period.

Previous studies suggested that initiation of XCI in females is preceded by pairing of the two Xic loci and that the process of choice was dependent on pairing, thereby restricting XCI to female cells (Bacher et al., 2006; Xu et al., 2006). Our data indicate that pairing of the two Xic and choice occur after initiation of XCI. However, I speculate that the requirement of two Xic for the process of pairing and choice to occur might still be one of the mechanisms ensuring that irreversible XCI takes place in female cells only. Moreover, although the negative regulation of *Xist* by the naïve transcription factor network is the same in male and female cells, all known *Xist* activators are located on the X-chromosome, meaning that they will be duplicated in females relative to males (Chureau et al., 2011; Jonkers et al., 2009; Tian et al., 2010). This will ensure that only female cells can overcome the threshold for permanent XCI to occur. It could be interesting to further understand how these and other mechanisms allow XCI to be maintained in females only.

In conclusion, our study re-defines the paradigm of XCI and opens up new avenues to investigate how this process is regulated.

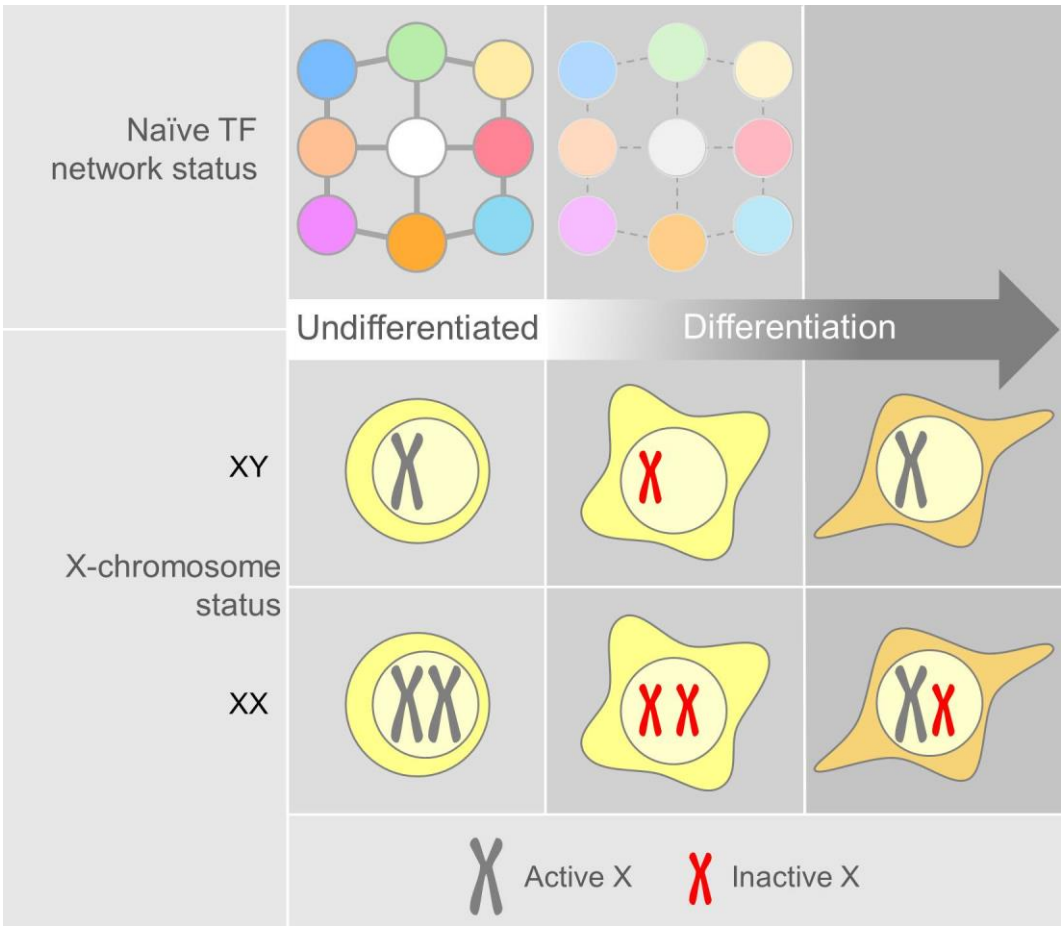

Figure 6.1: The link between naïve pluripotency and XCI.
Schematic representation of the main findings of this thesis. In both male and female nPSCs with a robust naïve transcription factor network, *Xist* is not expressed. At the onset of differentiation, and as the naïve network weakens, *Xist* transiently coats the single X-chromosome in males and both X-chromosomes in females. When these cells are fully differentiated, *Xist* expression is extinguished in males and there is coating of only one of the two X-chromosomes in females.

Chapter 7
References

Ahmed, K., Dehghani, H., Rugg-Gunn, P., Fussner, E., Rossant, J., and Bazett-Jones, D.P. (2010). Global chromatin architecture reflects pluripotency and lineage commitment in the early mouse embryo. PLoS One *5*, e10531.

Anguera, M.C., Ma, W., Clift, D., Namekawa, S., Kelleher, R.J., 3rd, and Lee, J.T. (2011). Tsx produces a long noncoding RNA and has general functions in the germline, stem cells, and brain. PLoS Genet *7*, e1002248.

Arnold, S.J., and Robertson, E.J. (2009). Making a commitment: cell lineage allocation and axis patterning in the early mouse embryo. Nat Rev Mol Cell Biol *10*, 91-103.

Auclair, G., Guibert, S., Bender, A., and Weber, M. (2014). Ontogeny of CpG island methylation and specificity of DNMT3 methyltransferases during embryonic development in the mouse. Genome Biol *15*, 545.

Augui, S., Filion, G.J., Huart, S., Nora, E., Guggiari, M., Maresca, M., Stewart, A.F., and Heard, E. (2007). Sensing X chromosome pairs before X inactivation via a novel X-pairing region of the Xic. Science *318*, 1632-1636.

Avilion, A.A., Nicolis, S.K., Pevny, L.H., Perez, L., Vivian, N., and Lovell-Badge, R. (2003). Multipotent cell lineages in early mouse development depend on SOX2 function. Genes Dev *17*, 126-140.

Avner, P., and Heard, E. (2001). X-chromosome inactivation: counting, choice and initiation. Nat Rev Genet *2*, 59-67.

Bacher, C.P., Guggiari, M., Brors, B., Augui, S., Clerc, P., Avner, P., Eils, R., and Heard, E. (2006). Transient colocalization of X-inactivation centres accompanies the initiation of X inactivation. Nat Cell Biol *8*, 293-299.

Bao, S., Tang, F., Li, X., Hayashi, K., Gillich, A., Lao, K., and Surani, M.A. (2009). Epigenetic reversion of post-implantation epiblast to pluripotent embryonic stem cells. Nature *461*, 1292-1295.

Barakat, T.S., Gunhanlar, N., Pardo, C.G., Achame, E.M., Ghazvini, M., Boers, R., Kenter, A., Rentmeester, E., Grootegoed, J.A., and Gribnau, J. (2011). RNF12 activates Xist and is essential for X chromosome inactivation. PLoS Genet *7*, e1002001.

Barakat, T.S., Loos, F., van Staveren, S., Myronova, E., Ghazvini, M., Grootegoed, J.A., and Gribnau, J. (2014). The trans-activator RNF12 and cis-acting elements effectuate X chromosome inactivation independent of X-pairing. Mol Cell *53*, 965-978.

Bates, L.E., and Silva, J.C. (2017). Reprogramming human cells to naive pluripotency: how close are we? Curr Opin Genet Dev *46*, 58-65.

Beard, C., Li, E., and Jaenisch, R. (1995). Loss of methylation activates Xist in somatic but not in embryonic cells. Genes Dev *9*, 2325-2334.

Beletskii, A., Hong, Y.K., Pehrson, J., Egholm, M., and Strauss, W.M. (2001). PNA interference mapping demonstrates functional domains in the noncoding RNA Xist. Proc Natl Acad Sci U S A *98*, 9215-9220.

Boeuf, H., Hauss, C., Graeve, F.D., Baran, N., and Kedinger, C. (1997). Leukemia inhibitory factor-dependent transcriptional activation in embryonic stem cells. J Cell Biol *138*, 1207-1217.

Boroviak, T., Loos, R., Bertone, P., Smith, A., and Nichols, J. (2014). The ability of inner-cell-mass cells to self-renew as embryonic stem cells is acquired following epiblast specification. Nat Cell Biol *16*, 516-528.

Boroviak, T., Loos, R., Lombard, P., Okahara, J., Behr, R., Sasaki, E., Nichols, J., Smith, A., and Bertone, P. (2015). Lineage-Specific Profiling Delineates the Emergence and Progression of Naive Pluripotency in Mammalian Embryogenesis. Dev Cell *35*, 366-382.

Borsani, G., Tonlorenzi, R., Simmler, M.C., Dandolo, L., Arnaud, D., Capra, V., Grompe, M., Pizzuti, A., Muzny, D., Lawrence, C.*, et al.* (1991). Characterization of a murine gene expressed from the inactive X chromosome. Nature *351*, 325-329.

Boumil, R.M., and Lee, J.T. (2001). Forty years of decoding the silence in X-chromosome inactivation. Hum Mol Genet *10*, 2225-2232.

Bourillot, P.Y., Aksoy, I., Schreiber, V., Wianny, F., Schulz, H., Hummel, O., Hubner, N., and Savatier, P. (2009). Novel STAT3 target genes exert distinct roles in the inhibition of mesoderm and endoderm differentiation in cooperation with Nanog. Stem Cells *27*, 1760-1771.

Bradley, A., Evans, M., Kaufman, M.H., and Robertson, E. (1984). Formation of germ-line chimaeras from embryo-derived teratocarcinoma cell lines. Nature *309*, 255-256.

Brockdorff, N., Ashworth, A., Kay, G.F., Cooper, P., Smith, S., McCabe, V.M., Norris, D.P., Penny, G.D., Patel, D., and Rastan, S. (1991). Conservation of position and exclusive expression of mouse Xist from the inactive X chromosome. Nature *351*, 329-331.

Brockdorff, N., Ashworth, A., Kay, G.F., McCabe, V.M., Norris, D.P., Cooper, P.J., Swift, S., and Rastan, S. (1992). The product of the mouse Xist gene is a 15 kb inactive X-specific transcript containing no conserved ORF and located in the nucleus. Cell *71*, 515-526.

Brons, I.G., Smithers, L.E., Trotter, M.W., Rugg-Gunn, P., Sun, B., Chuva de Sousa Lopes, S.M., Howlett, S.K., Clarkson, A., Ahrlund-Richter, L., Pedersen, R.A.*, et al.* (2007). Derivation of pluripotent epiblast stem cells from mammalian embryos. Nature *448*, 191-195.

Brook, F.A., and Gardner, R.L. (1997). The origin and efficient derivation of embryonic stem cells in the mouse. Proc Natl Acad Sci U S A *94*, 5709-5712.

Brown, C.J., Ballabio, A., Rupert, J.L., Lafreniere, R.G., Grompe, M., Tonlorenzi, R., and Willard, H.F. (1991). A gene from the region of the human X inactivation centre is expressed exclusively from the inactive X chromosome. Nature *349*, 38-44.

Brown, C.J., Hendrich, B.D., Rupert, J.L., Lafreniere, R.G., Xing, Y., Lawrence, J., and Willard, H.F. (1992). The human XIST gene: analysis of a 17 kb inactive X-specific RNA that contains conserved repeats and is highly localized within the nucleus. Cell *71*, 527-542.

Brown, C.J., and Willard, H.F. (1994). The human X-inactivation centre is not required for maintenance of X-chromosome inactivation. Nature *368*, 154-156.

Brown, S.D. (1991). XIST and the mapping of the X chromosome inactivation centre. Bioessays *13*, 607-612.

Buehr, M., Meek, S., Blair, K., Yang, J., Ure, J., Silva, J., McLay, R., Hall, J., Ying, Q.L., and Smith, A. (2008). Capture of authentic embryonic stem cells from rat blastocysts. Cell *135*, 1287-1298.

Burdon, T., Stracey, C., Chambers, I., Nichols, J., and Smith, A. (1999). Suppression of SHP-2 and ERK signalling promotes self-renewal of mouse embryonic stem cells. Dev Biol *210*, 30-43.

Carbognin, E., Betto, R.M., Soriano, M.E., Smith, A.G., and Martello, G. (2016). Stat3 promotes mitochondrial transcription and oxidative respiration during maintenance and induction of naive pluripotency. EMBO J *35*, 618-634.

Cattanach, B.M., and Williams, C.E. (1972). Evidence of non-random X chromosome activity in the mouse. Genet Res *19*, 229-240.

Chambers, I., Colby, D., Robertson, M., Nichols, J., Lee, S., Tweedie, S., and Smith, A. (2003). Functional expression cloning of Nanog, a pluripotency sustaining factor in embryonic stem cells. Cell *113*, 643-655.

Chambers, I., Silva, J., Colby, D., Nichols, J., Nijmeijer, B., Robertson, M., Vrana, J., Jones, K., Grotewold, L., and Smith, A. (2007). Nanog safeguards pluripotency and mediates germline development. Nature *450*, 1230-1234.

Chew, J.L., Loh, Y.H., Zhang, W., Chen, X., Tam, W.L., Yeap, L.S., Li, P., Ang, Y.S., Lim, B., Robson, P.*, et al.* (2005). Reciprocal transcriptional regulation of Pou5f1 and Sox2 via the Oct4/Sox2 complex in embryonic stem cells. Mol Cell Biol *25*, 6031-6046.

Chuma, S., and Nakatsuji, N. (2001). Autonomous transition into meiosis of mouse fetal germ cells in vitro and its inhibition by gp130-mediated signaling. Dev Biol *229*, 468-479.

Chureau, C., Chantalat, S., Romito, A., Galvani, A., Duret, L., Avner, P., and Rougeulle, C. (2011). Ftx is a non-coding RNA which affects Xist expression and chromatin structure within the X-inactivation center region. Hum Mol Genet *20*, 705-718.

Costanzi, C., Stein, P., Worrad, D.M., Schultz, R.M., and Pehrson, J.R. (2000). Histone macroH2A1 is concentrated in the inactive X chromosome of female preimplantation mouse embryos. Development *127*, 2283-2289.

Creyghton, M.P., Cheng, A.W., Welstead, G.G., Kooistra, T., Carey, B.W., Steine, E.J., Hanna, J., Lodato, M.A., Frampton, G.M., Sharp, P.A.*, et al.* (2010). Histone H3K27ac separates active from poised enhancers and predicts developmental state. Proc Natl Acad Sci U S A *107*, 21931-21936.

Csankovszki, G., Panning, B., Bates, B., Pehrson, J.R., and Jaenisch, R. (1999). Conditional deletion of Xist disrupts histone macroH2A localization but not maintenance of X inactivation. Nat Genet *22*, 323-324.

da Rocha, S.T., Boeva, V., Escamilla-Del-Arenal, M., Ancelin, K., Granier, C., Matias, N.R., Sanulli, S., Chow, J., Schulz, E., Picard, C.*, et al.* (2014). Jarid2 Is Implicated in the Initial Xist-Induced Targeting of PRC2 to the Inactive X Chromosome. Mol Cell *53*, 301-316.

de Napoles, M., Mermoud, J.E., Wakao, R., Tang, Y.A., Endoh, M., Appanah, R., Nesterova, T.B., Silva, J., Otte, A.P., Vidal, M.*, et al.* (2004). Polycomb group proteins Ring1A/B link ubiquitylation of histone H2A to heritable gene silencing and X inactivation. Dev Cell *7*, 663-676.

Desbaillets, I., Ziegler, U., Groscurth, P., and Gassmann, M. (2000). Embryoid bodies: an in vitro model of mouse embryogenesis. Exp Physiol *85*, 645-651.

Doetschman, T.C., Eistetter, H., Katz, M., Schmidt, W., and Kemler, R. (1985). The in vitro development of blastocyst-derived embryonic stem cell lines: formation of visceral yolk sac, blood islands and myocardium. J Embryol Exp Morphol *87*, 27-45.

Donohoe, M.E., Silva, S.S., Pinter, S.F., Xu, N., and Lee, J.T. (2009). The pluripotency factor Oct4 interacts with Ctcf and also controls X-chromosome pairing and counting. Nature *460*, 128-132.

Dunn, S.J., Martello, G., Yordanov, B., Emmott, S., and Smith, A.G. (2014). Defining an essential transcription factor program for naive pluripotency. Science *344*, 1156-1160.

Efroni, S., Duttagupta, R., Cheng, J., Dehghani, H., Hoeppner, D.J., Dash, C., Bazett-Jones, D.P., Le Grice, S., McKay, R.D., Buetow, K.H.*, et al.* (2008). Global transcription in pluripotent embryonic stem cells. Cell Stem Cell *2*, 437-447.

Eggan, K., Akutsu, H., Hochedlinger, K., Rideout, W., 3rd, Yanagimachi, R., and Jaenisch, R. (2000). X-Chromosome inactivation in cloned mouse embryos. Science *290*, 1578-1581.

Escamilla-Del-Arenal, M., da Rocha, S.T., and Heard, E. (2011). Evolutionary diversity and developmental regulation of X-chromosome inactivation. Hum Genet *130*, 307-327.

Evans, M.J., and Kaufman, M.H. (1981). Establishment in culture of pluripotential cells from mouse embryos. Nature *292*, 154-156.

Festuccia, N., Osorno, R., Halbritter, F., Karwacki-Neisius, V., Navarro, P., Colby, D., Wong, F., Yates, A., Tomlinson, S.R., and Chambers, I. (2012). Esrrb is a direct Nanog target gene that can substitute for Nanog function in pluripotent cells. Cell Stem Cell *11*, 477-490.

Ficz, G., Hore, T.A., Santos, F., Lee, H.J., Dean, W., Arand, J., Krueger, F., Oxley, D., Paul, Y.L., Walter, J.*, et al.* (2013). FGF signaling inhibition in ESCs drives rapid genome-wide demethylation to the epigenetic ground state of pluripotency. Cell Stem Cell *13*, 351-359.

Galupa, R., and Heard, E. (2015). X-chromosome inactivation: new insights into cis and trans regulation. Curr Opin Genet Dev *31*, 57-66.

Gillich, A., Bao, S., Grabole, N., Hayashi, K., Trotter, M.W., Pasque, V., Magnusdottir, E., and Surani, M.A. (2012). Epiblast stem cell-based system reveals reprogramming synergy of germline factors. Cell Stem Cell *10*, 425-439.

Gontan, C., Achame, E.M., Demmers, J., Barakat, T.S., Rentmeester, E., van, I.W., Grootegoed, J.A., and Gribnau, J. (2012). RNF12 initiates X-chromosome inactivation by targeting REX1 for degradation. Nature *485*, 386-390.

Goodrich, L., Panning, B., and Leung, K.N. (2016). Activators and repressors: A balancing act for X-inactivation. Semin Cell Dev Biol *56*, 3-8.

Goto, Y., Gomez, M., Brockdorff, N., and Feil, R. (2002). Differential patterns of histone methylation and acetylation distinguish active and repressed alleles at X-linked genes. Cytogenet Genome Res *99*, 66-74.

Grant, M., Zuccotti, M., and Monk, M. (1992). Methylation of CpG sites of two X-linked genes coincides with X-inactivation in the female mouse embryo but not in the germ line. Nat Genet *2*, 161-166.

Graves, J.A. (2006). Sex chromosome specialization and degeneration in mammals. Cell *124*, 901-914.

Grumbach, M.M., Morishima, A., and Taylor, J.H. (1963). Human Sex Chromosome Abnormalities in Relation to DNA Replication and Heterochromatinization. Proc Natl Acad Sci U S A *49*, 581-589.

Guo, G., Yang, J., Nichols, J., Hall, J.S., Eyres, I., Mansfield, W., and Smith, A. (2009). Klf4 reverts developmentally programmed restriction of ground state pluripotency. Development *136*, 1063-1069.

Habibi, E., Brinkman, A.B., Arand, J., Kroeze, L.I., Kerstens, H.H., Matarese, F., Lepikhov, K., Gut, M., Brun-Heath, I., Hubner, N.C.*, et al.* (2013). Whole-genome bisulfite sequencing of two distinct interconvertible DNA methylomes of mouse embryonic stem cells. Cell Stem Cell *13*, 360-369.

Hackett, J.A., Dietmann, S., Murakami, K., Down, T.A., Leitch, H.G., and Surani, M.A. (2013). Synergistic mechanisms of DNA demethylation during transition to ground-state pluripotency. Stem Cell Reports *1*, 518-531.

Hackett, J.A., Kobayashi, T., Dietmann, S., and Surani, M.A. (2017). Activation of Lineage Regulators and Transposable Elements across a Pluripotent Spectrum. Stem Cell Reports *8*, 1645-1658.

Han, D.W., Tapia, N., Joo, J.Y., Greber, B., Arauzo-Bravo, M.J., Bernemann, C., Ko, K., Wu, G., Stehling, M., Do, J.T.*, et al.* (2010). Epiblast stem cell subpopulations represent mouse embryos of distinct pregastrulation stages. Cell *143*, 617-627.

Harper, M.I., Fosten, M., and Monk, M. (1982). Preferential paternal X inactivation in extraembryonic tissues of early mouse embryos. J Embryol Exp Morphol *67*, 127-135.

Hassan-Zadeh, V., Rugg-Gunn, P., and Bazett-Jones, D.P. (2017). DNA methylation is dispensable for changes in global chromatin architecture but required for chromocentre formation in early stem cell differentiation. Chromosoma *126*, 605-614.

Hayashi, K., de Sousa Lopes, S.M.C., Tang, F., Lao, K., and Surani, M.A. (2008). Dynamic equilibrium and heterogeneity of mouse pluripotent stem cells with distinct functional and epigenetic states. Cell Stem Cell *3*, 391-401.

Hayashi, K., Ohta, H., Kurimoto, K., Aramaki, S., and Saitou, M. (2011). Reconstitution of the mouse germ cell specification pathway in culture by pluripotent stem cells. Cell *146*, 519-532.

Heard, E., Avner, P., and Rothstein, R. (1994). Creation of a deletion series of mouse YACs covering a 500 kb region around Xist. Nucleic Acids Res *22*, 1830-1837.

Heard, E., Rougeulle, C., Arnaud, D., Avner, P., Allis, C.D., and Spector, D.L. (2001). Methylation of histone H3 at Lys-9 is an early mark on the X chromosome during X inactivation. Cell *107*, 727-738.

Hendrich, B.D., Brown, C.J., and Willard, H.F. (1993). Evolutionary conservation of possible functional domains of the human and murine XIST genes. Hum Mol Genet *2*, 663-672.

Herzing, L.B., Romer, J.T., Horn, J.M., and Ashworth, A. (1997). Xist has properties of the X-chromosome inactivation centre. Nature *386*, 272-275.

Huang, S.M., Mishina, Y.M., Liu, S., Cheung, A., Stegmeier, F., Michaud, G.A., Charlat, O., Wiellette, E., Zhang, Y., Wiessner, S.*, et al.* (2009). Tankyrase inhibition stabilizes axin and antagonizes Wnt signalling. Nature *461*, 614-620.

Huang, Y., Osorno, R., Tsakiridis, A., and Wilson, V. (2012). In Vivo differentiation potential of epiblast stem cells revealed by chimeric embryo formation. Cell Rep *2*, 1571-1578.

Itskovitz-Eldor, J., Schuldiner, M., Karsenti, D., Eden, A., Yanuka, O., Amit, M., Soreq, H., and Benvenisty, N. (2000). Differentiation of human embryonic stem cells into embryoid bodies compromising the three embryonic germ layers. Mol Med *6*, 88-95.

Ivanova, N., Dobrin, R., Lu, R., Kotenko, I., Levorse, J., DeCoste, C., Schafer, X., Lun, Y., and Lemischka, I.R. (2006). Dissecting self-renewal in stem cells with RNA interference. Nature *442*, 533-538.

Jonkers, I., Barakat, T.S., Achame, E.M., Monkhorst, K., Kenter, A., Rentmeester, E., Grosveld, F., Grootegoed, J.A., and Gribnau, J. (2009). RNF12 is an X-Encoded dose-dependent activator of X chromosome inactivation. Cell *139*, 999-1011.

Kahan, B.W., and Ephrussi, B. (1970). Developmental potentialities of clonal in vitro cultures of mouse testicular teratoma. J Natl Cancer Inst *44*, 1015-1036.

Kalkan, T., Olova, N., Roode, M., Mulas, C., Lee, H.J., Nett, I., Marks, H., Walker, R., Stunnenberg, H.G., Lilley, K.S.*, et al.* (2017). Tracking the embryonic stem cell transition from ground state pluripotency. Development *144*, 1221-1234.

Kaslow, D.C., and Migeon, B.R. (1987). DNA methylation stabilizes X chromosome inactivation in eutherians but not in marsupials: evidence for multistep maintenance of mammalian X dosage compensation. Proc Natl Acad Sci U S A *84*, 6210-6214.

Kim, H., Wu, J., Ye, S., Tai, C.I., Zhou, X., Yan, H., Li, P., Pera, M., and Ying, Q.L. (2013). Modulation of beta-catenin function maintains mouse epiblast stem cell and human embryonic stem cell self-renewal. Nat Commun *4*, 2403.

Kiyonari, H., Kaneko, M., Abe, S., and Aizawa, S. (2010). Three inhibitors of FGF receptor, ERK, and GSK3 establishes germline-competent embryonic stem cells of C57BL/6N mouse strain with high efficiency and stability. Genesis *48*, 317-327.

Kohlmaier, A., Savarese, F., Lachner, M., Martens, J., Jenuwein, T., and Wutz, A. (2004). A chromosomal memory triggered by Xist regulates histone methylation in X inactivation. PLoS Biol *2*, E171.

Kunath, T., Saba-El-Leil, M.K., Almousailleakh, M., Wray, J., Meloche, S., and Smith, A. (2007). FGF stimulation of the Erk1/2 signalling cascade triggers transition of pluripotent embryonic stem cells from self-renewal to lineage commitment. Development *134*, 2895-2902.

Kurek, D., Neagu, A., Tastemel, M., Tuysuz, N., Lehmann, J., van de Werken, H.J., Philipsen, S., van der Linden, R., Maas, A., van, I.W.F.*, et al.* (2015). Endogenous WNT signals mediate BMP-induced and spontaneous differentiation of epiblast stem cells and human embryonic stem cells. Stem Cell Reports *4*, 114-128.

Kuroda, T., Tada, M., Kubota, H., Kimura, H., Hatano, S.Y., Suemori, H., Nakatsuji, N., and Tada, T. (2005). Octamer and Sox elements are required for transcriptional cis regulation of Nanog gene expression. Mol Cell Biol *25*, 2475-2485.

Lee, J.T. (2000). Disruption of imprinted X inactivation by parent-of-origin effects at Tsix. Cell *103*, 17-27.

Lee, J.T., Davidow, L.S., and Warshawsky, D. (1999). Tsix, a gene antisense to Xist at the X-inactivation centre. Nat Genet *21*, 400-404.

Lee, J.T., and Jaenisch, R. (1997). Long-range cis effects of ectopic X-inactivation centres on a mouse autosome. Nature *386*, 275-279.

Lee, J.T., and Lu, N. (1999). Targeted mutagenesis of Tsix leads to nonrandom X inactivation. Cell *99*, 47-57.

Lee, J.T., Strauss, W.M., Dausman, J.A., and Jaenisch, R. (1996). A 450 kb transgene displays properties of the mammalian X-inactivation center. Cell *86*, 83-94.

Leitch, H.G., McEwen, K.R., Turp, A., Encheva, V., Carroll, T., Grabole, N., Mansfield, W., Nashun, B., Knezovich, J.G., Smith, A.*, et al.* (2013). Naive pluripotency is associated with global DNA hypomethylation. Nat Struct Mol Biol *20*, 311-316.

Li, M., and Izpisua Belmonte, J.C. (2016). Looking to the future following 10 years of induced pluripotent stem cell technologies. Nat Protoc *11*, 1579-1585.

Li, M., and Izpisua Belmonte, J.C. (2018). Deconstructing the pluripotency gene regulatory network. Nat Cell Biol *20*, 382-392.

Li, P., Tong, C., Mehrian-Shai, R., Jia, L., Wu, N., Yan, Y., Maxson, R.E., Schulze, E.N., Song, H., Hsieh, C.L.*, et al.* (2008). Germline competent embryonic stem cells derived from rat blastocysts. Cell *135*, 1299-1310.

Luikenhuis, S., Wutz, A., and Jaenisch, R. (2001). Antisense transcription through the Xist locus mediates Tsix function in embryonic stem cells. Mol Cell Biol *21*, 8512-8520.

Lyon, M.F. (1961). Gene action in the X-chromosome of the mouse (Mus musculus L.). Nature *190*, 372-373.

Lyon, M.F. (1962). Sex chromatin and gene action in the mammalian X-chromosome. Am J Hum Genet *14*, 135-148.

Lyon, M.F. (1999). X-chromosome inactivation. Curr Biol *9*, R235-237.

Ma, M., and Strauss, W.M. (2005). Analysis of the Xist RNA isoforms suggests two distinctly different forms of regulation. Mamm Genome *16*, 391-404.

Maherali, N., Sridharan, R., Xie, W., Utikal, J., Eminli, S., Arnold, K., Stadtfeld, M., Yachechko, R., Tchieu, J., Jaenisch, R.*, et al.* (2007). Directly reprogrammed fibroblasts show global epigenetic remodeling and widespread tissue contribution. Cell Stem Cell *1*, 55-70.

Mak, W., Nesterova, T.B., de Napoles, M., Appanah, R., Yamanaka, S., Otte, A.P., and Brockdorff, N. (2004). Reactivation of the paternal X chromosome in early mouse embryos. Science *303*, 666-669.

Marahrens, Y., Panning, B., Dausman, J., Strauss, W., and Jaenisch, R. (1997). Xist-deficient mice are defective in dosage compensation but not spermatogenesis. Genes Dev *11*, 156-166.

Marks, H., Kalkan, T., Menafra, R., Denissov, S., Jones, K., Hofemeister, H., Nichols, J., Kranz, A., Stewart, A.F., Smith, A.*, et al.* (2012). The transcriptional and epigenomic foundations of ground state pluripotency. Cell *149*, 590-604.

Marks, H., Kerstens, H.H., Barakat, T.S., Splinter, E., Dirks, R.A., van Mierlo, G., Joshi, O., Wang, S.Y., Babak, T., Albers, C.A.*, et al.* (2015). Dynamics of gene silencing during X inactivation using allele-specific RNA-seq. Genome Biol *16*, 149.

Martello, G., Bertone, P., and Smith, A. (2013). Identification of the missing pluripotency mediator downstream of leukaemia inhibitory factor. EMBO J *32*, 2561-2574.

Martello, G., and Smith, A. (2014). The nature of embryonic stem cells. Annu Rev Cell Dev Biol *30*, 647-675.

Martello, G., Sugimoto, T., Diamanti, E., Joshi, A., Hannah, R., Ohtsuka, S., Gottgens, B., Niwa, H., and Smith, A. (2012). Esrrb is a pivotal target of the Gsk3/Tcf3 axis regulating embryonic stem cell self-renewal. Cell Stem Cell *11*, 491-504.

Martin, G.R. (1981). Isolation of a pluripotent cell line from early mouse embryos cultured in medium conditioned by teratocarcinoma stem cells. Proc Natl Acad Sci U S A *78*, 7634-7638.

Martin, G.R., Epstein, C.J., Travis, B., Tucker, G., Yatziv, S., Martin, D.W., Jr., Clift, S., and Cohen, S. (1978). X-chromosome inactivation during differentiation of female teratocarcinoma stem cells in vitro. Nature *271*, 329-333.

Martin, G.R., and Evans, M.J. (1975). Differentiation of clonal lines of teratocarcinoma cells: formation of embryoid bodies in vitro. Proc Natl Acad Sci U S A *72*, 1441-1445.

Masui, O., Bonnet, I., Le Baccon, P., Brito, I., Pollex, T., Murphy, N., Hupe, P., Barillot, E., Belmont, A.S., and Heard, E. (2011). Live-cell chromosome dynamics and outcome of X chromosome pairing events during ES cell differentiation. Cell *145*, 447-458.

Masui, S., Nakatake, Y., Toyooka, Y., Shimosato, D., Yagi, R., Takahashi, K., Okochi, H., Okuda, A., Matoba, R., Sharov, A.A.*, et al.* (2007). Pluripotency governed by Sox2 via regulation of Oct3/4 expression in mouse embryonic stem cells. Nat Cell Biol *9*, 625-635.

Matsuda, T., Nakamura, T., Nakao, K., Arai, T., Katsuki, M., Heike, T., and Yokota, T. (1999). STAT3 activation is sufficient to maintain an undifferentiated state of mouse embryonic stem cells. EMBO J *18*, 4261-4269.

Mermoud, J.E., Costanzi, C., Pehrson, J.R., and Brockdorff, N. (1999). Histone macroH2A1.2 relocates to the inactive X chromosome after initiation and propagation of X-inactivation. J Cell Biol *147*, 1399-1408.

Meshorer, E., and Misteli, T. (2006). Chromatin in pluripotent embryonic stem cells and differentiation. Nat Rev Mol Cell Biol *7*, 540-546.

Mietton, F., Sengupta, A.K., Molla, A., Picchi, G., Barral, S., Heliot, L., Grange, T., Wutz, A., and Dimitrov, S. (2009). Weak but uniform enrichment of the histone variant macroH2A1 along the inactive X chromosome. Mol Cell Biol *29*, 150-156.

Migeon, B.R. (2006). The role of X inactivation and cellular mosaicism in women's health and sex-specific diseases. JAMA *295*, 1428-1433.

Minkovsky, A., Barakat, T.S., Sellami, N., Chin, M.H., Gunhanlar, N., Gribnau, J., and Plath, K. (2013). The pluripotency factor-bound intron 1 of Xist is dispensable for X chromosome inactivation and reactivation in vitro and in vivo. Cell Rep *3*, 905-918.

Mitsui, K., Tokuzawa, Y., Itoh, H., Segawa, K., Murakami, M., Takahashi, K., Maruyama, M., Maeda, M., and Yamanaka, S. (2003). The homeoprotein Nanog is required for maintenance of pluripotency in mouse epiblast and ES cells. Cell *113*, 631-642.

Monk, M., and Harper, M.I. (1979). Sequential X chromosome inactivation coupled with cellular differentiation in early mouse embryos. Nature *281*, 311-313.

Monkhorst, K., de Hoon, B., Jonkers, I., Mulugeta Achame, E., Monkhorst, W., Hoogerbrugge, J., Rentmeester, E., Westerhoff, H.V., Grosveld, F., Grootegoed, J.A.*, et al.* (2009). The probability to initiate X chromosome inactivation is determined by the X to autosomal ratio and X chromosome specific allelic properties. PLoS One *4*, e5616.

Monkhorst, K., Jonkers, I., Rentmeester, E., Grosveld, F., and Gribnau, J. (2008). X inactivation counting and choice is a stochastic process: evidence for involvement of an X-linked activator. Cell *132*, 410-421.

Moreira de Mello, J.C., de Araujo, E.S., Stabellini, R., Fraga, A.M., de Souza, J.E., Sumita, D.R., Camargo, A.A., and Pereira, L.V. (2010). Random X inactivation and extensive mosaicism in human placenta revealed by analysis of allele-specific gene expression along the X chromosome. PLoS One *5*, e10947.

Morgani, S., Nichols, J., and Hadjantonakis, A.K. (2017). The many faces of Pluripotency: in vitro adaptations of a continuum of in vivo states. BMC Dev Biol *17*, 7.

Nakatake, Y., Fukui, N., Iwamatsu, Y., Masui, S., Takahashi, K., Yagi, R., Yagi, K., Miyazaki, J., Matoba, R., Ko, M.S.*, et al.* (2006). Klf4 cooperates with Oct3/4 and Sox2 to activate the Lefty1 core promoter in embryonic stem cells. Mol Cell Biol *26*, 7772-7782.

Navarro, P., Chambers, I., Karwacki-Neisius, V., Chureau, C., Morey, C., Rougeulle, C., and Avner, P. (2008). Molecular coupling of Xist regulation and pluripotency. Science *321*, 1693-1695.

Navarro, P., Moffat, M., Mullin, N.P., and Chambers, I. (2011). The X-inactivation trans-activator Rnf12 is negatively regulated by pluripotency factors in embryonic stem cells. Hum Genet *130*, 255-264.

Navarro, P., Oldfield, A., Legoupi, J., Festuccia, N., Dubois, A., Attia, M., Schoorlemmer, J., Rougeulle, C., Chambers, I., and Avner, P. (2010). Molecular coupling of Tsix regulation and pluripotency. Nature *468*, 457-460.

Navarro, P., Pichard, S., Ciaudo, C., Avner, P., and Rougeulle, C. (2005). Tsix transcription across the Xist gene alters chromatin conformation without affecting Xist transcription: implications for X-chromosome inactivation. Genes Dev *19*, 1474-1484.

Nesterova, T.B., Senner, C.E., Schneider, J., Alcayna-Stevens, T., Tattermusch, A., Hemberger, M., and Brockdorff, N. (2011). Pluripotency factor binding and Tsix expression act synergistically to repress Xist in undifferentiated embryonic stem cells. Epigenetics Chromatin *4*, 17.

Nesterova, T.B., Slobodyanyuk, S.Y., Elisaphenko, E.A., Shevchenko, A.I., Johnston, C., Pavlova, M.E., Rogozin, I.B., Kolesnikov, N.N., Brockdorff, N., and Zakian, S.M. (2001). Characterization of the genomic Xist locus in rodents reveals conservation of overall gene structure and tandem repeats but rapid evolution of unique sequence. Genome Res *11*, 833-849.

Ng, H.H., and Surani, M.A. (2011). The transcriptional and signalling networks of pluripotency. Nat Cell Biol *13*, 490-496.

Nichols, J., Silva, J., Roode, M., and Smith, A. (2009). Suppression of Erk signalling promotes ground state pluripotency in the mouse embryo. Development *136*, 3215-3222.

Nichols, J., and Smith, A. (2009). Naive and primed pluripotent states. Cell Stem Cell *4*, 487-492.

Nichols, J., Zevnik, B., Anastassiadis, K., Niwa, H., Klewe-Nebenius, D., Chambers, I., Scholer, H., and Smith, A. (1998). Formation of pluripotent stem cells in the mammalian embryo depends on the POU transcription factor Oct4. Cell *95*, 379-391.

Nishimoto, M., Fukushima, A., Okuda, A., and Muramatsu, M. (1999). The gene for the embryonic stem cell coactivator UTF1 carries a regulatory element which selectively interacts with a complex composed of Oct-3/4 and Sox-2. Mol Cell Biol *19*, 5453-5465.

Niwa, H., Burdon, T., Chambers, I., and Smith, A. (1998). Self-renewal of pluripotent embryonic stem cells is mediated via activation of STAT3. Genes Dev *12*, 2048-2060.

Niwa, H., Miyazaki, J., and Smith, A.G. (2000). Quantitative expression of Oct-3/4 defines differentiation, dedifferentiation or self-renewal of ES cells. Nat Genet *24*, 372-376.

Niwa, H., Ogawa, K., Shimosato, D., and Adachi, K. (2009). A parallel circuit of LIF signalling pathways maintains pluripotency of mouse ES cells. Nature *460*, 118-122.

O'Neill, L.P., Spotswood, H.T., Fernando, M., and Turner, B.M. (2008). Differential loss of histone H3 isoforms mono-, di- and tri-methylated at lysine 4 during X-inactivation in female embryonic stem cells. Biol Chem *389*, 365-370.

Okamoto, I., Arnaud, D., Le Baccon, P., Otte, A.P., Disteche, C.M., Avner, P., and Heard, E. (2005). Evidence for de novo imprinted X-chromosome inactivation independent of meiotic inactivation in mice. Nature *438*, 369-373.

Okamoto, I., Otte, A.P., Allis, C.D., Reinberg, D., and Heard, E. (2004). Epigenetic dynamics of imprinted X inactivation during early mouse development. Science *303*, 644-649.

Okamoto, I., Patrat, C., Thepot, D., Peynot, N., Fauque, P., Daniel, N., Diabangouaya, P., Wolf, J.P., Renard, J.P., Duranthon, V*., et al.* (2011). Eutherian mammals use diverse strategies to initiate X-chromosome inactivation during development. Nature *472*, 370-374.

Osorno, R., Tsakiridis, A., Wong, F., Cambray, N., Economou, C., Wilkie, R., Blin, G., Scotting, P.J., Chambers, I., and Wilson, V. (2012). The developmental dismantling of pluripotency is reversed by ectopic Oct4 expression. Development *139*, 2288-2298.

Panning, B., Dausman, J., and Jaenisch, R. (1997). X chromosome inactivation is mediated by Xist RNA stabilization. Cell *90*, 907-916.

Panning, B., and Jaenisch, R. (1996). DNA hypomethylation can activate Xist expression and silence X-linked genes. Genes Dev *10*, 1991-2002.

Park, S.H., Park, S.H., Kook, M.C., Kim, E.Y., Park, S., and Lim, J.H. (2004). Ultrastructure of human embryonic stem cells and spontaneous and retinoic acid-induced differentiating cells. Ultrastruct Pathol *28*, 229-238.

Pasque, V., Tchieu, J., Karnik, R., Uyeda, M., Sadhu Dimashkie, A., Case, D., Papp, B., Bonora, G., Patel, S., Ho, R*., et al.* (2014). X chromosome reactivation dynamics reveal stages of reprogramming to pluripotency. Cell *159*, 1681-1697.

Payer, B., Rosenberg, M., Yamaji, M., Yabuta, Y., Koyanagi-Aoi, M., Hayashi, K., Yamanaka, S., Saitou, M., and Lee, J.T. (2013). Tsix RNA and the germline factor, PRDM14, link X reactivation and stem cell reprogramming. Mol Cell *52*, 805-818.

Penny, G.D., Kay, G.F., Sheardown, S.A., Rastan, S., and Brockdorff, N. (1996). Requirement for Xist in X chromosome inactivation. Nature *379*, 131-137.

Petropoulos, S., Edsgard, D., Reinius, B., Deng, Q., Panula, S.P., Codeluppi, S., Reyes, A.P., Linnarsson, S., Sandberg, R., and Lanner, F. (2016). Single-Cell RNA-Seq Reveals Lineage and X Chromosome Dynamics in Human Preimplantation Embryos. Cell *167*, 285.

Plath, K., Fang, J., Mlynarczyk-Evans, S.K., Cao, R., Worringer, K.A., Wang, H., de la Cruz, C.C., Otte, A.P., Panning, B., and Zhang, Y. (2003). Role of histone H3 lysine 27 methylation in X inactivation. Science *300*, 131-135.

Plath, K., Mlynarczyk-Evans, S., Nusinow, D.A., and Panning, B. (2002). Xist RNA and the mechanism of X chromosome inactivation. Annu Rev Genet *36*, 233-278.

Plath, K., Talbot, D., Hamer, K.M., Otte, A.P., Yang, T.P., Jaenisch, R., and Panning, B. (2004). Developmentally regulated alterations in Polycomb repressive complex 1 proteins on the inactive X chromosome. J Cell Biol *167*, 1025-1035.

Rastan, S. (1983). Non-random X-chromosome inactivation in mouse X-autosome translocation embryos--location of the inactivation centre. J Embryol Exp Morphol *78*, 1-22.

Rastan, S., and Robertson, E.J. (1985). X-chromosome deletions in embryo-derived (EK) cell lines associated with lack of X-chromosome inactivation. J Embryol Exp Morphol *90*, 379-388.

Rodda, D.J., Chew, J.L., Lim, L.H., Loh, Y.H., Wang, B., Ng, H.H., and Robson, P. (2005). Transcriptional regulation of nanog by OCT4 and SOX2. J Biol Chem *280*, 24731-24737.

Rosner, M.H., Vigano, M.A., Ozato, K., Timmons, P.M., Poirier, F., Rigby, P.W., and Staudt, L.M. (1990). A POU-domain transcription factor in early stem cells and germ cells of the mammalian embryo. Nature *345*, 686-692.

Rougeulle, C., Chaumeil, J., Sarma, K., Allis, C.D., Reinberg, D., Avner, P., and Heard, E. (2004). Differential histone H3 Lys-9 and Lys-27 methylation profiles on the X chromosome. Mol Cell Biol *24*, 5475-5484.

Russell, L.B. (1963). Mammalian X-chromosome action: inactivation limited in spread and region of origin. Science *140*, 976-978.

Sado, T., Hoki, Y., and Sasaki, H. (2005). Tsix silences Xist through modification of chromatin structure. Dev Cell *9*, 159-165.

Sado, T., Li, E., and Sasaki, H. (2002). Effect of TSIX disruption on XIST expression in male ES cells. Cytogenet Genome Res *99*, 115-118.

Sado, T., Wang, Z., Sasaki, H., and Li, E. (2001). Regulation of imprinted X-chromosome inactivation in mice by Tsix. Development *128*, 1275-1286.

Sanchez-Castillo, M., Ruau, D., Wilkinson, A.C., Ng, F.S., Hannah, R., Diamanti, E., Lombard, P., Wilson, N.K., and Gottgens, B. (2015). CODEX: a next-generation sequencing experiment database for the haematopoietic and embryonic stem cell communities. Nucleic Acids Res *43*, D1117-1123.

Sarma, K., Levasseur, P., Aristarkhov, A., and Lee, J.T. (2010). Locked nucleic acids (LNAs) reveal sequence requirements and kinetics of Xist RNA localization to the X chromosome. Proc Natl Acad Sci U S A *107*, 22196-22201.

Schoeftner, S., Sengupta, A.K., Kubicek, S., Mechtler, K., Spahn, L., Koseki, H., Jenuwein, T., and Wutz, A. (2006). Recruitment of PRC1 function at the initiation of X inactivation independent of PRC2 and silencing. EMBO J *25*, 3110-3122.

Schulz, E.G., Meisig, J., Nakamura, T., Okamoto, I., Sieber, A., Picard, C., Borensztein, M., Saitou, M., Bluthgen, N., and Heard, E. (2014). The two active X chromosomes in female ESCs block exit from the pluripotent state by modulating the ESC signaling network. Cell Stem Cell *14*, 203-216.

Sheardown, S.A., Duthie, S.M., Johnston, C.M., Newall, A.E., Formstone, E.J., Arkell, R.M., Nesterova, T.B., Alghisi, G.C., Rastan, S., and Brockdorff, N. (1997). Stabilization of Xist RNA mediates initiation of X chromosome inactivation. Cell *91*, 99-107.

Shin, J., Bossenz, M., Chung, Y., Ma, H., Byron, M., Taniguchi-Ishigaki, N., Zhu, X., Jiao, B., Hall, L.L., Green, M.R*., et al.* (2010). Maternal Rnf12/RLIM is required for imprinted X-chromosome inactivation in mice. Nature *467*, 977-981.

Shin, J., Wallingford, M.C., Gallant, J., Marcho, C., Jiao, B., Byron, M., Bossenz, M., Lawrence, J.B., Jones, S.N., Mager, J*., et al.* (2014). RLIM is dispensable for X-chromosome inactivation in the mouse embryonic epiblast. Nature *511*, 86-89.

Shy, B.R., Wu, C.I., Khramtsova, G.F., Zhang, J.Y., Olopade, O.I., Goss, K.H., and Merrill, B.J. (2013). Regulation of Tcf7l1 DNA binding and protein stability as principal mechanisms of Wnt/beta-catenin signaling. Cell Rep *4*, 1-9.

Silva, J., Barrandon, O., Nichols, J., Kawaguchi, J., Theunissen, T.W., and Smith, A. (2008). Promotion of reprogramming to ground state pluripotency by signal inhibition. PLoS Biol *6*, e253.

Silva, J., Mak, W., Zvetkova, I., Appanah, R., Nesterova, T.B., Webster, Z., Peters, A.H., Jenuwein, T., Otte, A.P., and Brockdorff, N. (2003). Establishment of histone h3 methylation on the inactive X chromosome requires transient recruitment of Eed-Enx1 polycomb group complexes. Dev Cell *4*, 481-495.

Silva, J., Nichols, J., Theunissen, T.W., Guo, G., van Oosten, A.L., Barrandon, O., Wray, J., Yamanaka, S., Chambers, I., and Smith, A. (2009). Nanog is the gateway to the pluripotent ground state. Cell *138*, 722-737.

Smith, A. (2017). Formative pluripotency: the executive phase in a developmental continuum. Development *144*, 365-373.

Smith, A.G., Heath, J.K., Donaldson, D.D., Wong, G.G., Moreau, J., Stahl, M., and Rogers, D. (1988). Inhibition of pluripotential embryonic stem cell differentiation by purified polypeptides. Nature *336*, 688-690.

Smith, Z.D., Chan, M.M., Mikkelsen, T.S., Gu, H., Gnirke, A., Regev, A., and Meissner, A. (2012). A unique regulatory phase of DNA methylation in the early mammalian embryo. Nature *484*, 339-344.

Soma, M., Fujihara, Y., Okabe, M., Ishino, F., and Kobayashi, S. (2014). Ftx is dispensable for imprinted X-chromosome inactivation in preimplantation mouse embryos. Sci Rep *4*, 5181.

Splinter, E., de Wit, E., Nora, E.P., Klous, P., van de Werken, H.J., Zhu, Y., Kaaij, L.J., van Ijcken, W., Gribnau, J., Heard, E.*, et al.* (2011). The inactive X chromosome adopts a unique three-dimensional conformation that is dependent on Xist RNA. Genes Dev *25*, 1371-1383.

Stavridis, M.P., Lunn, J.S., Collins, B.J., and Storey, K.G. (2007). A discrete period of FGF-induced Erk1/2 signalling is required for vertebrate neural specification. Development *134*, 2889-2894.

Stavropoulos, N., Lu, N., and Lee, J.T. (2001). A functional role for Tsix transcription in blocking Xist RNA accumulation but not in X-chromosome choice. Proc Natl Acad Sci U S A *98*, 10232-10237.

Stevens, L.C., and Little, C.C. (1954). Spontaneous Testicular Teratomas in an Inbred Strain of Mice. Proc Natl Acad Sci U S A *40*, 1080-1087.

Stuart, H.T., van Oosten, A.L., Radzisheuskaya, A., Martello, G., Miller, A., Dietmann, S., Nichols, J., and Silva, J.C. (2014). NANOG amplifies STAT3 activation and they synergistically induce the naive pluripotent program. Curr Biol *24*, 340-346.

Sugimoto, M., Kondo, M., Koga, Y., Shiura, H., Ikeda, R., Hirose, M., Ogura, A., Murakami, A., Yoshiki, A., Chuva de Sousa Lopes, S.M.*, et al.* (2015). A simple and robust method for establishing homogeneous mouse epiblast stem cell lines by wnt inhibition. Stem Cell Reports *4*, 744-757.

Sumi, T., Oki, S., Kitajima, K., and Meno, C. (2013). Epiblast ground state is controlled by canonical Wnt/beta-catenin signaling in the postimplantation mouse embryo and epiblast stem cells. PLoS One *8*, e63378.

Sun, S., Del Rosario, B.C., Szanto, A., Ogawa, Y., Jeon, Y., and Lee, J.T. (2013). Jpx RNA activates Xist by evicting CTCF. Cell *153*, 1537-1551.

Tada, M., Takahama, Y., Abe, K., Nakatsuji, N., and Tada, T. (2001). Nuclear reprogramming of somatic cells by in vitro hybridization with ES cells. Curr Biol *11*, 1553-1558.

Tai, C.I., and Ying, Q.L. (2013). Gbx2, a LIF/Stat3 target, promotes reprogramming to and retention of the pluripotent ground state. J Cell Sci *126*, 1093-1098.

Takagi, N., and Sasaki, M. (1975). Preferential inactivation of the paternally derived X chromosome in the extraembryonic membranes of the mouse. Nature *256*, 640-642.

Takagi, N., Yoshida, M.A., Sugawara, O., and Sasaki, M. (1983). Reversal of X-inactivation in female mouse somatic cells hybridized with murine teratocarcinoma stem cells in vitro. Cell *34*, 1053-1062.

Takahashi, K., and Yamanaka, S. (2006). Induction of pluripotent stem cells from mouse embryonic and adult fibroblast cultures by defined factors. Cell *126*, 663-676.

Takahashi, K., and Yamanaka, S. (2016). A decade of transcription factor-mediated reprogramming to pluripotency. Nat Rev Mol Cell Biol *17*, 183-193.

Tesar, P.J., Chenoweth, J.G., Brook, F.A., Davies, T.J., Evans, E.P., Mack, D.L., Gardner, R.L., and McKay, R.D. (2007). New cell lines from mouse epiblast share defining features with human embryonic stem cells. Nature *448*, 196-199.

Thomson, J.A., Itskovitz-Eldor, J., Shapiro, S.S., Waknitz, M.A., Swiergiel, J.J., Marshall, V.S., and Jones, J.M. (1998). Embryonic stem cell lines derived from human blastocysts. Science *282*, 1145-1147.

Tian, D., Sun, S., and Lee, J.T. (2010). The long noncoding RNA, Jpx, is a molecular switch for X chromosome inactivation. Cell *143*, 390-403.

Tokuzawa, Y., Kaiho, E., Maruyama, M., Takahashi, K., Mitsui, K., Maeda, M., Niwa, H., and Yamanaka, S. (2003). Fbx15 is a novel target of Oct3/4 but is dispensable for embryonic stem cell self-renewal and mouse development. Mol Cell Biol *23*, 2699-2708.

Tomioka, M., Nishimoto, M., Miyagi, S., Katayanagi, T., Fukui, N., Niwa, H., Muramatsu, M., and Okuda, A. (2002). Identification of Sox-2 regulatory region which is under the control of Oct-3/4-Sox-2 complex. Nucleic Acids Res *30*, 3202-3213.

Tosolini, M., and Jouneau, A. (2016). From Naive to Primed Pluripotency: In Vitro Conversion of Mouse Embryonic Stem Cells in Epiblast Stem Cells. Methods Mol Biol *1341*, 209-216.

Toyooka, Y., Shimosato, D., Murakami, K., Takahashi, K., and Niwa, H. (2008). Identification and characterization of subpopulations in undifferentiated ES cell culture. Development *135*, 909-918.

Vallot, C., Patrat, C., Collier, A.J., Huret, C., Casanova, M., Liyakat Ali, T.M., Tosolini, M., Frydman, N., Heard, E., Rugg-Gunn, P.J.*, et al.* (2017). XACT Noncoding RNA Competes with XIST in the Control of X Chromosome Activity during Human Early Development. Cell Stem Cell *20*, 102-111.

van den Berg, D.L., Zhang, W., Yates, A., Engelen, E., Takacs, K., Bezstarosti, K., Demmers, J., Chambers, I., and Poot, R.A. (2008). Estrogen-related receptor beta interacts with Oct4 to positively regulate Nanog gene expression. Mol Cell Biol *28*, 5986-5995.

van Oosten, A.L., Costa, Y., Smith, A., and Silva, J.C. (2012). JAK/STAT3 signalling is sufficient and dominant over antagonistic cues for the establishment of naive pluripotency. Nat Commun *3*, 817.

Veillard, A.C., Marks, H., Bernardo, A.S., Jouneau, L., Laloe, D., Boulanger, L., Kaan, A., Brochard, V., Tosolini, M., Pedersen, R.*, et al.* (2014). Stable methylation at promoters distinguishes epiblast stem cells from embryonic stem cells and the in vivo epiblasts. Stem Cells Dev *23*, 2014-2029.

West, J.D., Frels, W.I., Chapman, V.M., and Papaioannou, V.E. (1977). Preferential expression of the maternally derived X chromosome in the mouse yolk sac. Cell *12*, 873-882.

Williams, L.H., Kalantry, S., Starmer, J., and Magnuson, T. (2011). Transcription precedes loss of Xist coating and depletion of H3K27me3 during X-chromosome reprogramming in the mouse inner cell mass. Development *138*, 2049-2057.

Williams, R.L., Hilton, D.J., Pease, S., Willson, T.A., Stewart, C.L., Gearing, D.P., Wagner, E.F., Metcalf, D., Nicola, N.A., and Gough, N.M. (1988). Myeloid leukaemia inhibitory factor maintains the developmental potential of embryonic stem cells. Nature *336*, 684-687.

Wray, J., Kalkan, T., Gomez-Lopez, S., Eckardt, D., Cook, A., Kemler, R., and Smith, A. (2011). Inhibition of glycogen synthase kinase-3 alleviates Tcf3 repression of the pluripotency network and increases embryonic stem cell resistance to differentiation. Nat Cell Biol *13*, 838-845.

Wray, J., Kalkan, T., and Smith, A.G. (2010). The ground state of pluripotency. Biochem Soc Trans *38*, 1027-1032.

Wutz, A., and Jaenisch, R. (2000). A shift from reversible to irreversible X inactivation is triggered during ES cell differentiation. Mol Cell *5*, 695-705.

Wutz, A., Rasmussen, T.P., and Jaenisch, R. (2002). Chromosomal silencing and localization are mediated by different domains of Xist RNA. Nat Genet *30*, 167-174.

Xu, N., Tsai, C.L., and Lee, J.T. (2006). Transient homologous chromosome pairing marks the onset of X inactivation. Science *311*, 1149-1152.

Yang, J., van Oosten, A.L., Theunissen, T.W., Guo, G., Silva, J.C., and Smith, A. (2010). Stat3 activation is limiting for reprogramming to ground state pluripotency. Cell Stem Cell *7*, 319-328.

Ye, S., Li, P., Tong, C., and Ying, Q.L. (2013). Embryonic stem cell self-renewal pathways converge on the transcription factor Tfcp2l1. EMBO J *32*, 2548-2560.

Yen, Z.C., Meyer, I.M., Karalic, S., and Brown, C.J. (2007). A cross-species comparison of X-chromosome inactivation in Eutheria. Genomics *90*, 453-463.

Yeom, Y.I., Fuhrmann, G., Ovitt, C.E., Brehm, A., Ohbo, K., Gross, M., Hubner, K., and Scholer, H.R. (1996). Germline regulatory element of Oct-4 specific for the totipotent cycle of embryonal cells. Development *122*, 881-894.

Yi, F., Pereira, L., Hoffman, J.A., Shy, B.R., Yuen, C.M., Liu, D.R., and Merrill, B.J. (2011). Opposing effects of Tcf3 and Tcf1 control Wnt stimulation of embryonic stem cell self-renewal. Nat Cell Biol *13*, 762-770.

Ying, Q.L., Nichols, J., Chambers, I., and Smith, A. (2003). BMP induction of Id proteins suppresses differentiation and sustains embryonic stem cell self-renewal in collaboration with STAT3. Cell *115*, 281-292.

Ying, Q.L., Wray, J., Nichols, J., Batlle-Morera, L., Doble, B., Woodgett, J., Cohen, P., and Smith, A. (2008). The ground state of embryonic stem cell self-renewal. Nature *453*, 519-523.

Young, R.A. (2011). Control of the embryonic stem cell state. Cell *144*, 940-954.

Yuan, H., Corbi, N., Basilico, C., and Dailey, L. (1995). Developmental-specific activity of the FGF-4 enhancer requires the synergistic action of Sox2 and Oct-3. Genes Dev *9*, 2635-2645.

Zhao, J., Sun, B.K., Erwin, J.A., Song, J.J., and Lee, J.T. (2008). Polycomb proteins targeted by a short repeat RNA to the mouse X chromosome. Science *322*, 750-756.

Zylicz, J.J., Dietmann, S., Gunesdogan, U., Hackett, J.A., Cougot, D., Lee, C., and Surani, M.A. (2015). Chromatin dynamics and the role of G9a in gene regulation and enhancer silencing during early mouse development. Elife *4*.

Appendix

Short Article

Cell Stem Cell

Exit from Naive Pluripotency Induces a Transient X Chromosome Inactivation-like State in Males

Graphical Abstract

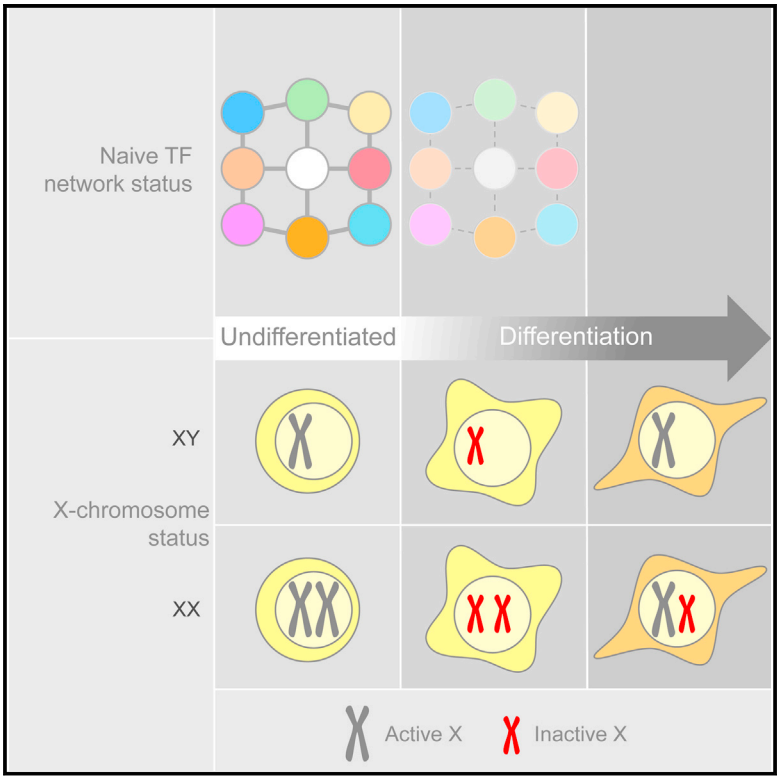

Authors

Elsa J. Sousa, Hannah T. Stuart, Lawrence E. Bates, Mohammadmersad Ghorbani, Jennifer Nichols, Sabine Dietmann, José C.R. Silva

Correspondence

jcs64@cam.ac.uk

In Brief

Silva and colleagues report that the initiation of X chromosome inactivation takes place in males and on both X chromosomes in females. This is transient and rapid and is triggered by downregulation of naive pluripotent transcription factors during the onset of differentiation.

Highlights

- A robust naive pluripotent transcription factor network abolishes expression of Xist
- Xist accumulates on the male X and both female Xs at the onset of differentiation
- Males undergo transient and rapid partial XCI
- Male XCI is triggered by downregulation of the naive identity

Sousa et al., 2018, Cell Stem Cell *22*, 919–928
June 1, 2018
https://doi.org/10.1016/j.stem.2018.05.001

CellPress

Cell Stem Cell
Short Article

Exit from Naive Pluripotency Induces a Transient X Chromosome Inactivation-like State in Males

Elsa J. Sousa,[1,2] Hannah T. Stuart,[1,3] Lawrence E. Bates,[1,3] Mohammadmersad Ghorbani,[1] Jennifer Nichols,[1,4] Sabine Dietmann,[1] and José C.R. Silva[1,3,5,*]
[1]Wellcome-MRC Cambridge Stem Cell Institute, University of Cambridge, Cambridge CB2 1QR, UK
[2]Graduate Program in Areas of Basic and Applied Biology, Instituto de Ciências Biomédicas Abel Salazar, Universidade do Porto, 4050-313 Porto, Portugal
[3]Department of Biochemistry, University of Cambridge, Cambridge CB2 1GA, UK
[4]Department of Physiology, Development and Neuroscience, University of Cambridge, Cambridge CB2 3EG, UK
[5]Lead Contact
*Correspondence: jcs64@cam.ac.uk
https://doi.org/10.1016/j.stem.2018.05.001

SUMMARY

A hallmark of naive pluripotency is the presence of two active X chromosomes in females. It is not clear whether prevention of X chromosome inactivation (XCI) is mediated by gene networks that preserve the naive state. Here, we show that robust naive pluripotent stem cell (nPSC) self-renewal represses expression of *Xist*, the master regulator of XCI. We found that nPSCs accumulate *Xist* on the male X chromosome and on both female X chromosomes as they become NANOG negative at the onset of differentiation. This is accompanied by the appearance of a repressive chromatin signature and partial X-linked gene silencing, suggesting a transient and rapid XCI-like state in male nPSCs. In the embryo, *Xist* is transiently expressed in males and in females from both X chromosomes at the onset of naive epiblast differentiation. In conclusion, we propose that XCI initiation is gender independent and triggered by destabilization of naive identity, suggesting that gender-specific mechanisms follow, rather than precede, XCI initiation.

INTRODUCTION

In order to achieve dosage compensation, female mammals have one inactive X chromosome (Xi). However, in female murine embryos, the Xi is reactivated in the pre-implantation blastocyst (Mak et al., 2004; Okamoto et al., 2004) specifically in the cells of the naive pluripotent epiblast (Silva et al., 2009). Their *in vitro* counterpart, naive pluripotent stem cells (nPSCs), retain this embryonic feature, making them an excellent model system to study X chromosome inactivation (XCI). XCI is initiated upon differentiation of female nPSCs and is characterized by monoallelic upregulation of *Xist*, the non-coding RNA which coats the future Xi in *cis* (Panning et al., 1997; Sheardown et al., 1997). In contrast, *Xist* expression is extinguished during differentiation of male nPSCs.

The link between a naive pluripotent cellular identity and the lack of a Xi in females is still poorly understood. In the pre-implantation blastocyst, reactivation of the Xi occurs in cells expressing the nPSC marker NANOG (Silva et al., 2009). Moreover, NANOG and other members of the naive transcriptional network were found to bind to *Xist* intron 1 (Navarro et al., 2008). Deletion of *Nanog* and *Oct4* was shown to induce a moderate upregulation of *Xist* (Navarro et al., 2008), but deletion of *Xist* intron 1 was shown to be dispensable for XCI and did not affect *Xist* expression (Minkovsky et al., 2013).

X chromosome reactivation (XCR) is also a feature during *in vitro* nuclear reprogramming to naive pluripotent cell identity (Tada et al., 2001). The general consensus is that naive pluripotent gene regulators must play a role both *in vivo* and *in vitro* XCR (Navarro et al., 2008, 2010, 2011; Pasque and Plath, 2015; Pasque et al., 2014; Payer et al., 2013; Silva et al., 2009).

Studies investigating the process of XCI have largely been conducted *in vitro* and using nPSCs cultured in serum/LIF (SL) conditions. This is known to be suboptimal, as it induces transcriptional heterogeneity of pluripotency factors (Chambers et al., 2007), promotes an overall weak naive transcription factor (TF) network in which spontaneous differentiation and increased expression of lineage markers are observed (Marks et al., 2012), and exhibits epigenetic constraints (Ficz et al., 2013; Habibi et al., 2013; Leitch et al., 2013; Marks et al., 2012). It is also known to reduce reprogramming efficiency (Silva et al., 2008) and to decrease the ability of nPSCs to enter embryonic development (Alexandrova et al., 2016). Using defined serum-free medium containing LIF and inhibitors of mitogen-activated protein kinase signaling and glycogen synthase kinase-3β (2iL), these limitations have been overcome (Silva et al., 2008; Silva et al., 2009; Ying et al., 2008). 2iL acts on the TF network governing the naive identity by boosting its expression (Martello and Smith, 2014). In addition, nPSCs cultured in 2iL exhibit a transcriptional signature that is similar to the naive pluripotent epiblast (Boroviak et al., 2015). However, it is unknown whether increased transcriptional homogeneity and pluripotent TF robustness have an impact on the process of XCI.

Here, we assessed the relationship between naive pluripotent cell identity and the process of XCI. This uncovered unexpected XCI events during differentiation of both male and female nPSCs.

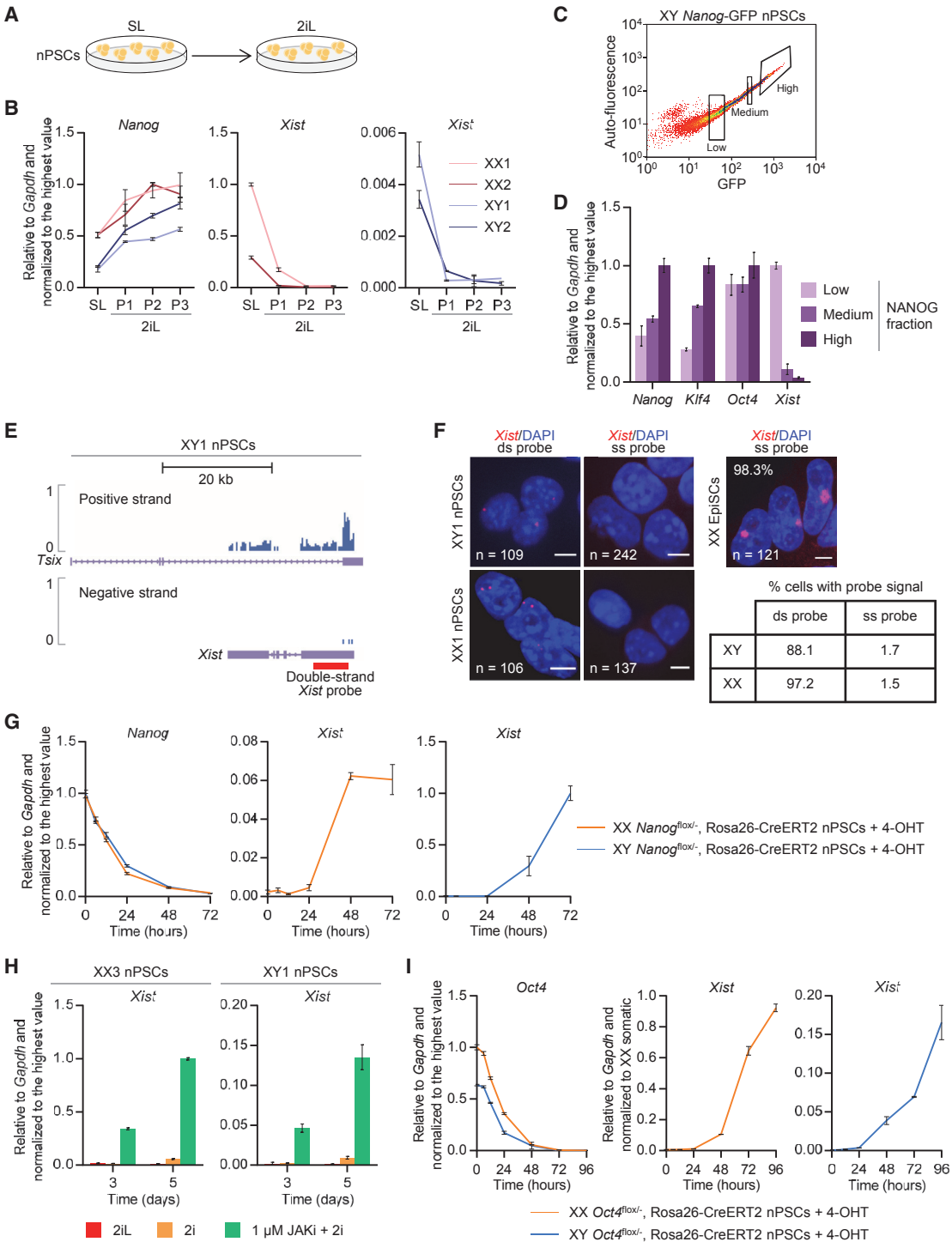

Figure 1. *Xist* Expression Is Abolished by a Robust Naive Pluripotent Network

(A) Schematic illustrating the experiment performed to evaluate the impact of the nPSC culture conditions on the expression of *Xist*.

(B) qRT-PCR analysis of *Nanog* and *Xist* in XX1, XX2, XY1, and XY2 ESC lines in SL versus 2iL. P indicates number of passages in 2iL. Error bars represent ± SD.

(C) Flow cytometry analysis of male SL *Nanog*-GFP ESCs and subsequent sorting into three *Nanog*-GFP populations: low, medium, and high.

(D) qRT-PCR analysis of *Nanog*, *Klf4*, *Oct4*, and *Xist* in low, medium, and high *Nanog*-GFP ESCs. Error bars represent ± SD.

(E) Strand-specific RNA-seq showing expression of the positive and negative strands at the *Xist* locus in male 2iL ESCs. The double-strand *Xist* probe used in (F) is represented in red.

(legend continued on next page)

These observations impact our understanding of XCI and its relationship with the naive pluripotent identity.

RESULTS

Robust nPSC Self-Renewal Abolishes *Xist* Expression

To evaluate the impact of gene expression homogeneity and increased naive pluripotent gene expression on the levels of *Xist*, we analyzed two male and two female SL-derived embryonic stem cell (ESC) lines before and after passaging in 2iL (Figures 1A, S1A, and S1B). As expected, upregulation of naive pluripotent network components was observed after transferring cells from SL to 2iL (Figures 1B and S1C). Remarkably, 2iL conditions led to repression of *Xist* in both male and female ESCs after only one passage (Figure 1B).

ESCs in SL present heterogeneous levels of naive markers (Chambers et al., 2007), rendering these cells a useful tool to study the relationship between naive network status and *Xist* expression. Male SL ESCs with *Nanog*-GFP reporter were sorted into low, medium, and high GFP populations (Figures 1C and S1D). *Oct4* levels were maintained in all three fractions, whereas the pluripotency factor *Klf4* positively correlated with *Nanog* expression (Figure 1D). Interestingly, *Xist* expression was 28-fold lower in *Nanog*-high than *Nanog*-low cells (Figure 1D).

To validate the qRT-PCR data, we performed strand-specific RNA sequencing (RNA-seq) in 2iL-cultured male nPSCs. This clearly showed that expression at the *Xist* locus was exclusively antisense (Figure 1E). We also analyzed the pattern of *Xist* by RNA fluorescence *in situ* hybridization (FISH) using a single-strand (ss) *Xist*-specific probe and a conventional double-strand (ds) probe detecting *Xist* exon 1 and also any present antisense transcript. When using the ds probe and depending on the gender, one or two pinpoints were detected in 88% or 97% of cells, respectively (Figure 1F). In contrast, with the ss probe, *Xist* was detected in less than 2% of cells (Figure 1F). Together, these data demonstrate that *Xist* is not expressed in robust self-renewing nPSCs.

2iL culture medium allows the removal of otherwise essential components of the naive TF network (Ying et al., 2008). Thus, we assessed the effect of the withdrawal of these on *Xist* expression over 3 days. We performed 4-hydroxytamoxifen (4-OHT)-mediated Cre deletion of *Nanog* from *Nanog*$^{flox/-}$, Rosa26-CreERT2 ESCs (Figures 1G and S1F–S1H). We found an inverse correlation between the expression of *Nanog* and *Xist*, which was highly upregulated in both females and males (Figure 1G). As expected, *Nanog* deletion also had an effect on the expression of its downstream targets such as *Klf4* and *Esrrb*, but not on *Oct4* or other naive pluripotency genes (Figure S1H).

JAK/STAT3 signaling plays an important role in the maintenance of pluripotency (Martello and Smith, 2014). In addition, activated STAT3 (p-STAT3) and its downstream target genes have binding sites within the X-inactivation center (XIC) that harbors *Xist* and other genes involved in its regulation (Sánchez-Castillo et al., 2015). Here, inhibition of JAK/STAT3 signaling was achieved by treatment of ESCs with a JAK inhibitor (JAKi) and confirmed by depletion of p-STAT3 (Figures 1H, S1I, and S1J) and downregulation of its target *Socs3* (Figure S1K). Interestingly, treatment with 1 μM JAKi induced upregulation of *Xist* in both female and male ESC lines (Figure 1H).

Overall, these data show that perturbing the naive pluripotent network leads to a sharp upregulation of *Xist* in both male and female ESCs. However, inhibition of JAK/STAT3 signaling also impacted expression of naive factors, such as *Oct4* (Figure S1K), which are known to be required for the integrity of the pluripotency network. This raised the need to investigate whether the observed sharp upregulation of *Xist* in males is indeed associated with a weaker but nonetheless naive identity or/and a consequence of naive cell differentiation. To investigate this, we analyzed *Xist* expression kinetics upon 4-OHT-mediated Cre deletion of *Oct4* in male and female *Oct4*$^{flox/-}$, Rosa26-CreERT2 ESCs (Figures 1I, S1L, S1M, and S1N). In this context, the naive network collapses and cells lose the naive identity. Importantly, concomitantly with *Oct4* deletion, both female and male cells exhibited a striking increase in the expression of *Xist* (Figure 1I). In males, this reached 16% of *Xist* female somatic cell levels.

Together, these data link the loss of naive gene expression and identity to the upregulation of *Xist*.

Xist Is Highly Expressed in a Transient and Rapid Fashion at the Onset of Male nPSC Differentiation

It is defined in the literature that *Xist* is repressed as male nPSCs undergo differentiation both *in vivo* and *in vitro* (Panning et al., 1997; Sheardown et al., 1997). Intriguingly, our results above showed a surprisingly high upregulation of *Xist* in males with a compromised naive network, leading us to revisit the kinetics of *Xist* expression during male nPSC differentiation. To address this, we induced differentiation of male ESCs that had previously been cultured in either traditional SL or optimal 2iL (Figure 2A). Surprisingly, a striking upregulation of *Xist* was observed in differentiating male 2iL ESCs (Figure 2B). Moreover, this was independent of the differentiation condition applied. *Xist* upregulation was transient and rapid, occurring between 1.5 and 2 days after induction of differentiation (Figure 2B). Although less apparent, this pattern was also observed in differentiating male SL ESCs (Figure 2B). These results were confirmed using independent male ESC and induced pluripotent stem cell (iPSC) lines (Figures S2A and S2B).

Recent reports highlighted that erosion of imprints can occur during the culture of nPSCs (Choi et al., 2017; Yagi et al.,

(F) RNA FISH in male and female 2iL ESCs with a double-strand (ds) probe (left) or with a single-strand (ss) probe detecting only *Xist* (right). The percentage of cells with probe signal is indicated. Female EpiSCs were used as a control for the ss probe. The scale bar represents 5 μm.

(G) qRT-PCR analysis of *Nanog* and *Xist* in female and male *Nanog*$^{flox/-}$, Rosa26-CreERT2 ESCs in 2iL at indicated time points following treatment with 4-OHT. Error bars represent ± SD.

(H) qRT-PCR analysis of *Xist* in XX3 and XY1 ESCs in 2iL, 2i or after 3 and 5 days in 1 μM JAKi + 2i. Error bars represent ± SD.

(I) qRT-PCR analysis of *Oct4* and *Xist* in female and male *Oct4*$^{flox/-}$, Rosa26-CreERT2 ESCs in 2iL at indicated time points following treatment with 4-OHT. Female somatic cells were used as control for *Xist* expression. Error bars represent ± SD.

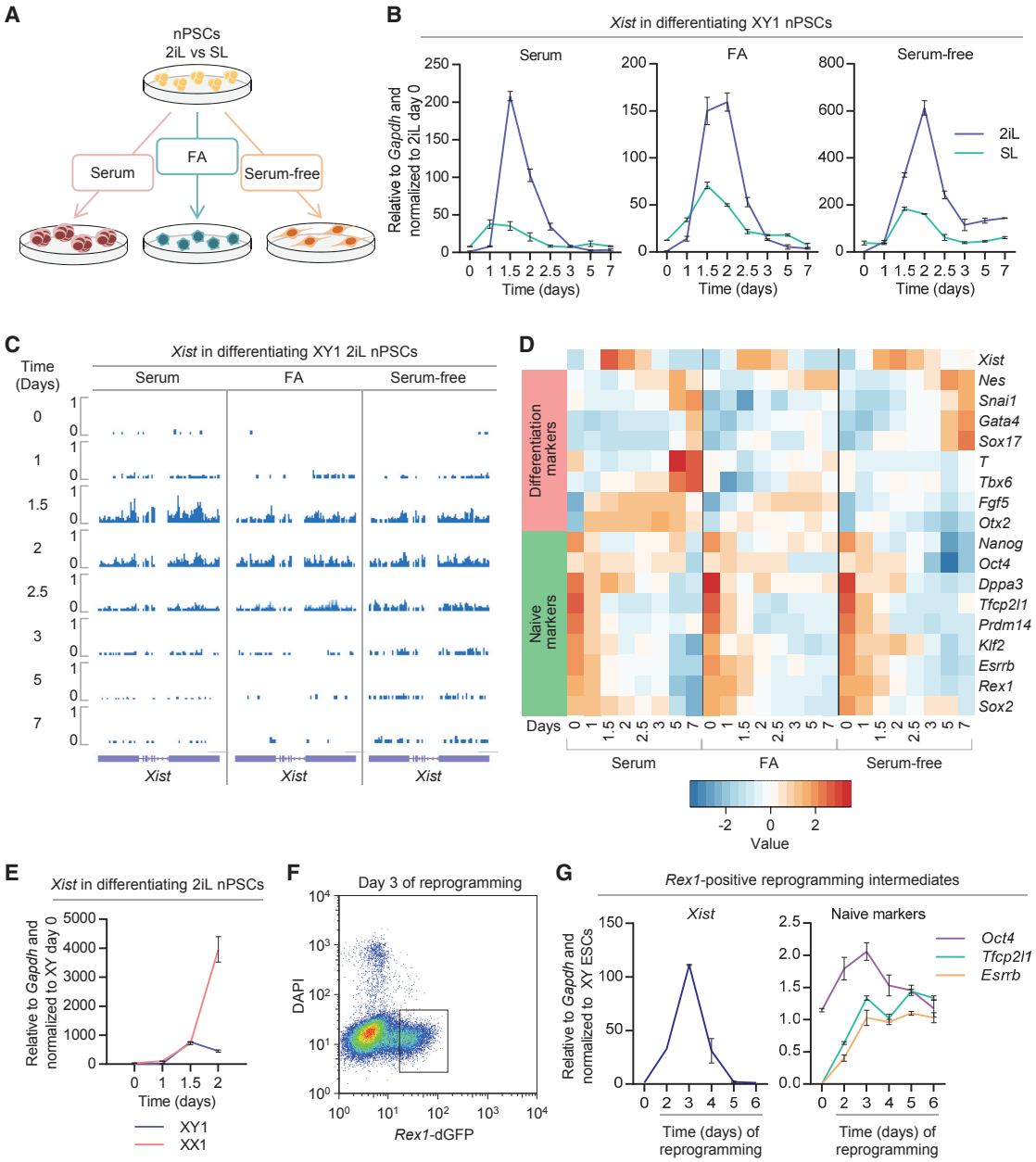

Figure 2. *Xist* Is Transiently and Rapidly Upregulated in Male nPSC Differentiation and Male EpiSC Reprogramming

(A) Schematic illustrating three conditions employed to differentiate 2iL and SL nPSCs: suspension culture in serum to generate EBs or adherent monolayer culture in serum-free media ± Fgf2+ActivinA (FA).

(B) qRT-PCR analysis of *Xist* during differentiation of male ESCs in three different conditions. Before differentiation, ESCs were maintained in 2iL or SL conditions, as indicated. Error bars represent ± SD.

(C) Strand-specific RNA-seq (negative strand only) showing expression of *Xist* during differentiation of male 2iL ESCs in three different conditions. Scale represents reads per million (RPM).

(D) Heatmap showing expression profile of *Xist*, differentiation markers, and naive markers during differentiation of male 2iL ESCs, as indicated. Scale represents *Z* scores of log2-transformed expression values.

(E) qRT-PCR analysis of *Xist* during EB differentiation of male versus female 2iL ESCs. Error bars represent ± SD.

(F) Flow cytometry analysis of male GY118F *Rex1*+/dGFP EpiSCs following reprogramming induction with GCSF in 2iL. Cells were sorted at different time points, with *Rex1*-dGFP reporter activation indicating the subset of cells successfully transitioning to the naive identity. A representative plot from day 3 is shown.

(G) qRT-PCR analysis of *Xist* and naive markers (*Oct4*, *Tfcp2l1*, and *Esrrb*) in male *Rex1*-positive reprogramming intermediates at different time points after induction of reprogramming with 2iL+GCSF/GY118F. Parental EpiSCs (day 0) and ESCs in 2iL were used as controls. Error bars represent ± SD.

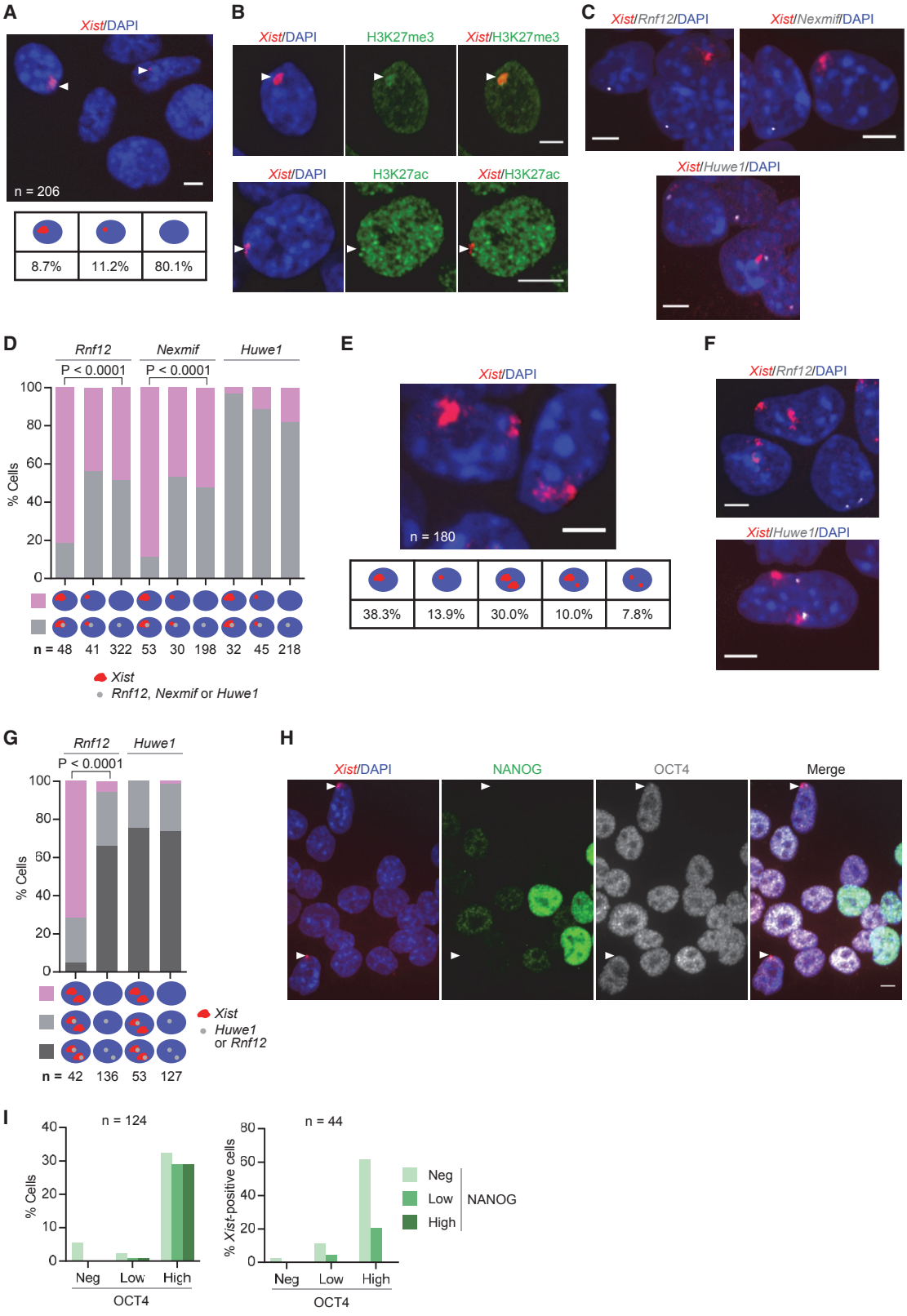

Figure 3. Males Undergo Transient XCI

(A) RNA FISH for *Xist* (red) in male 2iL ESCs at 1.5 days of differentiation in FA using a strand-specific probe. White arrowheads indicate *Xist* signals. Quantification of the different *Xist* RNA patterns is shown.

(legend continued on next page)

2017). However, *Xist* is unlikely to have its expression pattern affected, as it is not an imprinted gene in either the naive epiblast or nPSCs.

Independent differentiation time courses were analyzed by strand-specific RNA-seq. In agreement with the qRT-PCR data, when male 2iL ESCs are differentiated, there is a surge of *Xist* expression that starts 1.5 days following induction of differentiation and lasts approximately 12 hr (Figure 2C). Principal-component analysis (PCA) based on differentially expressed genes showed that 2iL ESCs have a more undifferentiated starting point in relation to SL ESCs (Figure S2C), which corroborates our qRT-PCR data showing that transferring nPSCs from SL to 2iL increases the expression of naive pluripotency markers. The expression of known regulators of *Xist* was also analyzed. *Ftx*, *Jpx*, and *Tsx* also appear to be downregulated by 2iL conditions in comparison to SL at day 0 (Figure S2D). Upon differentiation, positive and negative regulators of *Xist* are also transiently upregulated (Figures S2D–S2F). Global analysis of the expression pattern of long non-coding RNAs showed that *Xist* follows a pattern during differentiation that is distinct from other long non-coding RNAs (Figure S3A).

To position *Xist* upregulation in the sequence of events taking place during differentiation, we compared its timing relative to naive pluripotent and lineage marker gene expression (Figure 2D). Importantly, downregulation of the naive pluripotency factors *Sox2*, *Nanog*, *Rex1*, *Esrrb*, *Klf2*, *Prdm14*, and *Tfcp2l1* preceded *Xist* upregulation. In contrast, expression of lineage markers was detected only after *Xist* upregulation. In combination with the effects of naive network perturbations on *Xist* expression (Figure 1), these results indicate that the upregulation of *Xist* observed in male cells upon induction of differentiation is caused by a weakening naive pluripotent network.

The differentiation experiments were also performed in a female ESC line. Remarkably, 1.5 days after induction of embryoid body (EB) differentiation, *Xist* expression reaches very similar levels in male and female cells (Figure 2E). However, while *Xist* expression keeps increasing in female cells, it starts declining in male cells.

Together, these results reveal that at the onset of differentiation, males upregulate *Xist* at a level similar to that of females.

Xist Is Transiently Upregulated during Reprogramming of Male Cells

The aforementioned mechanistic association between a functional naive TF network and the repression of *Xist* led us to investigate whether these are correlated in the context of reprogramming to naive pluripotency in 2iL. We analyzed the productive reprogramming intermediates of male EpiSCs using STAT3 activation (Yang et al., 2010) and *Rex1*-dGFP reporter activity (Kalkan et al., 2017) to induce and monitor reprogramming, respectively (Figures 2F and S3B). As expected, *Xist* was repressed in both male EpiSCs and control ESCs (Figure 2G). However, in productive reprogramming intermediates, *Xist* was sharply upregulated (Figure 2G) prior to establishment of a consolidated nPSC identity. It is possible that this is due to loss of tight control of gene expression. Alternatively, it could reflect the fragile nature of the nascent naive network during reprogramming.

Male X Chromosome Exhibits Hallmarks of XCI upon *Xist* Upregulation

Next, we analyzed whether the observed *Xist* upregulation in males was linked to events associated with the initiation of XCI as previously described for females. To look at this, we assessed the nuclear pattern of *Xist* by RNA FISH. Surprisingly, 1.5 days after male 2iL ESCs were induced to differentiate in FA, 20% of cells showed *Xist* RNA expression. Interestingly, nearly half of these exhibited *Xist* RNA clouds, with various sizes, characteristic of XCI (Figure 3A). Although in a smaller proportion, male SL ESCs induced to differentiate also exhibited cells showing *Xist* RNA accumulation (Figure S4A). Appearance of an *Xist* RNA cloud during male nPSC differentiation has been reported before (Monkhorst et al., 2008). However, the percentage of cells exhibiting this pattern was less than 0.5%, a much smaller proportion than reported in this study. The difference in the results could be explained by the homogeneity and robust self-renewal of our 2iL nPSC cultures and by the choice of time point to conduct the analysis.

Another event associated with XCI in females is accumulation of the repressive histone mark trimethyl-H3K27 (H3K27me3) (Plath et al., 2003; Silva et al., 2003) on the future Xi. Interestingly, H3K27me3 accumulation was observed in 63% of male cells showing *Xist* RNA cloud (Figures 3B, S4B, and S4C).

We then addressed the status of acetyl-H3K27 (H3K27ac), which is a mark of active enhancers (Creyghton et al., 2010). This was found hypoacetylated at the male *Xist* RNA cloud (Figures 3B, S4B, and S4D). Together, these results indicate that a silencing epigenetic signature has formed in the *Xist*-coated male X chromosome.

To examine whether *Xist* accumulation was inducing gene silencing, we performed RNA FISH analysis for nascent transcripts of 5 X-linked genes (*Rnf12*, *Nexmif*, *Nsdhl*, *Wbp5*, and *Huwe1*). The percentage of cells expressing *Rnf12*, *Nsdhl*, and *Nexmif* was between 3- and 4-fold lower in male cells showing *Xist* cloud that in male cells lacking *Xist* accumulation, and in

(B) Immuno-RNA FISH for *Xist* (red) and H3K27me3 or H3K27ac (green) in male 2iL ESCs at 1.5 days of differentiation in FA. White arrowheads indicate *Xist* cloud.
(C) RNA FISH for *Xist* (red) and *Rnf12*, *Nexmif*, or *Huwe1* (grayscale) in male 2iL ESCs at 1.5 days of differentiation in FA.
(D) Quantification of RNA FISH patterns for the X-linked genes *Rnf12*, *Nexmif*, or *Huwe1* and *Xist* as shown in (C). Gray indicates the presence of *Rnf12*/*Nexmif*/*Huwe1* signal, and pink indicates the absence of *Rnf12*/*Nexmif*/*Huwe1* signal.
(E) RNA FISH for *Xist* (red) in female 2iL ESCs at 1.5 days of differentiation in FA using ss probe. Quantification of different *Xist* RNA patterns is shown.
(F) RNA FISH for *Xist* (red) and *Rnf12* or *Huwe1* (grayscale) in female 2iL ESCs at 1.5 days of differentiation in FA.
(G) Quantification of RNA FISH patterns for X-linked genes *Rnf12* or *Huwe1* and *Xist* as shown in (F). Dark gray indicates biallelic *Rnf12*/*Huwe1* signal, light gray indicates monoallelic *Rnf12*/*Huwe1* signal, and pink indicates the absence of *Rnf12*/*Huwe1* signal.
(H) Immuno-RNA FISH for *Xist* (red), NANOG (green), and OCT4 (grayscale) in male 2iL ESCs at 1.5 days of differentiation in FA. White arrowheads indicate *Xist* clouds.
(I) Percentage of NANOG- and OCT4-expressing cells in the population (left) and in cells exhibiting *Xist* cloud (right) as shown in (H).
Fisher's exact test was used for statistical analysis. ESC lines used were XY1 and XX1. Scale bar represents 5 μm.

the case of *Wbp5*, no examples of gene expression were found at the male X chromosome coated by *Xist* (Figures 3C, 3D, and S4E). In contrast, *Huwe1* showed no difference. *Rnf12*, *Nsdhl*, *Wbp5*, and *Nexmif* are in closer proximity to the *Xist* locus than *Huwe1* and are also known to be silenced early during XCI, unlike *Huwe1*, which is silenced at a late stage (Marks et al., 2015). At the cell population level, *Nexmif* was also downregulated (Figure S4F). However, *Xist*-mediated silencing did not affect population levels of *Rnf12* expression (Figure S4F). These data are consistent with a rapid transient *Xist* upregulation in males, a transience that is sufficient to have an impact on early-silencing genes but not lasting long enough to affect late-silencing ones.

Together these results show that males undergo XCI. which had so far only been associated with females. However, unlike females, male XCI is partial, transient, and rapid.

Females Exhibit Partial XCI of Both X Chromosomes at the Onset of Differentiation

The observed upregulation of *Xist* in males, which possess only one X chromosome, questions the existence of a choice mechanism preceding initiation of XCI in females. To address this, we performed *Xist* RNA FISH in differentiating female nPSCs. Analysis of these cells in 2iL self-renewing conditions showed that *Xist* is not expressed (Figure 1F). Strikingly, at 1.5 days of differentiation, we observed that 30% of the female cells expressing *Xist* display RNA accumulation on both X chromosomes (Figure 3E). Control experiments revealed that 99% of the cells in this female line have no more than two X chromosomes, demonstrating that these results cannot be explained by the presence of tetraploid cells in culture (Figures S1B and S4G).

To assess whether *Xist* accumulation is inducing gene silencing on both X chromosomes, we performed RNA FISH analysis for nascent transcripts of *Rnf12* and *Huwe1* (Figures 3F and 3G). The incidence of biallelic silencing of *Rnf12* was 12-fold greater in female cells exhibiting *Xist* RNA accumulation on both X chromosomes than in cells not expressing *Xist*, while *Huwe1* showed no difference.

These results indicate that the choice of which X chromosome is going to be irreversibly silenced may follow rather than precede the initiation of XCI.

Transient *Xist* RNA Patterns Occur as Differentiating Cells Become NANOG Negative

To investigate whether *Xist* upregulation is consistent with a particular differentiation stage, we analyzed the expression of NANOG and OCT4 relative to *Xist* at the single-cell level. Due to asynchrony in nPSC differentiation, NANOG expression was variable while most cells remained OCT4-high at 1.5 days. Interestingly, *Xist* upregulation in males occurred in cells that were NANOG-low or -negative (Figures 3H and 3I). Likewise, we found biallelic *Xist* upregulation in female cells that were OCT4-high/NANOG-low or -negative (Figures S4H and S4I). The expression of active CASPASE-3, which is an early marker of apoptosis, was evaluated to confirm the viability of the *Xist*-positive male cells. Importantly, all analyzed *Xist*-positive cells were negative for active CASPASE-3 (Figure S4J).

These results are in agreement with a transient *Xist* upregulation occurring in a defined developmental window and in close relationship with the downregulation of the naive network.

In Vivo Transient *Xist* Expression in Males and in Females on Both X Chromosomes

The embryonic day 4.5 (E4.5) naive epiblast is molecularly and functionally highly similar to *in vitro* 2iL nPSCs (Boroviak et al., 2015). Given the observed transient upregulation of *Xist* RNA during nPSC differentiation, we investigated whether this also occurs during *in vivo* differentiation of the pluripotent naive epiblast. In agreement with our findings in nPSCs, we found that E4.5 naive epiblast cells do not display *Xist* expression in either sex (Figure 4A). From E4.5, the embryo starts implanting and naive pluripotent gene expression is rapidly downregulated (Boroviak et al., 2015). Thus, we analyzed E5.5 male and female post-implantation embryos as a naive epiblast differentiation time point. At E5.5, we also failed to detect *Xist* expression in males, whereas female cells already exhibited one *Xist* RNA cloud in nearly all cells, which is the pattern associated with female differentiated cells. This led us to analyze earlier time points. Interestingly, at E4.75–E5.0, we found 1–3 cells per male epiblast exhibiting *Xist* RNA expression (Figure 4B). When analyzing female epiblast cells for the same time points, we observed that *Xist* was biallelically expressed in 10% of the epiblast cells showing *Xist* expression (Figures 4B and 4C). Together, these data are indicative that at implantation stage, and correlating with the downregulation of the naive epiblast network, male and female epiblast cells undergo transient and rapid monoallelic and biallelic expression of *Xist* respectively.

DISCUSSION

Our results show that *Xist* is fully repressed in both male and female nPSCs provided they have a robust naive TF network. This may be the result of a combination of direct and indirect mechanisms at the XIC, which contains multiple genomic binding sites occupied by naive pluripotent-associated TFs located at the *Xist* locus and at other non-coding and coding genes involved in *Xist* regulation (Sánchez-Castillo et al., 2015).

We showed that *Xist* accumulates transiently at the male X chromosome and induces partial epigenetic and transcriptional silencing in early differentiating cells. We have also demonstrated that this is linked to downregulation of the naive TF network. In this context, known positive regulators of *Xist*, such as *Jpx* (Tian et al., 2010), *Ftx* (Chureau et al., 2011), and RNF12 (Jonkers et al., 2009; Barakat et al., 2017), may transiently gain the upper hand and drive *Xist* expression. However, *Xist* is subsequently rapidly suppressed, suggesting that other mechanisms of *Xist* silencing are readily available. In agreement with this, deletion of *Tsix*, one of the non-coding RNAs implicated in *Xist* silencing, was previously found to correlate with the presence of an *Xist* RNA cloud in a proportion of differentiating male nPSCs (Sado et al., 2002). Likewise, *Dnmt1* mutant nPSCs exhibit *Xist* upregulation and silencing of X-linked genes in differentiating male cells (Beard et al., 1995; Panning and Jaenisch, 1996).

It has been proposed that initiation of XCI is related to the X chromosome/ploidy ratio (Monkhorst et al., 2008). Our study proposes downregulation of the naive TF network as the trigger for the initiation of XCI. It will now be interesting to investigate how these relate to each other.

XCI is defined as having five key phases in the following order: counting, choice, initiation, spreading, and maintenance (Augui

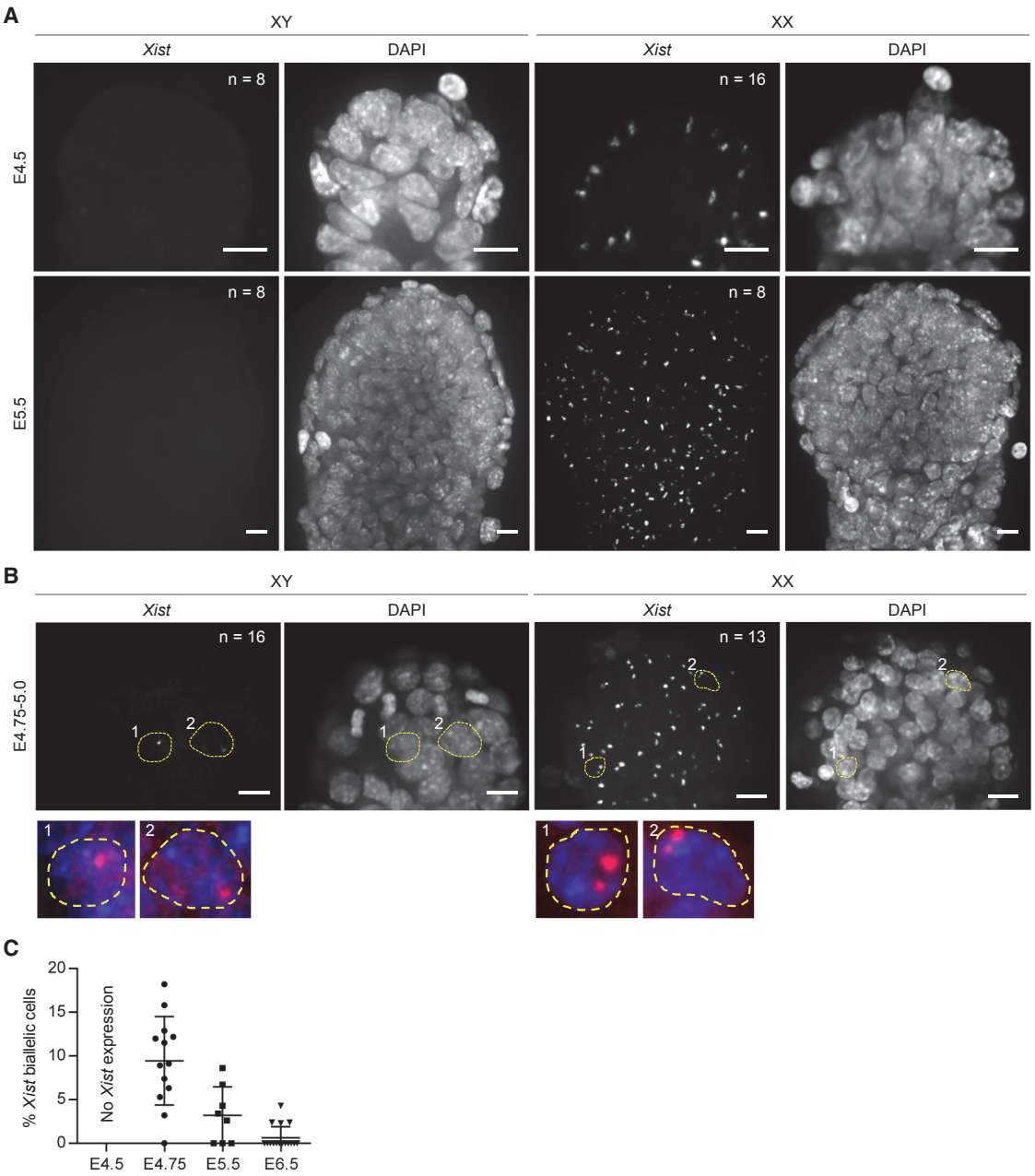

Figure 4. *Xist* Is Transiently Upregulated Monoallelically in Males and Biallelically in Females *In Vivo*

(A and B) RNA FISH for *Xist* in representative male and female epiblasts of embryos at E4.5 and E5.5 (A) and at E4.75–E5.0 (B).

(B) Examples of cells with monoallelic *Xist* expression in males and biallelic expression in females are delineated with yellow dashed lines. Higher magnification of these cells is displayed in the bottom panels.

(C) Percentage of cells with biallelic *Xist* over total number of epiblast cells expressing *Xist* in female embryos at indicated developmental stages. Error bars represent ± SD.

Scale bar represents 10 μm.

et al., 2011). However, our data suggest that counting and choice between the two X chromosomes is not a requirement for XCI initiation. Furthermore, we show that the initiation and spreading phases also occur in males. Importantly, the initiation and spreading of XCI in males take place within a defined window of time where the process of XCI is known to be reversible (Wutz and Jaenisch, 2000), meaning that as long as *Xist* expression ceases within 3 days of differentiation, any induced changes on the X chromosome are fully reversible. Consistent with this, our data showed that *Xist* expression was already downregulated by day 3 of male cell differentiation. Therefore, we hypothesize that in the mouse species a counting mechanism, which relies on gender differences during the reversible period, occurs after XCI initiation.

It has been proposed that initiation of XCI in females is preceded by pairing of the two XIC loci and that the process of choice was dependent on pairing, therefore restricting XCI to female cells (Bacher et al., 2006; Xu et al., 2006). Moreover, although the negative regulation of *Xist* by the naive TF network is the same in male and female cells, the X-linked *Xist* activators adjacent to *Xist* and known to also work in *trans* will be duplicated in females. These and other mechanisms must somehow ensure that all but one X chromosome undergo irreversible XCI. It will now be important to further understand how these mechanisms allow XCI to be maintained in females only.

Human naive-like cells and human embryos cultured *in vitro* were found to have an intriguing *Xist* pattern (Petropoulos et al., 2016; Sahakyan et al., 2017; Vallot et al., 2017). In both cases, the presence of one or two *Xist* RNA clouds was reported for a proportion of male and female cells, respectively. As suggested by the authors, this may indicate species differences. However, it may also be akin to what we are reporting here, that is, as a result of a perturbed naive TF network, human naive cells may exhibit monoallelic and biallelic *Xist* upregulation in both males and females respectively.

In conclusion, our study redefines the paradigm of XCI and opens up new avenues to investigate how this process is regulated.

STAR★METHODS

Detailed methods are provided in the online version of this paper and include the following:

- KEY RESOURCES TABLE
- CONTACT FOR REAGENT AND RESOURCE SHARING
- EXPERIMENTAL MODEL AND SUBJECT DETAILS
  - Cell lines
  - Cell culture
  - Cell differentiation
  - Reprogramming
  - Embryos
- METHOD DETAILS
  - RNA isolation, cDNA synthesis and qRT-PCR
  - Flow cytometry
  - DNA extraction
  - Gender PCR
  - Western blotting
  - *Xist* RNA FISH with double-stranded probe
  - RNA FISH with single-stranded probe
  - RNA FISH of mouse embryos
  - Immunofluorescence
  - Metaphase spread
  - DNA FISH chromosome painting
  - Microscopy and image analysis
  - RNA-seq
- QUANTIFICATION AND STATISTICAL ANALYSES
  - RNA-seq analysis
- DATA AND SOFTWARE AVAILABILITY

SUPPLEMENTAL INFORMATION

Supplemental Information includes four figures and can be found with this article online at https://doi.org/10.1016/j.stem.2018.05.001.

ACKNOWLEDGMENTS

We thank Yael Costa, Charlotte Handford, and Kathryn Tremble for critical reading of the manuscript. We are also grateful to Carla Mulas and Ayaka Yanagida for help with the embryo dissections, Rebecca Lloyd for assistance in cloning of the GY118F transgene, and Peter Humphreys and Andy Riddell for assistance with imaging and flow cell sorting, respectively. We also thank Neil Brockdorff and Tatyana Nesterova for technical help. This study was supported by a Wellcome Trust Fellowship (WT101861) to J.C.R.S., who is a Wellcome Trust Senior Research Fellow. E.J.S. is the recipient of a Ph.D. fellowship from the Portuguese Foundation for Science and Technology, FCT (SFRH/BD/52197/2013). H.T.S. and L.E.B. are recipients of MRC Ph.D. studentships (1233706 and 1509066).

AUTHOR CONTRIBUTIONS

J.C.R.S. conceived the study, designed experiments, and wrote and approved the manuscript. E.J.S. designed and performed the experiments and wrote the manuscript. H.T.S. designed and performed the reprogramming experiment. J.N. derived the *Oct4*$^{flox/-}$, Rosa26-CreERT2 ESCs. L.E.B. designed and performed the *Oct4* deletion experiment. S.D. designed and performed bioinformatics analysis. M.G. performed bioinformatics analysis.

DECLARATION OF INTERESTS

The authors declare no competing interests.

Received: August 10, 2017
Revised: December 21, 2017
Accepted: May 1, 2018
Published: May 24, 2018; corrected online June 6, 2018

REFERENCES

Alexandrova, S., Kalkan, T., Humphreys, P., Riddell, A., Scognamiglio, R., Trumpp, A., and Nichols, J. (2016). Selection and dynamics of embryonic stem cell integration into early mouse embryos. Development *143*, 24–34.

Augui, S., Nora, E.P., and Heard, E. (2011). Regulation of X-chromosome inactivation by the X-inactivation centre. Nat. Rev. Genet. *12*, 429–442.

Bacher, C.P., Guggiari, M., Brors, B., Augui, S., Clerc, P., Avner, P., Eils, R., and Heard, E. (2006). Transient colocalization of X-inactivation centres accompanies the initiation of X inactivation. Nat. Cell Biol. *8*, 293–299.

Barakat, T.S., Gunhanlar, N., Pardo, C.G., Achame, E.M., Ghazvini, M., Boers, R., Kenter, A., Rentmeester, E., Grootegoed, J.A., and Gribnau, J. (2017). RNF12 activates Xist and is essential for X chromosome inactivation. PLoS Genet. *27*, e1002001.

Beard, C., Li, E., and Jaenisch, R. (1995). Loss of methylation activates Xist in somatic but not in embryonic cells. Genes Dev. *9*, 2325–2334.

Boroviak, T., Loos, R., Lombard, P., Okahara, J., Behr, R., Sasaki, E., Nichols, J., Smith, A., and Bertone, P. (2015). Lineage-specific profiling delineates the emergence and progression of naive pluripotency in mammalian embryogenesis. Dev. Cell *35*, 366–382.

Chambers, I., Silva, J., Colby, D., Nichols, J., Nijmeijer, B., Robertson, M., Vrana, J., Jones, K., Grotewold, L., and Smith, A. (2007). Nanog safeguards pluripotency and mediates germline development. Nature *450*, 1230–1234.

Choi, J., Huebner, A.J., Clement, K., Walsh, R.M., Savol, A., Lin, K., Gu, H., Di Stefano, B., Brumbaugh, J., Kim, S.Y., et al. (2017). Prolonged Mek1/2 suppression impairs the developmental potential of embryonic stem cells. Nature *548*, 219–223.

Chuma, S., and Nakatsuji, N. (2001). Autonomous transition into meiosis of mouse fetal germ cells in vitro and its inhibition by gp130-mediated signaling. Dev. Biol. *229*, 468–479.

Chureau, C., Chantalat, S., Romito, A., Galvani, A., Duret, L., Avner, P., and Rougeulle, C. (2011). Ftx is a non-coding RNA which affects Xist expression and chromatin structure within the X-inactivation center region. Hum. Mol. Genet. *20*, 705–718.

Creyghton, M.P., Cheng, A.W., Welstead, G.G., Kooistra, T., Carey, B.W., Steine, E.J., Hanna, J., Lodato, M.A., Frampton, G.M., Sharp, P.A., et al. (2010). Histone H3K27ac separates active from poised enhancers and predicts developmental state. Proc. Natl. Acad. Sci. USA *107*, 21931–21936.

Ficz, G., Hore, T.A., Santos, F., Lee, H.J., Dean, W., Arand, J., Krueger, F., Oxley, D., Paul, Y.L., Walter, J., et al. (2013). FGF signaling inhibition in ESCs drives rapid genome-wide demethylation to the epigenetic ground state of pluripotency. Cell Stem Cell *13*, 351–359.

Habibi, E., Brinkman, A.B., Arand, J., Kroeze, L.I., Kerstens, H.H., Matarese, F., Lepikhov, K., Gut, M., Brun-Heath, I., Hubner, N.C., et al. (2013). Whole-genome bisulfite sequencing of two distinct interconvertible DNA methylomes of mouse embryonic stem cells. Cell Stem Cell *13*, 360–369.

Jonkers, I., Barakat, T.S., Achame, E.M., Monkhorst, K., Kenter, A., Rentmeester, E., Grosveld, F., Grootegoed, J.A., and Gribnau, J. (2009). RNF12 is an X-encoded dose-dependent activator of X chromosome inactivation. Cell *139*, 999–1011.

Kalkan, T., Olova, N., Roode, M., Mulas, C., Lee, H.J., Nett, I., Marks, H., Walker, R., Stunnenberg, H.G., Lilley, K.S., et al. (2017). Tracking the embryonic stem cell transition from ground state pluripotency. Development *144*, 1221–1234.

Leitch, H.G., McEwen, K.R., Turp, A., Encheva, V., Carroll, T., Grabole, N., Mansfield, W., Nashun, B., Knezovich, J.G., Smith, A., et al. (2013). Naive pluripotency is associated with global DNA hypomethylation. Nat. Struct. Mol. Biol. *20*, 311–316.

Mak, W., Nesterova, T.B., de Napoles, M., Appanah, R., Yamanaka, S., Otte, A.P., and Brockdorff, N. (2004). Reactivation of the paternal X chromosome in early mouse embryos. Science *303*, 666–669.

Marks, H., Kalkan, T., Menafra, R., Denissov, S., Jones, K., Hofemeister, H., Nichols, J., Kranz, A., Stewart, A.F., Smith, A., and Stunnenberg, H.G. (2012). The transcriptional and epigenomic foundations of ground state pluripotency. Cell *149*, 590–604.

Marks, H., Kerstens, H.H., Barakat, T.S., Splinter, E., Dirks, R.A., van Mierlo, G., Joshi, O., Wang, S.Y., Babak, T., Albers, C.A., et al. (2015). Dynamics of gene silencing during X inactivation using allele-specific RNA-seq. Genome Biol. *16*, 149.

Martello, G., and Smith, A. (2014). The nature of embryonic stem cells. Annu. Rev. Cell Dev. Biol. *30*, 647–675.

Minkovsky, A., Barakat, T.S., Sellami, N., Chin, M.H., Gunhanlar, N., Gribnau, J., and Plath, K. (2013). The pluripotency factor-bound intron 1 of Xist is dispensable for X chromosome inactivation and reactivation in vitro and in vivo. Cell Rep. *3*, 905–918.

Monkhorst, K., Jonkers, I., Rentmeester, E., Grosveld, F., and Gribnau, J. (2008). X inactivation counting and choice is a stochastic process: evidence for involvement of an X-linked activator. Cell *132*, 410–421.

Navarro, P., Chambers, I., Karwacki-Neisius, V., Chureau, C., Morey, C., Rougeulle, C., and Avner, P. (2008). Molecular coupling of Xist regulation and pluripotency. Science *321*, 1693–1695.

Navarro, P., Oldfield, A., Legoupi, J., Festuccia, N., Dubois, A., Attia, M., Schoorlemmer, J., Rougeulle, C., Chambers, I., and Avner, P. (2010). Molecular coupling of Tsix regulation and pluripotency. Nature *468*, 457–460.

Navarro, P., Moffat, M., Mullin, N.P., and Chambers, I. (2011). The X-inactivation trans-activator Rnf12 is negatively regulated by pluripotency factors in embryonic stem cells. Hum. Genet. *130*, 255–264.

Okamoto, I., Otte, A.P., Allis, C.D., Reinberg, D., and Heard, E. (2004). Epigenetic dynamics of imprinted X inactivation during early mouse development. Science *303*, 644–649.

Panning, B., and Jaenisch, R. (1996). DNA hypomethylation can activate Xist expression and silence X-linked genes. Genes Dev. *10*, 1991–2002.

Panning, B., Dausman, J., and Jaenisch, R. (1997). X chromosome inactivation is mediated by Xist RNA stabilization. Cell *90*, 907–916.

Pasque, V., and Plath, K. (2015). X chromosome reactivation in reprogramming and in development. Curr. Opin. Cell Biol. *37*, 75–83.

Pasque, V., Tchieu, J., Karnik, R., Uyeda, M., Sadhu Dimashkie, A., Case, D., Papp, B., Bonora, G., Patel, S., Ho, R., et al. (2014). X chromosome reactivation dynamics reveal stages of reprogramming to pluripotency. Cell *159*, 1681–1697.

Payer, B., Rosenberg, M., Yamaji, M., Yabuta, Y., Koyanagi-Aoi, M., Hayashi, K., Yamanaka, S., Saitou, M., and Lee, J.T. (2013). Tsix RNA and the germline factor, PRDM14, link X reactivation and stem cell reprogramming. Mol. Cell *52*, 805–818.

Petropoulos, S., Edsgärd, D., Reinius, B., Deng, Q., Panula, S.P., Codeluppi, S., Reyes, A.P., Linnarsson, S., Sandberg, R., and Lanner, F. (2016). Single-cell RNA-seq reveals lineage and X chromosome dynamics in human preimplantation embryos. Cell *167*, 285.

Plath, K., Fang, J., Mlynarczyk-Evans, S.K., Cao, R., Worringer, K.A., Wang, H., de la Cruz, C.C., Otte, A.P., Panning, B., and Zhang, Y. (2003). Role of histone H3 lysine 27 methylation in X inactivation. Science *300*, 131–135.

Sado, T., Li, E., and Sasaki, H. (2002). Effect of TSIX disruption on XIST expression in male ES cells. Cytogenet. Genome Res. *99*, 115–118.

Sahakyan, A., Kim, R., Chronis, C., Sabri, S., Bonora, G., Theunissen, T.W., Kuoy, E., Langerman, J., Clark, A.T., Jaenisch, R., and Plath, K. (2017). Human naive pluripotent stem cells model X chromosome dampening and X inactivation. Cell Stem Cell *20*, 87–101.

Sánchez-Castillo, M., Ruau, D., Wilkinson, A.C., Ng, F.S., Hannah, R., Diamanti, E., Lombard, P., Wilson, N.K., and Gottgens, B. (2015). CODEX: a next-generation sequencing experiment database for the haematopoietic and embryonic stem cell communities. Nucleic Acids Res. *43*, D1117–D1123.

Sheardown, S.A., Duthie, S.M., Johnston, C.M., Newall, A.E., Formstone, E.J., Arkell, R.M., Nesterova, T.B., Alghisi, G.C., Rastan, S., and Brockdorff, N. (1997). Stabilization of Xist RNA mediates initiation of X chromosome inactivation. Cell *91*, 99–107.

Silva, J., Mak, W., Zvetkova, I., Appanah, R., Nesterova, T.B., Webster, Z., Peters, A.H., Jenuwein, T., Otte, A.P., and Brockdorff, N. (2003). Establishment of histone h3 methylation on the inactive X chromosome requires transient recruitment of Eed-Enx1 polycomb group complexes. Dev. Cell *4*, 481–495.

Silva, J., Barrandon, O., Nichols, J., Kawaguchi, J., Theunissen, T.W., and Smith, A. (2008). Promotion of reprogramming to ground state pluripotency by signal inhibition. PLoS Biol. *6*, e253.

Silva, J., Nichols, J., Theunissen, T.W., Guo, G., van Oosten, A.L., Barrandon, O., Wray, J., Yamanaka, S., Chambers, I., and Smith, A. (2009). Nanog is the gateway to the pluripotent ground state. Cell *138*, 722–737.

Tada, M., Takahama, Y., Abe, K., Nakatsuji, N., and Tada, T. (2001). Nuclear reprogramming of somatic cells by in vitro hybridization with ES cells. Curr. Biol. *11*, 1553–1558.

Tian, D., Sun, S., and Lee, J.T. (2010). The long noncoding RNA, Jpx, is a molecular switch for X chromosome inactivation. Cell *143*, 390–403.

Vallot, C., Patrat, C., Collier, A.J., Huret, C., Casanova, M., Liyakat Ali, T.M., Tosolini, M., Frydman, N., Heard, E., Rugg-Gunn, P.J., and Rougeulle, C. (2017). XACT noncoding RNA competes with XIST in the control of X chromosome activity during human early development. Cell Stem Cell *20*, 102–111.

Wutz, A., and Jaenisch, R. (2000). A shift from reversible to irreversible X inactivation is triggered during ES cell differentiation. Mol. Cell *5*, 695–705.

Xu, N., Tsai, C.L., and Lee, J.T. (2006). Transient homologous chromosome pairing marks the onset of X inactivation. Science *311*, 1149–1152.

Yagi, M., Kishigami, S., Tanaka, A., Semi, K., Mizutani, E., Wakayama, S., Wakayama, T., Yamamoto, T., and Yamada, Y. (2017). Derivation of ground-state female ES cells maintaining gamete-derived DNA methylation. Nature *548*, 224–227.

Yang, J., van Oosten, A.L., Theunissen, T.W., Guo, G., Silva, J.C., and Smith, A. (2010). Stat3 activation is limiting for reprogramming to ground state pluripotency. Cell Stem Cell *7*, 319–328.

Ying, Q.L., Wray, J., Nichols, J., Batlle-Morera, L., Doble, B., Woodgett, J., Cohen, P., and Smith, A. (2008). The ground state of embryonic stem cell self-renewal. Nature *453*, 519–523.

STAR★METHODS

KEY RESOURCES TABLE

REAGENT or RESOURCE	SOURCE	IDENTIFIER
Antibodies		
Monoclonal mouse anti-alpha-Tubulin	Abcam	Cat# ab7291, RRID:AB_2241126
Polyclonal rabbit anti-Nanog	Bethyl Laboratories	Cat# A300-397A, RRID:AB_386108
Monoclonal rat anti-Nanog	ThermoFisher Scientific	Cat# 14-5761-80, RRID:AB_763613
Monoclonal rabbit anti-Oct4	Cell Signaling Technology	Cat# 83932, RRID:AB_2721046
Polyclonal goat anti-Oct4	Santa Cruz Biotechnology	Cat# sc-8628, RRID:AB_653551
Monoclonal rabbit anti-Phospho-Stat3 (Tyr705)	Cell Signaling Technology	Cat# 9145, RRID:AB_2491009
Polyclonal rabbit anti-H3K27me3	Merck Millipore	Cat# 07-449, RRID:AB_310624
Polyclonal rabbit anti-H3K37ac	Abcam	Cat# ab4729, RRID:AB_2118291
Monoclonal rabbit anti-Cleaved Caspase-3 (Asp175)	Cell Signaling Technology	Cat# 9664, RRID:AB_2070042
Polyclonal rabbit anti-Rnf12	Merck Millipore	Cat# ABE1949, RRID:AB_2721047
HPR-conjugated donkey anti-rabbit	GE Healthcare	Cat# NA934, RRID:AB_772206
HPR-conjugated sheep anti-mouse	GE Healthcare	Cat# NA931, RRID:AB_772210
HPR-conjugated donkey anti-goat	Santa Cruz Biotechnology	Cat# sc-2020, RRID:AB_631728
Donkey anti-rabbit IgG (H+L) Highly Cross-Adsorbed Secondary Antibody, Alexa Fluor 488	ThermoFisher Scientific	Cat# A-21206, RRID:AB_2535792
Donkey anti-Rabbit IgG (H+L) Highly Cross-Adsorbed Secondary Antibody, Alexa Fluor 647	ThermoFisher Scientific	Cat# A-31573, RRID:AB_2536183
Donkey Anti-Rat IgG (H+L) Highly Cross-Adsorbed Secondary Antibody, Alexa Fluor 488	ThermoFisher Scientific	Cat# A-21208, RRID:AB_2535794
Goat biotinylated anti-Avidin	Vector Laboratories	Cat# BA-0300, RRID:AB_2336108
Chemicals, Peptides, and Recombinant Proteins		
N2	Cambridge Stem Cell Institute	N/A
B27	ThermoFisher Scientific	Cat# 17504044
Murine LIF	Hyvönen lab, Cambridge	N/A
CHIR99021	Stewart lab, Dresden	N/A
PD0325901	Stewart lab, Dresden	N/A
FBS	Labtech	Cat# FB-1001S/500
Egf	Peprotech	Cat# 315-09
Fgf2	Hyvönen lab, Cambridge	N/A
Activin A	Hyvönen lab, Cambridge	N/A
XAV 939	Tocris, Bio-techne	Cat# 3748
4-Hydroxytamoxifen	Sigma-Aldrich	Cat# 7904
InSolution JAK Inhibitor I	Merck-Millipore	Cat# 420097
GCSF	Peprotech	Cat# 300-23
KaryoMAX Colcemid Solution in HBSS	ThermoFisher Scientific	*Cat# 15210040*
Taq DNA Polymerase	QIAGEN	*Cat# 201205*
Critical Commercial Assays		
DNeasy Blood & Tissue Kit	QIAGEN	Cat# 69504
RNeasy Mini Kit	QIAGEN	Cat# 74104
SuperScript III First-Strand Synthesis SuperMix	ThermoFisher Scientific	Cat# 18080400
TaqMan Fast Universal PCR Master Mix (2X), no AmpErase UNG	ThermoFisher Scientific	Cat# 4352042
Esrrb TaqMan Gene Expression Assay	ThermoFisher Scientific	Mm00442411_m1
Ftx TaqMan Gene Expression Assay	ThermoFisher Scientific	Mm03455830_m1

(*Continued on next page*)

Continued

REAGENT or RESOURCE	SOURCE	IDENTIFIER
Gapdh TaqMan Gene Expression Assay	ThermoFisher Scientific	4352339E
Klf2 TaqMan Gene Expression Assay	ThermoFisher Scientific	Mm01244979_g1
Klf4 TaqMan Gene Expression Assay	ThermoFisher Scientific	Mm00516104_m1
Klf5 TaqMan Gene Expression Assay	ThermoFisher Scientific	Mm00456521_m1
Nanog TaqMan Gene Expression Assay	ThermoFisher Scientific	Mm02384862_g1
Nexmif TaqMan Gene Expression Assay	ThermoFisher Scientific	Mm01239465_g1
Oct4 TaqMan Gene Expression Assay	ThermoFisher Scientific	Mm00658129_gH
Rex1 TaqMan Gene Expression Assay	ThermoFisher Scientific	Mm03053975_g1
Rnf12 TaqMan Gene Expression Assay	ThermoFisher Scientific	Mm00488044_m1
Socs3 TaqMan Gene Expression Assay	ThermoFisher Scientific	Mm01249143_g1
Sox2 TaqMan Gene Expression Assay	ThermoFisher Scientific	Mm03053810_s1
Tfcp2l1 TaqMan Gene Expression Assay	ThermoFisher Scientific	Mm00470119_m1
Xist TaqMan Gene Expression Assay	ThermoFisher Scientific	Mm01232884_m1
Biotin-Nick Translation Mix	Sigma-Aldrich	Cat# 11745824910
Illustra MicroSpin S-300 HR columns	GE Healthcare	Cat# 27513001
Salmon Sperm DNA, sheared	ThermoFisher Scientific	*Cat# AM9680*
Mouse Cot-1 DNA	ThermoFisher Scientific	*18440016*
Ribonucleoside Vanadyl Complex	New England Biolabs	*S1402S*
Texas Red Avidin DCS	Vector Laboratories	*A-2016*
Mouse Xist Stellaris RNA FISH Probe with Quasar 570 Dye	BioSearch Technologies	Cat# SMF-3011-1
Mouse Xist Stellaris RNA FISH Probe with Quasar 670 Dye	BioSearch Technologies	Cat# VSMF-3095-5
Custom Stellaris RNA FISH Probe with FISH Probe with Quasar 570 Dye	BioSearch Technologies	Cat# SMF-1063-5
Mouse Chromosome X Whole Chromosome Painting Probe, Green Label	MetaSystems Probes	Cat# D-1420-050-FI
Mouse Chromosome Y Whole Chromosome Painting Probe, Orange Label	MetaSystems Probes	Cat# D-1421-050-OR
Deposited Data		
RNA seq data	This paper	GEO: GSE109173
Experimental Models: Cell Lines		
E14tg2a ESC line	Smith lab, Cambridge	N/A
EFC ESC line	Smith lab, Cambridge	N/A
LF1 ESC line	Smith lab, Cambridge	N/A
LF2 ESC line	Smith lab, Cambridge	N/A
C6 ESC line	Smith lab, Cambridge	N/A
Nanog$^{flox/-}$, Rosa26-CreERT2 ESC line	This paper	N/A
Oct4$^{flox/-}$, Rosa26-CreERT2 ESC line	This paper	N/A
Rex1-dGFP EpiSC line	This paper	N/A
Rex1-dGFP NSC line	This paper	N/A
Nanog-GFP EpiSC line	Smith lab, Cambridge	N/A
Experimental Models: Organisms/Strains		
Mouse CD-1	Charles River	Cat# 022
Oligonucleotides		
Gender PCR primer Ube1XA (5′ to 3′): TGGTC TGGACCCAAACGCTGTCCACA	(Chuma and Nakatsuji, 2001)	N/A
Gender PCR primer Ube1XB (5′ to 3′): GGCA GCAGCCATCACATAATCCAGATG	(Chuma and Nakatsuji, 2001)	N/A

(*Continued on next page*)

Continued

REAGENT or RESOURCE	SOURCE	IDENTIFIER
Software and Algorithms		
Fiji	Open Source	http://imagej.net/Fiji/Downloads
R	The R Project	https://www.r-project.org/
GraphPad Prism 6	GraphPad Software	https://www.graphpad.com/scientific-software/prism/
FlowJo	FlowJo, LLC	https://www.flowjo.com/
TrimGalore	Babraham Institute	http://www.bioinformatics.babraham.ac.uk/projects/trim_galore
TopHat2	Johns Hopkins University	https://ccb.jhu.edu/software/tophat
featureCounts	Walter and Eliza Hall Institute of Medical Research	http://bioinf.wehi.edu.au/featureCounts
DESeq2	Bioconductor	https://bioconductor.org/packages/release/bioc/html/DESeq2.html

CONTACT FOR REAGENT AND RESOURCE SHARING

Further information and requests for resources and reagents should be directed to and will be fulfilled by the Lead Contact, José Silva (jcs64@cam.ac.uk).

EXPERIMENTAL MODEL AND SUBJECT DETAILS

Cell lines

Male wild-type ESC lines included E14tg2a (XY1) and EFC (XY2). Female wild-type ESC lines included LF1 (XX1), LF2 (XX2) and C6 (XX3). The cell sorting experiment was performed in male *Nanog*-GFP ESCs. Female *Nanog*-GFP EpiSCs were used as control in *Xist* RNA FISH. *Nanog* deletion was performed in male and female *Nanog*$^{flox/-}$, Rosa26-CreERT2 ESC lines. *Oct4* deletion was performed in male and female *Oct4*$^{flox/-}$, Rosa26-CreERT2 ESC lines. Male iPSC line used was derived from *Rex1*-dGFP NSCs. Reprogramming was performed in male *Rex1*-dGFP EpiSCs.

Cell culture

Mouse ESCs and iPSCs were cultured in 2i+LIF (2iL), 2i, or serum+LIF (SL) as indicated. 2iL medium was composed of N2B27, 3 μM CHIR99021, 1 μM PD0325901 (Stewart lab, Dresden), and 20 ng ml^{-1} of murine LIF (Hyvönen lab, Cambridge). N2B27 medium comprised 1:1 DMEM/F-12 and Neurobasal (ThermoFisher Scientific), 2 mM L-glutamine (ThermoFisher Scientific), 1x penicillin-streptomycin (Sigma-Aldrich), 0.1 mM 2-mercaptoethanol (ThermoFisher Scientific), 1% B27 (ThermoFisher Scientific) and 0.5% N2 (homemade). SL medium contained GMEM (Sigma-Aldrich), 10% fetal bovine serum (Labtech), 1x non-essential amino acids (ThermoFisher Scientific), 1 mM sodium pyruvate (Sigma-Aldrich), 2 mM L-glutamine, 1X penicillin-streptomycin, 0.1 mM 2-mercaptoethanol and 20 ng ml^{-1} of LIF. EpiSCs were cultured in FAX medium composed of N2B27 supplemented with 12.5 ng ml^{-1} Fgf2, 20 ng ml^{-1} Activin A (Hyvönen lab, Cambridge) and 6.25 μg ml^{-1} XAV 939 (Bio-Techne). 4-OHT (Sigma-Aldrich) was used at a concentration of 500 nM and InSolution JAKi I (Merck Millipore) at a concentration of 1 μM. During expansion of *Nanog*$^{flox/-}$ cell lines, selection with 200 μg ml^{-1} G418 (ThermoFisher Scientific) was applied to select for pluripotent cells based on *Nanog* promoter activity at the null allele. For ESCs and iPSCs, tissue-culture flasks were coated with 0.1% gelatin (Sigma-Aldrich) in PBS (Sigma-Aldrich). For EpiSCs, tissue-culture flasks were coated with 10 μg ml^{-1} fibronectin (Merck Millipore) in PBS (Sigma-Aldrich).

Cell differentiation

For embryoid body differentiation, 1.5 × 10^6 cells were plated on 10 cm low-attachment dishes in serum-containing medium without LIF. For differentiation in adherent monolayer culture, 6 × 10^5 cells were plated on gelatin-coated 10 cm dishes in serum-free (N2B27) or N2B27 supplemented with Fgf2 and Activin A (FA). XY1 and XX1 ESCs were not passaged more than 3 times in 2iL prior to the differentiation assays.

Reprogramming

Embryo-derived male EpiSCs with *Rex1*+/dGFP reporter (Kalkan et al., 2017) were used that constitutively express the GY118F receptor transgene known to drive EpiSC reprogramming via STAT3 activation (Yang et al., 2010). For reprogramming, EpiSCs were plated at 10,000 cells per fibronectin-coated 6-well in FAX maintenance medium. The following day, reprogramming was induced by switch to 2iL plus GCSF (30 ng ml^{-1} human GCSF, Peprotech). On days 2, 3, 4, 5 and 6, multiple reprogramming wells were harvested using accutase, stained with DAPI to eliminate nonviable cells, and sorted by flow cytometry to isolate the *Rex1*-dGFP-positive subpopulation for further analysis. Parental EpiSCs and male *Rex1*+/dGFP ESCs were used as negative and positive gating controls respectively.

Embryos

Embryos were collected from CD1 female mice (Charles River Laboratories, UK). Use of animals in this project was approved by the Animal Welfare and Ethical Review Body for the University of Cambridge (Procedure Project Licenses P76777883 and 80/2597).

METHOD DETAILS

RNA isolation, cDNA synthesis and qRT-PCR

Total RNA was isolated from cells using the RNeasy mini kit (QIAGEN) in accordance with the manufacturer's protocol. One microgram of total RNA was reverse-transcribed using SuperScript III First-Strand Synthesis SuperMix (ThermoFisher Scientific). Reverse Transcription Quantitative Real-Time PCR (qRT-PCR) reactions were set up in triplicate using TaqMan Universal PCR Master Mix (ThermoFisher Scientific) and TaqMan gene expression assays (ThermoFisher Scientific). qRT-PCR experiments were performed on a StepOnePlus Real Time PCR System (ThermoFisher Scientific). Delta Ct (ΔCt) values compared to Gapdh were calculated and relative quantities calculated as 2 to the power of -ΔCt. The means of three values were calculated and normalized as indicated.

Flow cytometry

Nanog-GFP ESCs were resuspended in PBS containing 3.5% BSA (ThermoFisher Scientific) and sorting was performed using a MoFlo high-speed cell sorter (Beckman Coulter). A 514/10BP filter was used for GFP and a 580/30BP filter was used for autofluorescence. *Rex1*-dGFP positive reprogramming intermediates were sorted using a BD Influx 5 cell sorter (BD Biosciences). A 460/50 filter was used for DAPI and a 530/40 filter was used for GFP.

DNA extraction

In the case of the cell lines, DNA was isolated using the DNeasy Blood & Tissue Kit (QIAGEN) in accordance with the manufacturer's protocol. In the case of the embryos, these were collected from the slides after RNA FISH and imaging and then lysed in 0.2% Triton X-100 and Proteinase K at 56°C for 10 minutes followed by 95°C for 15 minutes.

Gender PCR

Cell lines were sexed by PCR using primers Ube1XA and Ube1XB, which results in two products of distinct sizes from the Ube1x and Ube1y genes on the X and Y chromosome respectively (Chuma and Nakatsuji, 2001) . PCR reactions were performed in a final volume of 20 μL with 100 ng of DNA, 1X CoralLoad buffer, 0.2 mM dNTPs, 0.35 μM primers and 2.5 units Taq DNA Polymerase (QIAGEN) and run on a thermal cycler with the following conditions: 94°C for 3 minutes, 30 cycles with 94°C for 30 s, 66°C for 30 s, and 72°C for 30 s, followed by 72°C for 10 minutes. In the case of the embryos 4 μL per embryo lysate were added to the PCR reaction. Products were electrophoresed on 2% agarose gel.

Western blotting

Dissociated cells were lysed in RIPA buffer (as described by Sigma-Aldrich) containing Complete-ULTRA protease-inhibitor and PhosStop phosphatase-inhibitor cocktails (Roche), and sonicated with Bioruptor200 (Diagenode) at high frequency, alternating 30 s on/off for 3 minutes. SDS-PAGE electrophoresis was performed using Bolt 10% Bis-Tris Plus gels (ThermoFisher Scientific) in a Novex MiniCell (ThermoFisher Scientific). Protein transfer was performed using semi-dry iBlot 2 system (ThermoFisher Scientific) and iBlot Transfer Stacks (ThermoFisher Scientific). The following primary antibodies dilutions were used: mouse monoclonal against α-Tubulin (1:5,000) from Abcam, rabbit polyclonal against NANOG (1:5,000) from Bethyl Laboratories, rabbit monoclonal against p-Y705-STAT3 (1:1,000) from Cell Signaling Technology, rabbit polyclonal against RNF12 (1:1,000) from Merck Millipore, and goat polyclonal against OCT4 (1:1,000) from Santa Cruz Biotechnology. Detection was achieved using HRP-linked secondary antibodies against the appropriate species (GE Healthcare) and ECL Plus Western Blotting Detection System (GE Healthcare).

Xist RNA FISH with double-stranded probe

Cells were plated on SuperFrost Plus Adhesion slides (ThermoFisher Scientific) and permeabilised in cytoskeletal buffer (100 mM NaCl, 300 mM sucrose, 3 mM MgCl2, 10 mM PIPES) containing 0.5% Triton X-100 (Sigma-Aldrich), 1 mM EGTA pH 8 and vanadyl ribonucleoside (New England Biolabs) for 5 minutes on ice. They were subsequently fixed in 4% paraformaldehyde (Sigma-Aldrich) for 10 minutes, briefly washed in 1X PBS and dehydrated through 70, 80, 95, and 100% ethanol, after which the slides were air-dried. At this stage, a denatured *Xist* probe was applied onto the slides and these were incubated overnight at 37°C.

The probe was prepared by labeling plasmid DNA containing a mouse *Xist* exon 1 fragment sequence (kindly provided by Professor Neil Brockdorff, University of Oxford, UK) with a Biotin-Nick Translation Mix (Sigma-Aldrich) according to manufacturer's instructions and non-incorporated nucleotides were removed with Illustra MicroSpin S-300 HR columns (GE Healthcare). To 20 ng of probe, 10 μg of sheared salmon sperm DNA (ThermoFisher Scientific) and 3 μg of mouse Cot-1 DNA (ThermoFisher Scientific) were added. Finally, the probe was dehydrated by vacuum and resuspended in deionized formamide (VWR). Before applying to the slide, the probe was denatured at 80°C and 2X hybridization buffer (4X SSC, 20% dextran sulfate, 2 mg ml^{-1} BSA, 2 mM vanadyl ribonucleoside) was added.

The following day, the slides were washed at 42°C in 2X SSC/50% formamide for 15 minutes, then three times in 2X SSC for 5 minutes each. They were then transferred to 4X SSC/0.1% Tween 20 at room temperature and blocked in 4 mg ml^{-1} BSA in

4X SSC/0.1% Tween 20 at 37°C for 30 minutes. Probe detection was performed by first applying Avidin conjugated to Texas Red (1:500, Vector Laboratories), then a biotinylated anti-avidin antibody (1:200, Vector Laboratories), followed by a second layer of Avidin-Texas Red. All detection reagents were diluted in 4 mg ml^{-1} BSA in 4X SSC/0.1%Tween 20 and incubated at 37°C for 30 minutes followed by three washes in 4X SSC/0.1% Tween 20 in between each step. Finally, the slides were mounted in Vectashield Mounting Medium containing DAPI (Vector Laboratories).

RNA FISH with single-stranded probe

RNA FISH protocol was modified from the Stellaris (Biosearch Technologies) protocol for adherent mammalian cells. Cells were plated on SuperFrost Plus Adhesion slides (ThermoFisher Scientific) and fixed in 4% PFA (Sigma-Aldrich) at room temperature for 10 minutes. They were subsequently washed in 1X PBS and permeabilised in cytoskeletal buffer (100 mM NaCl, 300 mM sucrose, 3 mM MgCl2, 10 mM PIPES) containing 0.5% Triton X-100, 1 mM EGTA pH 8 and vanadyl ribonucleoside (New England Biolabs) for 5 minutes on ice. Following washing in 1X PBS, they were incubated in 70% ethanol at 4°C overnight. Cells were incubated in 10% formamide (VWR) in 2X SSC (Sigma-Aldrich) for 10 minutes and then in 250 nM Stellaris Probes diluted in 100 mg mL^{-1} dextran sulfate (MP Biomedicals) and 10% formamide in 2X SSC at 37°C overnight. *Xist* was recognized using Stellaris FISH Probes labeled with either Quasar 570 or Quasar 670 (BioSearch Technologies). *Rnf12*, *Nexmif*, *Nsdhl*, *Wbp5* and *Huwe1* were recognized using Custom Stellaris FISH Probes labeled with Quasar 570 (BioSearch Technologies). The sequences of 48 oligonucleotides designed against unique intronic sequences using the online Stellaris Probe Designer tool (BioSearch Technologies). The *Rnf12* and *Huwe1* probes sequences were kindly provided by Prof. Neil Brockdorff and Dr. Tatyana Nesterova (University of Oxford, UK). After hybridization, cells were incubated in 10% formamide in 2X SSC at 37°C for 30 minutes followed by a wash in 2X SSC at room temperature for 5 minutes. Cells were mounted with Vectashield Antifade Mounting Medium with DAPI (Vector Laboratories).

RNA FISH of mouse embryos

Mouse embryos were collected from CD1 mice and fixed in 4% PFA at room temperature for 15 minutes. Embryos were further processed for RNA FISH using Stellaris probes (BioSearch Technologies) according to the procedure described above.

Immunofluorescence

Immunofluorescence was always performed in combination with RNA FISH using Stellaris probes. Sequential immunofluorescence and RNA FISH protocol was modified from the Stellaris (Biosearch Technologies) protocol for adherent mammalian cells. Cells were fixed and permeabilised as for RNA FISH. They were then washed in 1X PBS and incubated with primary antibody diluted in 1X PBS at 37°C for 2 hours. Primary antibodies were used as follows: rabbit polyclonal against H3K27me3 (1:500) from Merck Millipore, rabbit polyclonal against H3K27ac (1:500) from Abcam, rat monoclonal against NANOG (1:300) from ThermoFisher Scientific, rabbit monoclonal against OCT4 (1:300) from Cell Signaling Technology and rabbit monoclonal against cleaved CASPASE-3 (1:100) from Cell Signaling Technology. Following washing in 1X PBS, cells were incubated with secondary antibody diluted in 1X PBS at 37°C for 1 hour. An appropriate Alexa Fluor conjugated secondary antibody (1:1,000) from ThermoFisher Scientific was used. Cells were then washed in 1X PBS and fixed again in 4% PFA at room temperature for 10 minutes. Following washing with 1X PBS, RNA FISH protocol was carried out as described above, starting from the incubation in 10% formamide in 2X SSC.

Metaphase spread

ESCs were plated onto a gelatinised 6-well 2 days prior preparation of the chromosome spreads. Cultures were then arrested in metaphase by addition of 0.5 μg mL^{-1} KaryoMAX colcemid (ThermoFisher Scientific) and incubation at 37°C for 3 hours. Cell were then washed in PBS, harvested with accutase and centrifuged at 300 g for 5 minutes. Following aspiration of the supernatant, the pellet was resuspended in 5 mL of 0.075 M KCl solution and incubated at 37°C for 15 minutes. Then 100 μL of ice cold methanol:glacial acetic acid (3:1) fixative solution were added drop-wise followed by an incubation on ice for 10 minutes. Following incubation, cells were centrifuged at 300 g for 5 minutes, supernatant was aspirated leaving 500 μL in the tube and 5 mL of fixative solution were added to the cells. Again 500 μL of the supernatant were kept in the tube after centrifugation and spread onto a glass slide. After at least 3 hours at room temperature, the slide was stained or stored at −20°C for further analysis.

DNA FISH chromosome painting

Prior to X and Y chromosome painting, immune RNA FISH was performed, slides were imaged and x-y coordinates were marked for future reference. After removal of the coverslip, slides were washed in 2X SSC at room temperature. X and Y chromosome painting was also performed on metaphase spreads. Slides were dehydrated through an ice-cold ethanol series (70%, 80%. 95% and 100%) for 3 minutes each and then allowed to air dry. X and/or Y chromosome paint probe (Metasystems) was added to the slide, denaturation was carried out at 75°C for 2 minutes and slides were incubated at 37°C overnight. After hybridization, slides were incubated in 0.4X SSC at 72°C for 2 minutes followed by a wash with 0.05% Tween-20 in 2X SSC at room temperature for 30 s. Slides were rinsed in water, allowed to air dry and mounted with Vectashield Antifade Mounting Medium with DAPI (Vector Laboratories).

Microscopy and image analysis

Images were taken with an Eclipse Ti Spinning Disk confocal microscope (Nikon) equipped with an Andor Revolution XD System using either 40X or 60X objectives. Images were processed and analyzed with ImageJ. Presented images are maximum intensity

projections of Z stack slices or, in the case of embryos, selected Z stack slices. Scoring of RNA FISH signals was done by eye from images.

RNA-seq

RNA integrity was assessed on a Qubit Fluorometer (ThermoFisher Scientific) and Agilent Bioanalyzer Nano Chips (Agilent Technologies). Depletion of ribosomal RNA was performed on 2-5 μg of total RNA using the Ribo-Zero rRNA Removal Kit (Illumina) and libraries were produced from 10-100ng of ribosomal-depleted RNA using NextFlex Rapid Directional RNA-seq Kit (Bioo Scientific) with 12 cycles of PCR amplification. Libraries were pooled in equimolar quantities and sequenced on the HiSeq4000 platform (Illumina) at CRUK.

QUANTIFICATION AND STATISTICAL ANALYSES

Where indicated, statistical analysis was performed by Fisher's exact test using GraphPad Prism. "n" values in figures represent the number of embryos or number of cells analyzed. All qRT-PCR data represent the mean of three technical replicates. All error bars represent ± standard deviation (SD).

RNA-seq analysis

RNA-seq reads were adaptor-trimmed with TrimGalore (http://www.bioinformatics.babraham.ac.uk/projects/trim_galore) and mapped to the mouse reference genome (GRCm38/mm10) with TopHat2 (https://ccb.jhu.edu/software/tophat) allowing for one mismatch and alignments guided by Ensembl gene models (Ensembl release 82). Strand-specific read counts were obtained with featureCounts (http://bioinf.wehi.edu.au/featureCounts). Transcript counts were normalized, and the statistical significance of differential expression between samples was assessed using the R Bioconductor DESeq2 package (https://bioconductor.org/packages/release/bioc/html/DESeq2.html). Transcript counts normalized by DESeq2 size factors were subsequently normalized by their length/1000. Principal component analysis (PCA) was performed by singular value composition using the R prcomp() function on scaled expression values.

DATA AND SOFTWARE AVAILABILITY

The accession number for the RNA-seq data reported in this paper is GEO: GSE109173.

Cell Stem Cell, Volume *22*

Supplemental Information

Exit from Naive Pluripotency Induces a Transient X Chromosome Inactivation-like State in Males

Elsa J. Sousa, Hannah T. Stuart, Lawrence E. Bates, Mohammadmersad Ghorbani, Jennifer Nichols, Sabine Dietmann, and José C.R. Silva

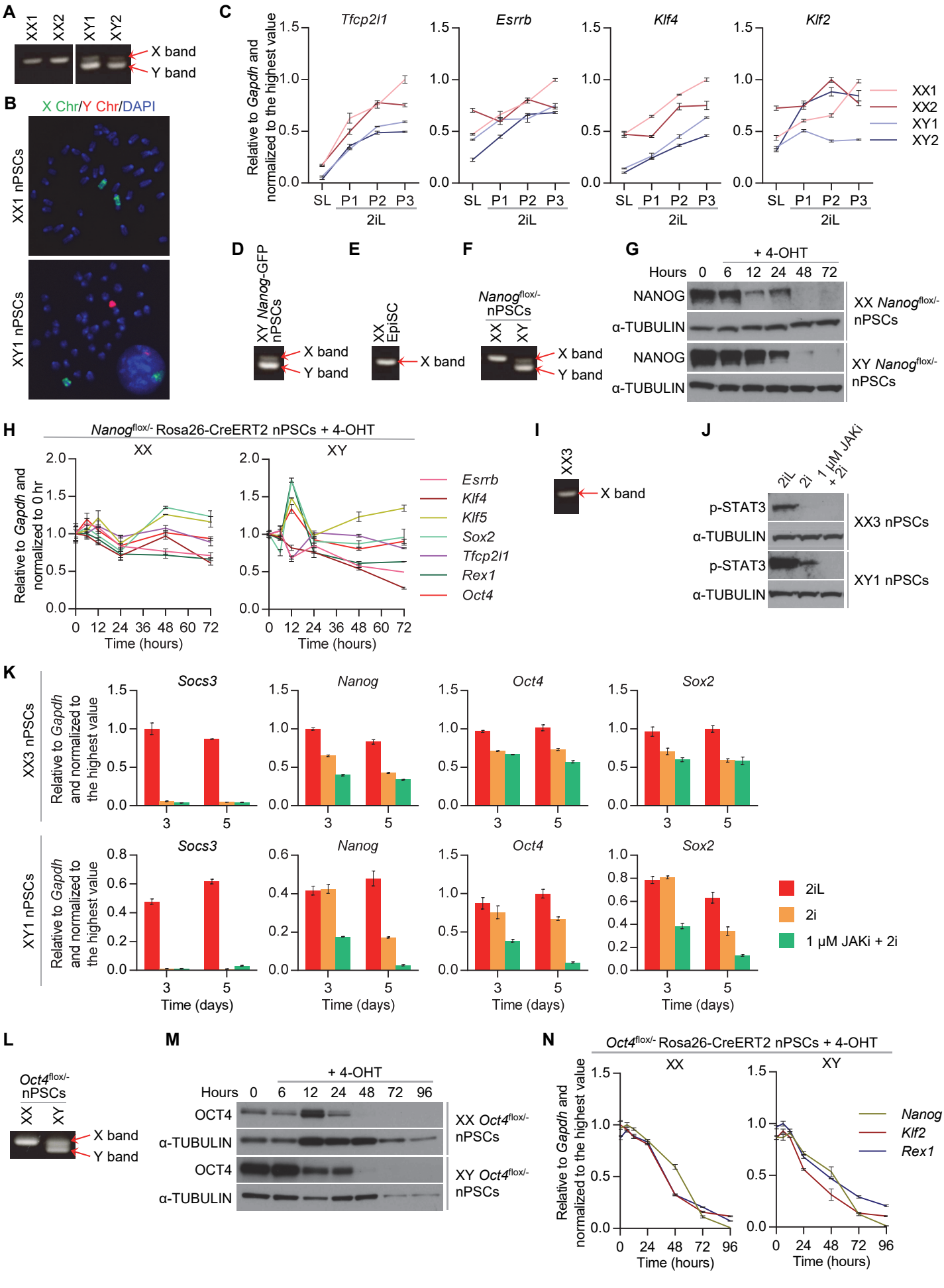
A
XX1
XX2
XY1
XY2
X band
Y band
B
X Chr/Y Chr/DAPI
XX1 nPSCs
XY1 nPSCs
C
Tfcp2l1
Esrrb
Klf4
Klf2
Relative to Gapdh and normalized to the highest value
SL P1 P2 P3
2iL
XX1
XX2
XY1
XY2
D
XY Nanog-GFP nPSCs
X band
Y band
E
XX EpiSC
X band
F
Nanogflox/- nPSCs
XX XY
X band
Y band
G
+ 4-OHT
Hours 0 6 12 24 48 72
NANOG
α-TUBULIN
XX Nanogflox/- nPSCs
XY Nanogflox/- nPSCs
H
Nanogflox/- Rosa26-CreERT2 nPSCs + 4-OHT
XX
XY
Relative to Gapdh and normalized to 0 hr
Time (hours)
Esrrb
Klf4
Klf5
Sox2
Tfcp2l1
Rex1
Oct4
I
XX3
X band
J
2iL
2i
1 μM JAKi + 2i
p-STAT3
α-TUBULIN
XX3 nPSCs
XY1 nPSCs
K
XX3 nPSCs
XY1 nPSCs
Relative to Gapdh and normalized to the highest value
Socs3
Nanog
Oct4
Sox2
Time (days)
2iL
2i
1 μM JAKi + 2i
L
Oct4flox/- nPSCs
XX XY
X band
Y band
M
+ 4-OHT
Hours 0 6 12 24 48 72 96
OCT4
α-TUBULIN
XX Oct4flox/- nPSCs
XY Oct4flox/- nPSCs
N
Oct4flox/- Rosa26-CreERT2 nPSCs + 4-OHT
XX
XY
Relative to Gapdh and normalized to the highest value
Time (hours)
Nanog
Klf2
Rex1

Figure S1. *Xist* expression is abolished by a robust naive pluripotent network, Related to Figure 1.

(A) PCR-based gender determination of the cell lines LF1 (XX1), LF2 (XX2), E14tg2a (XY1), and EFC (XY2).

(B) X (green) and Y (red) DNA FISH chromosome painting of metaphase spreads of the ESC lines LF1 (XX1) and E14tg2a (XY1).

(C) qRT-PCR analysis of naive markers (*Tfcp2l1*, *Esrrb*, *Klf4*, and *Klf2*) in two female, LF1 (XX1) and LF2 (XX2), and two male, E14tg2a (XY1) and EFC (XY2), ESC lines in SL versus 2iL conditions. P indicates the number of passages in 2iL. Data shown are the mean of 3 technical replicates. Error bars represent ± SD.

(D) PCR-based gender determination of the *Nanog*-GFP ESC line.

(E) PCR-based gender determination of the control EpiSC line.

(F) PCR-based gender determination of the *Nanog*$^{flox/-}$, Rosa26-CreERT2 ESC lines.

(G) Western blot analysis of NANOG in female and male *Nanog*$^{flox/-}$, Rosa26-CreERT2 ESCs in 2iL (0 hours) and at different time points following treatment with 4-OHT.

(H) qRT-PCR analysis of naive markers (*Esrrb*, *Klf4*, *Klf5*, *Sox2*, *Tfcp2l1*, *Rex1*, and *Oct4*) in female and male *Nanog*$^{flox/-}$, Rosa26-CreERT2 ESCs in 2iL (0 hours) and at different time points following treatment with 4-OHT. Data shown are the mean of 3 technical replicates. Error bars represent ± SD.

(I) PCR-based gender determination of the C6 ESC line (XX3).

(J) Western blot analysis of p-STAT3 in female (C6 – XX3) and male (E14tg2a – XY1) ESCs in 2iL, 2i or after 3 days in 1 μM JAKi + 2i.

(K) qRT-PCR analysis of the STAT3-target *Socs3* and naive markers (*Nanog*, *Oct4*, and *Sox2*) in female (C6 – XX3) and male (E14tg2a – XY1) ESCs in 2iL, 2i or after 3 and 5 days in 1 μM JAKi + 2i. Data shown are the mean of 3 technical replicates. Error bars represent ± SD.

(L) PCR-based gender determination of the *Oct4*$^{flox/-}$, Rosa26-CreERT2 ESC lines.

(M) Western blot analysis of OCT4 in female and male *Oct4*$^{flox/-}$, Rosa26-CreERT2 ESCs in 2iL (0 hours) and at different time points following treatment with 4-OHT.

(N) qRT-PCR analysis of naive markers (*Nanog*, *Klf2*, and *Rex1*) in female and male *Oct4*$^{flox/-}$, Rosa26-CreERT2 ESCs in 2iL (0 hours) and at different time points following treatment with 4-OHT. Data shown are the mean of 3 technical replicates. Error bars represent ± SD.

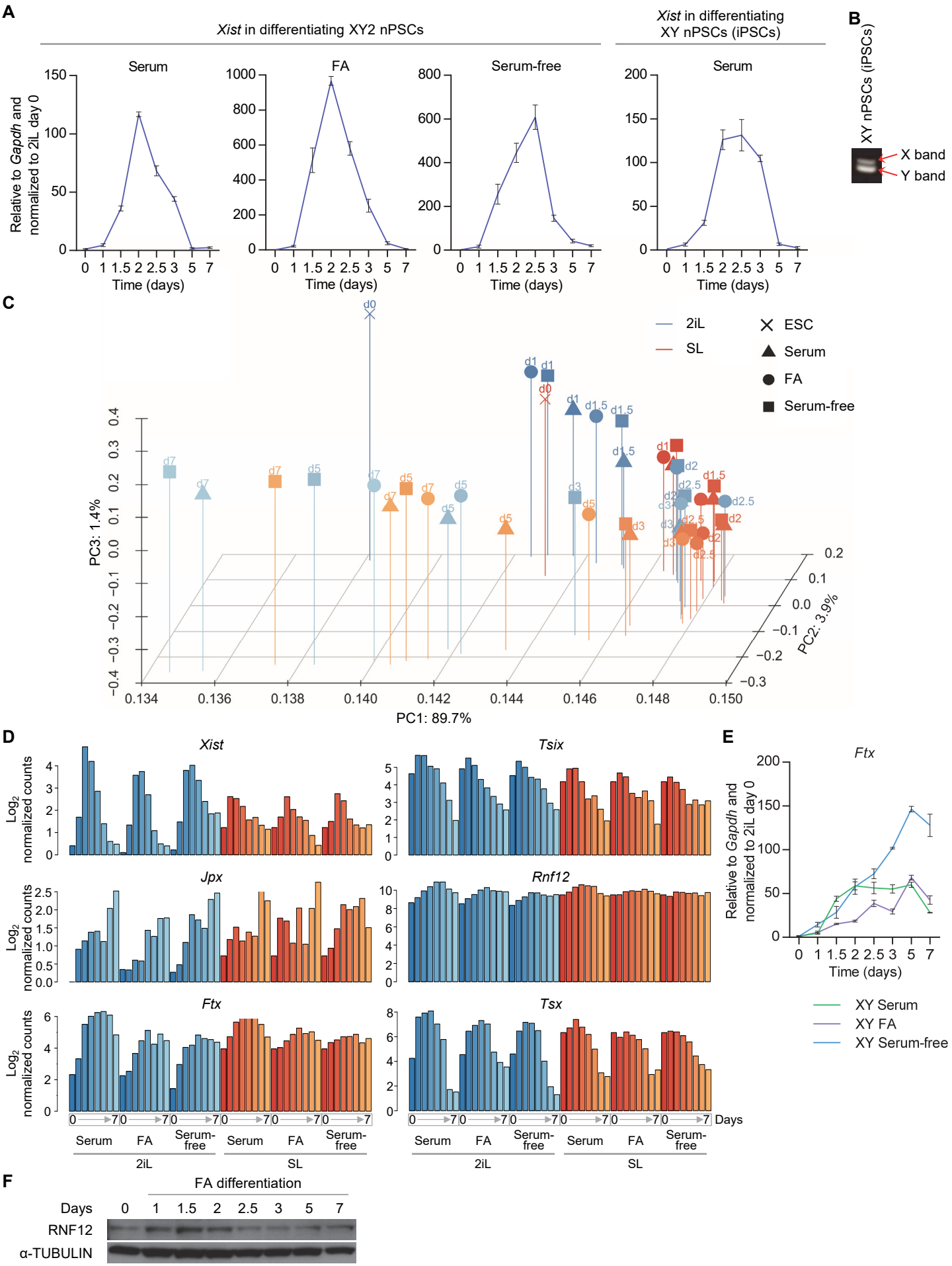
A
Xist in differentiating XY2 nPSCs
Xist in differentiating XY nPSCs (iPSCs)
Serum
FA
Serum-free
Serum
Relative to Gapdh and normalized to 2iL day 0
Time (days)
B
XY nPSCs (iPSCs)
X band
Y band
C
2iL
SL
ESC
Serum
FA
Serum-free
PC1: 89.7%
PC2: 3.9%
PC3: 1.4%
D
Xist
Tsix
Jpx
Rnf12
Ftx
Tsx
Log2 normalized counts
Days
Serum
FA
Serum-free
2iL
SL
E
Ftx
Relative to Gapdh and normalized to 2iL day 0
Time (days)
XY Serum
XY FA
XY Serum-free
F
FA differentiation
Days
RNF12
α-TUBULIN

Figure S2. *Xist* is transiently and rapidly upregulated in male nPSC differentiation, Related to Figure 2.

(A) qRT-PCR analysis of *Xist* during differentiation of male (EFC – XY2) ESCs using different conditions, and during embryoid body differentiation of male iPSCs derived from *Rex1*-dGFP neural stem cells. Before differentiation, cells were maintained in 2iL. Data shown are the mean of 3 technical replicates. Error bars represent ± SD.

(B) PCR-based gender determination of the iPSC line.

(C) PCA of differentiating male (E14tg2a – XY1) cells based on differential expression of genes that had an expression of at least Log_2 (normalized counts) 4.5 in at least one of the samples. Before differentiation, ESCs were maintained in 2iL or SL media, as indicated. Data was obtained by strand-specific RNA-seq.

(D) Expression levels are shown during differentiation of male (E14tg2a – XY1) ESCs for *Xist* and other elements of the XIC that have been implicated in the regulation of *Xist*. Before differentiation, ESCs were maintained in 2iL or SL media, as indicated. Data were obtained by strand-specific RNA-seq. Scale represents Log_2 transformed expression value.

(E) qRT-PCR analysis of *Ftx* during differentiation of male (E14tg2a – XY1) ESCs using different conditions. Before differentiation, cells were maintained in 2iL. Data shown are the mean of 3 technical replicates. Error bars represent ± SD.

(F) Western blot analysis of RNF12 during differentiation of male (E14tg2a – XY1) ESCs in FA. Before differentiation, cells were maintained in 2iL.

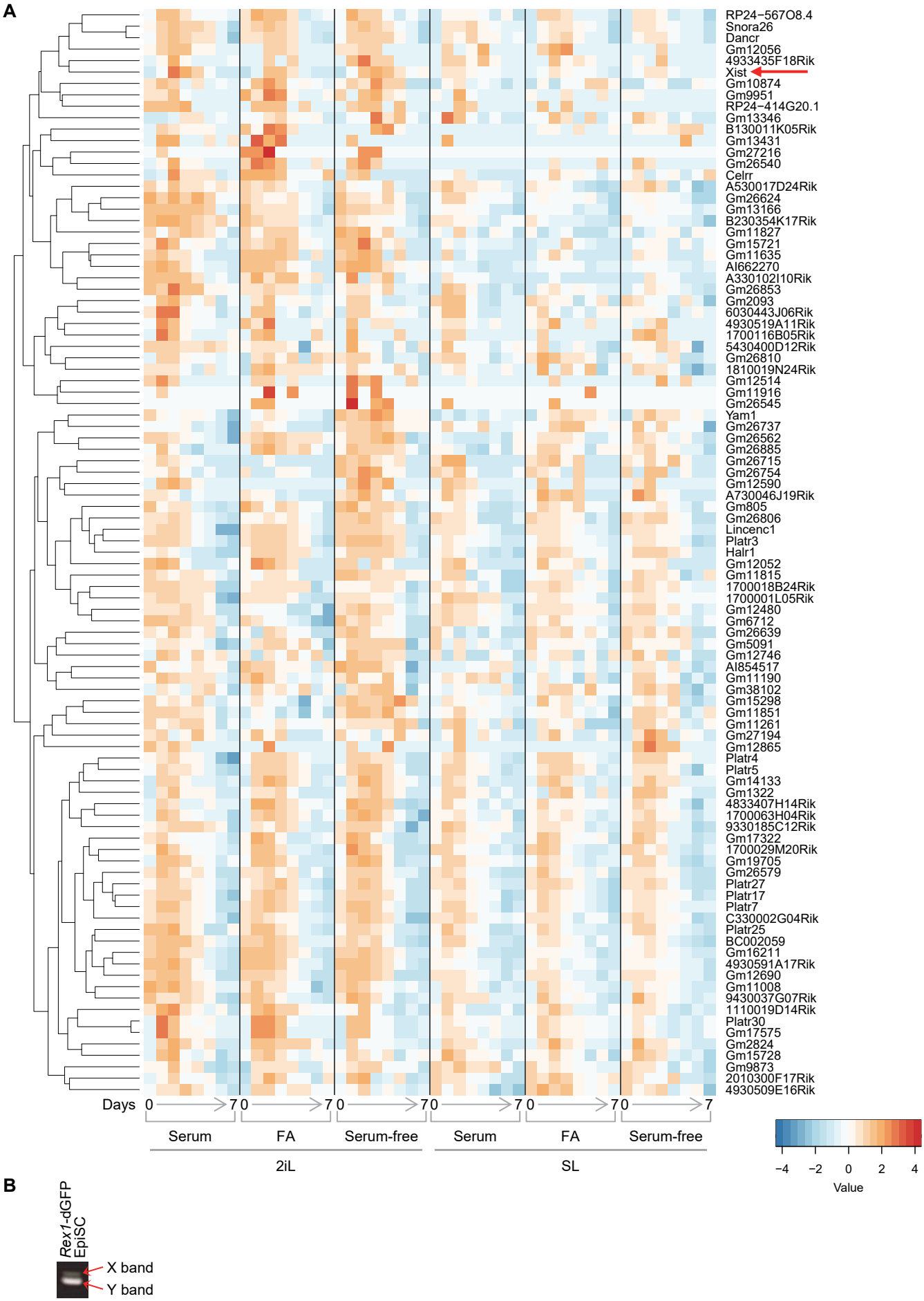
A
RP24−567O8.4
Snora26
Dancr
Gm12056
4933435F18Rik
Xist
Gm10874
Gm9951
RP24−414G20.1
Gm13346
B130011K05Rik
Gm13431
Gm27216
Gm26540
Celrr
A530017D24Rik
Gm26624
Gm13166
B230354K17Rik
Gm11827
Gm15721
Gm11635
AI662270
A330102I10Rik
Gm26853
Gm2093
6030443J06Rik
4930519A11Rik
1700116B05Rik
5430400D12Rik
Gm26810
1810019N24Rik
Gm12514
Gm11916
Gm26545
Yam1
Gm26737
Gm26562
Gm26885
Gm26715
Gm26754
Gm12590
A730046J19Rik
Gm805
Gm26806
Lincenc1
Platr3
Halr1
Gm12052
Gm11815
1700018B24Rik
1700001L05Rik
Gm12480
Gm6712
Gm26639
Gm5091
Gm12746
AI854517
Gm11190
Gm38102
Gm15298
Gm11851
Gm11261
Gm27194
Gm12865
Platr4
Platr5
Gm14133
Gm1322
4833407H14Rik
1700063H04Rik
9330185C12Rik
Gm17322
1700029M20Rik
Gm19705
Gm26579
Platr27
Platr17
Platr7
C330002G04Rik
Platr25
BC002059
Gm16211
4930591A17Rik
Gm12690
Gm11008
9430037G07Rik
1110019D14Rik
Platr30
Gm17575
Gm2824
Gm15728
Gm9873
2010300F17Rik
4930509E16Rik
Days 0 7 0 7 0 7 0 7 0 7 0 7
Serum FA Serum-free Serum FA Serum-free
2iL SL
−4 −2 0 2 4
Value
B
Rex1-dGFP EpiSC
X band
Y band

Figure S3. Expression pattern of long non-coding RNAs in differentiating male nPSCs, Related to Figure 2.

(A) Heatmap depicting the expression profile of long non-coding RNAs during differentiation of male (E14tg2a – XY1) ESCs. Before differentiation, ESCs were maintained in 2iL or SL media, as indicated. Data was obtained by strand-specific RNA-seq. Scale represents z-scores of Log_2 transformed expression values. *Xist* is indicated with a red arrow.

(B) PCR-based gender determination of the *Rex1*-dGFP EpiSC line.

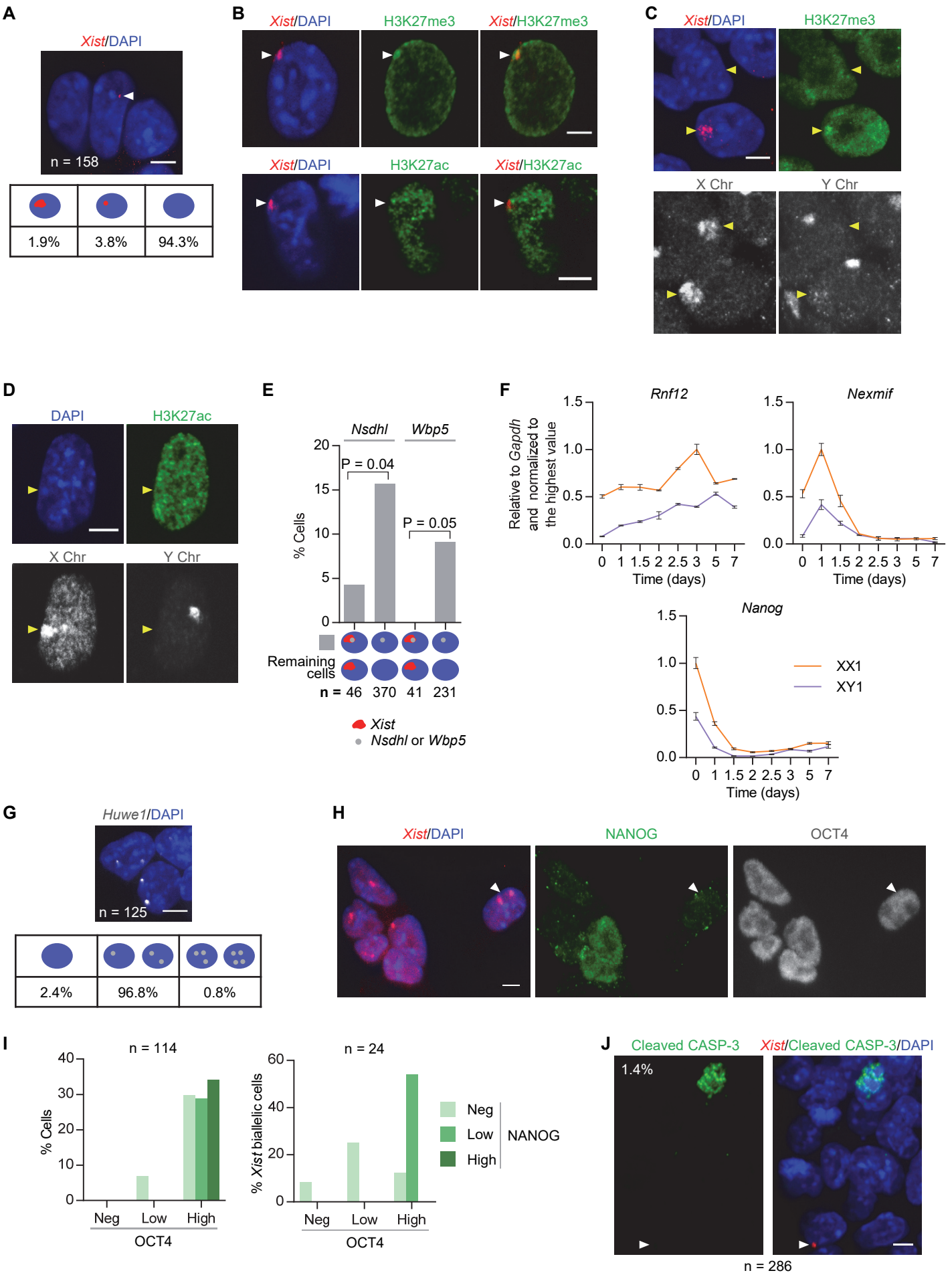
A
Xist/DAPI
n = 158
1.9%
3.8%
94.3%
B
Xist/DAPI
H3K27me3
Xist/H3K27me3
Xist/DAPI
H3K27ac
Xist/H3K27ac
C
Xist/DAPI
H3K27me3
X Chr
Y Chr
D
DAPI
H3K27ac
X Chr
Y Chr
E
Nsdhl
Wbp5
% Cells
P = 0.04
P = 0.05
Remaining cells
n = 46 370 41 231
Xist
Nsdhl or Wbp5
F
Rnf12
Nexmif
Nanog
Relative to Gapdh and normalized to the highest value
Time (days)
XX1
XY1
G
Huwe1/DAPI
n = 125
2.4%
96.8%
0.8%
H
Xist/DAPI
NANOG
OCT4
I
n = 114
n = 24
% Cells
% Xist biallelic cells
Neg
Low
High
OCT4
NANOG
J
Cleaved CASP-3
Xist/Cleaved CASP-3/DAPI
1.4%
n = 286

Figure S4. Males undergo transient XCI, Related to Figure 3.

(A) RNA FISH for *Xist* (red) in male 2iL ESCs at 1.5 days of differentiation in FA using strand-specific probe. Nuclei are shown in blue (DAPI staining). White arrowhead indicates the location of the *Xist* signal. Quantification of the different *Xist* RNA patterns is shown.

(B) Immuno RNA FISH for *Xist* (red) and H3K27me3 or H3K27ac (green) in male 2iL ESCs at 1.5 days of differentiation in FA. Nuclei are shown in blue (DAPI staining). White arrowheads indicate the location of the *Xist* cloud.

(C) Immuno RNA FISH for *Xist* (red) and H3K27me3 (green) in male 2iL ESCs at 1.5 days of differentiation in FA with subsequent DNA FISH XY paint (grayscale). Nuclei are shown in blue (DAPI staining). Yellow arrowheads indicate the location of the X chromosome. A cell lacking H3K27me3 on the X chromosome is shown as a negative control.

(D) Immunofluorescence for H3K27ac (green) in male 2iL ESCs at 1.5 days of differentiation in FA with subsequent DNA FISH XY paint (grayscale). Nuclei are shown in blue (DAPI staining). Yellow arrowheads indicate the location of the X chromosome. A cell showing existence of H3K27ac on the X chromosome is shown as a negative control.

(E) Quantification of the RNA FISH patterns for the X-linked genes *Nsdhl* or *Wbp5* and *Xist* in male 2iL ESCs at 1.5 days of differentiation in FA. Fisher's exact test was used for statistical analysis.

(F) qRT-PCR analysis of *Rnf12*, *Nexmif*, and *Nanog* during differentiation in FA of female (LF1 – XX1) and male (E14tg2a – XY1) ESCs. Before differentiation, cells were maintained in 2iL. Data shown are the mean of 3 technical replicates. Error bars represent ± SD.

(G) RNA FISH in female (LF1) 2iL ESCs with a strand-specific probe detecting X-encoded nascent RNA of *Huwe1* (grayscale). Nuclei are shown in blue (DAPI staining). Quantification of the different RNA FISH patterns is shown.

(H) Immuno RNA FISH for *Xist* (red), NANOG (green) and OCT4 (greyscale) in female (LF1 – XX1) 2iL ESCs at 1.5 days of differentiation in FA. Nuclei are shown in blue (DAPI staining). White arrowhead indicates the location of a cell with biallelic *Xist* upregulation.

(I) Quantification of *Nanog* and *Oct4* expression profile in the bulk population (left) and in cells with biallelic *Xist* expression (right) as shown in (B).

(J) Immuno RNA FISH for *Xist* (red) and cleaved CASPASE-3 (green) in male (E14tg2a) 2iL ESCs at 1.5 days of differentiation in FA. Nuclei are shown in blue (DAPI staining). White arrowhead indicates the location of an *Xist* RNA cloud. The percentage of cleaved CASPASE-3-positive cells is indicated. None of the cells analyzed were positive for both *Xist* and cleaved CASPASE-3.

The scale bar represents 5 μm.